arXiv:1604.07920v1 [astro-ph.SR] 27 Apr 2016

The Rotation-Activity Correlations in K and M dwarfs. I. Stellar parameters, compilations of $v \sin i$ and $P/\sin i$ for a large sample of late-K and M dwarfs [1]

E.R. Houdebine
Armagh Observatory, College Hill, BT61 9DG Armagh, Northern Ireland
Université de Toulouse, UPS-Observatoire Midi-Pyrénées, IRAP, Toulouse, France
CNRS, Institut de Recherche en Astrophysique et Planétologie, 14 av. E. Belin, F–31400 Toulouse, France
eric_houdebine@yahoo.fr

D.J. Mullan
Department of Physics and Astronomy, University of Delaware, Newark, DE 19716, USA

F. Paletou
Université de Toulouse, UPS-Observatoire Midi-Pyrénées, IRAP, Toulouse, France
CNRS, Institut de Recherche en Astrophysique et Planétologie, 14 av. E. Belin, F–31400 Toulouse, France
and

M. Gebran
Department of Physics & Astronomy, Notre Dame University-Louaize, PO Box 72, Zouk Mikaël, Lebanon

ABSTRACT

Reliable determination of Rotation-Activity Correlation (RAC's) depends on precise measurements of the following stellar parameters: T_{eff}, parallax, radius, metallicity, and rotational speed $v \sin i$. In this paper, our goal is to focus on the determination of these parameters for a sample of K and M dwarfs. In a future paper (Paper II), we will combine our rotational data with activity data in order to construct RAC's.

Here, we report on a determination of effective temperatures based on the $(\text{R-I})_C$ color from the calibrations of Mann et al. (2015) and Kenyon & Hartmann (1995) for four samples of late-K, dM2, dM3 and dM4 stars. We also determine stellar parameters (T_{eff}, $log(g)$ and [M/H]) using the PCA-based inversion technique for a sample of 105 late-K dwarfs. We compile all effective temperatures from the literature for this sample. We determine empirical radius-[M/H] correlations in our stellar samples. This allows us to propose new effective temperatures, stellar radii, and metallicities for a large sample of 612 late-K and M dwarfs. Our mean radii agree well with those of Boyajian et al. (2012).

We analyze HARPS and SOPHIE spectra of 105 late-K dwarfs, and have detected $v \sin i$ in 92 stars. In combination with our previous $v \sin i$ measurements in M and K dwarfs, we now derive $P/sini$ measures for a sample of 418 K and M dwarfs. We investigate the distributions of $P/sini$ and we show that they are different from one spectral sub-type to another at a 99.9% confidence level.

Subject headings: Stars: late-type dwarfs - Stars: late-type subdwarfs - Stars: rotation - Stars: Fundamental parameters

1. Introduction

The determination of fundamental stellar parameters (T_{eff}, R_*, [M/H] and $v \sin i$), notably for nearby stars, are essential to many astrophysical studies. This is especially true for studies of Rotation-Activity Correlations (RAC's), i.e., studies of how various indices of magnetic activity (e.g. R'_{HK}, L_X) vary as a function of the rotation period of the star. In this paper, we focus on quantities which are relevant to determining rotational properties, including T_{eff}, R_*, [M/H], and $v \sin i$. We shall postpone the discussion of activity indices to Paper II, when the RAC's will be constructed.

Various techniques have been used in the past to derive values of T_{eff} and [M/H]. Here we use two different approaches to determine these parameters in samples of late-K and M dwarfs. In the first approach, we use the PCA-based inversion technique of Paletou et al. (2015a), by applying it to the Na I resonance doublet in our K dwarf sample (105 stars). For this sample of K dwarfs, we also compiled all published values of T_{eff} in the literature and further derived new values of T_{eff} based on measurements of the (R-I)$_C$ color: our conversion from (R-I)$_C$ to T_{eff} uses the extensive calibration of Kenyon & Hartmann (1995). We find good agreement between our values rederived from (R-I)$_C$ and the published values ($3\sigma \sim 70$ K).

In the second approach, for our M dwarf samples (M2, M3 and M4), we find that a tight correlation between T_{eff} and (R-I)$_C$ exists among the recent measurements of Mann et al. (2015). It had been shown in the past that the (R-I)$_C$ color is a good effective temperature diagnostic for M dwarfs (e.g. Leggett 1992), with a relatively low sensitivity on the metallicity (e.g. Ramirez & Melendez 2005). In an on-going determination of T_{eff} derived from (R-I)C for samples of M dwarfs ranging in spectral subtype from M2 to M7, Houdebine et al. (2016, in preparation) find a very good agreement with a compilation of all published values of T_{eff} in the literature. Therefore, for our present samples of M2, M3 and M4 dwarfs, we have used the calibration of Mann et al. (2015) to determine T_{eff}.

Houdebine (2008, Paper VII) found a relatively tight correlation between [M/H] and R_* in a sample of M2 dwarfs. [M/H] decreases with decreasing R_* in normal dwarfs and subdwarfs, such that all subdwarfs have very low [M/H] and R_*. In the present paper, we perform extensive compilations of [M/H] from the literature and correlate [M/H] and R_* for our samples of late-K, M3, and M4 dwarfs. This allows us to obtain values of [M/H] for all of our target stars. The determination of [M/H] will be essential when we eventually attempt to construct meaningful RAC's for the Ca II line fluxes. The reason is that an ongoing NLTE-radiation tranfer modelling study (Houdebine & Panagi 2016, in preparation) of the Ca II line formation as a function of the metallicity confirms that the *Ca II line resonance doublet is not a good diagnostic of magnetic activity unless it is first corrected for the influence of metallicity.*

As a preliminary to constructing RAC's in K and M dwarfs, we have reported over the past several years, improved spectroscopic measurements of rotational broadening $v \sin i$ in stars of spectral sub-types dK4 (Houdebine 2011a, Paper XVI thereafter), dK6 (present study), dM2 (Houdebine 2008, Paper VIII, Houdebine 2010a, Paper XIV), dM3 (Houdebine & Mullan 2015) and dM4 (Houdebine 2012a, Paper XVII). An important aspect of our $v \sin i$ measurements has to do with the use of the HARPS and SOPHIE spectrographs: these spectrographs are designed initially for exoplanet searches and are therefore very stable in wavelength in the long term (about 1 m/s for HARPS). These data give us access to rotational velocities which are significantly smaller than in previous spectroscopic studies of K and M dwarfs. Because of the smallness of some of our $v \sin i$ values, we need to verify the precision of our data. We assess the uncertainties on our $v \sin i$ measurements in Section 5 below. We shall find that the uncertainties δv in $v \sin i$ may be as small as $\pm\sigma = 0.27\ km\ s^{-1}$ for $v \sin i < 1\ km\ s^{-1}$, $\pm\sigma = 0.32\ km\ s^{-1}$ for $1 < v \sin i < 5\ km\ s^{-1}$, and $\pm\sigma = 0.60\ km\ s^{-1}$ for $v \sin i > 5\ km\ s^{-1}$.

The occurrence of such uncertainties imposes an upper limit $P_{max}/\sin i$ on the rotational period of stars which are accessible to our approach. E.g., for stars near the transition to complete convection (TTCC), where $R_* \approx$0.3-0.4 $R_\odot$, we

[1]Based on observations available at Observatoire de Haute Provence and the European Southern Observatory databases and on Hipparcos parallax measurements.

can in principle measure the rotation periods of TTCC stars with confidence only up to values of $P_{max}/\sin i = 2\pi R_*/\delta_v \sim$ 15-40 days. With a random distribution of inclinations, the average value of $\sin i$ is $2/\pi = 0.64$. Therefore, the longest rotational periods P_{max} that we can hope to measure near the TTCC would be no greater than 10-26 days. For our sample of dK6 stars, where the average $R_* = 0.647 R_\odot$ (see Table 6), the upper limit on $P_{max}/\sin i$ is 33-66 days. Again correcting for $\sin i = 0.64$, we find P_{max} for dK6 stars to be 21-42 days. Interestingly, these ranges in period overlap with the upper limit (about 30 days) which was obtained from early studies of rotational modulation in Kepler photometry (Nielsen et al. 2013). It is encouraging to find that by pushing spectroscopic studies of rotation to better limits, we can now study stars whose rotational periods would previously have been accessible only to photometric studies. To be sure, our approach is still subject to the $\sin i$ limitation, whereas this does not affect photometric analysis.

In the present study, we report on a new analysis of high resolution HARPS and SOPHIE spectra of 105 late-K dwarfs. We have detected $v \sin i$ in 92 of these stars. By combining these data with analyses in our earlier papers, we now investigate the distributions of $P/\sin i$ for our samples of stars at spectral subtypes dK6, dM2, dM3, and dM4. In total, the present compilation of $P/\sin i$ measures includes measurements for 418 different K and M dwarfs. As already reported in paper XVI and in Houdebine & Mullan (2015, hereafter HM), we confirm here that these distributions vary with spectral subtype: the distributions among dK6, dM2, dM3 and dM4 stars are statistically different from one another. These findings imply that in order to study RAC's, one must construct RAC's separately for each different spectral sub-type.

Our data confirm that the mean rotation periods of stars in the range dK4-dM4 in general decrease with decreasing effective temperature for slow rotators (HM). However, we also find that something unusual happens in the rotation rates between dM2 and dM4. The overall trend towards decreasing rotation period as we go from dK4 to dM4 is interrupted at spectral sub-type dM3 where the period increases to a local peak where the rotational period is longer than the overall trend would have predicted (HM). When the investigation is extended (as in the present paper) to include fast rotators among the dK4-dM4 stars, one finds the following overall trend: the mean rotation period tends to increase slightly from dK4 to dM4. But once again, at dM3, an exception is found: the mean rotation period of fast rotators at dM3 is locally significantly longer than the overall trend would have predicted (HM). HM interpreted the abnormally long rotation periods at sub-type dM3 as possibly being associated with the occurrence of increasing coronal loop lengths (reported by Mullan et al. 2006). The mean rotation period of the slow rotators is an important constraint on the past evolution of the dynamo mechanisms and magnetic braking mechanisms (HM and this study).

The plan of this paper is as follows. In Section 2, we describe how the spectroscopic data were selected for a sample of late-K dwarfs. In Section 3, we describe how values of T_{eff}, R_*, and [M/H] have been extracted for our target stars, first for the K dwarfs, and then for the M dwarfs. In Section 4, we describe how a cross-correlation technique is used to determine the value of $v \sin i$ for our sample of dK6 stars using all spectral lines within a preferred band of the spectrum. Uncertainties in the values of $v \sin i$ for K and M dwarfs are discussed in Section 5. In Section 6, we present the distributions of $P/\sin i$ values for the stars of different spectral sub-types, and discuss the statistical significance of differences between the distributions. Our conclusions are in Section 7.

We stress that the contents of Paper I are only a first step in a two-step process which aims to derive RAC's for each spectral sub-type. The second step in this process will be discussed in Paper II. The present paper focusses on obtaining reliable data for the "Rotation" axis of the RAC. The subsequent paper will focus at first on obtaining reliable data for the "Activity" axis of the RAC. Once reliable data are available for both axes, a search will then be undertaken (in Paper II) to determine if any significant correlation exists between Rotation and Activity for each spectral sub-type.

2. Selection of spectroscopic data

Stepien (1989, 1993, 1994) has reported that RAC's exhibit certain differences at different spectral types. As an extension of this finding, we have

found, in previous studies (Paper XVIII, HM), that it is important in constructing RAC's to select samples of stars with T_{eff} values which are confined within a narrow range. There are two principal reasons for this, one related to our analysis of chromospheric emission lines, and one related to the choice of an optimal set of photospheric absorption lines.

As regards *chromospheric* analysis, it is important to deal with stars with closely similar T_{eff} when we are attempting to quantify with as much precision as possible the EW of the chromospheric lines (Ca II resonance doublet and H_α). These lines inevitably include some contributions from the background photospheric continuum and from the temperature minimum region (e.g.Houdebine & Doyle 1994, Cram & Mullan 1979, Houdebine & Stempels 1997, Paper XV). Initially, our samples of stars had been selected for the purpose of chromospheric modelling studies (e.g. Houdebine & Stempels 1997, Houdebine 2009b Paper XII, Houdebine 2010b Paper IX), and in these studies the selection of stars with closely similar spectral types was essential in order to develop reliable grids of semi-empirical model chromospheres, each of which would be superposed on a particular photospheric model.

As regards *photospheric* analysis, our principal goal is to extract precise $v \sin i$ values by applying cross-correlation methods to multiple absorption lines over a $\sim$100 Å swath of spectrum. We have found that it is important to select certain optimal ranges of wavelengths so that the spectral lines which lie within those ranges will contribute maximally to enhancing the precision of $v \sin i$: the precision is optimized in spectral ranges where there are large numbers of weak and unsaturated narrow spectral lines. As it turns out, the photospheric continuum also contributes to which wavelengths ranges are optimal for our purposes: even within the relatively narrow range of dK4 to dM4, changes in the continuum from one spectral subtype to another give rise to detectable differences in optimizing the choice of the wavelength range. These factors reinforce our decision to study homogeneous samples where the stars are confined to a narrow range of T_{eff} (e.g., Papers XIV, XVI, XVII, this study). Not only do RAC's vary with the spectral type (e.g. Stepien, 1989, 1993, 1994, Houdebine et al., 2016), but also the distributions of rotation periods varies from one spectral subtype to another (HM and this paper).

Based on our previous papers, we have found that the most suitable initial selection parameter when we wish to identify a homogeneous sample of K or M dwarfs belonging to a specific sub-type is the (R-I) color: this color is sensitive to T_{eff}, but less so to metallicity (e.g. Leggett 1992, Ramirez & Melendez 2005). Moreover, broad-band colors of high precision are widely available in the literature for many of the cool dwarfs which are of interest to us.

2.1. Selection of a sample of late K dwarfs

We selected a sample of 419 late K dwarfs on the basis of (R-I) measurements available in the literature. Our sample contains stars with $(R\text{-}I)_C$ (i.e. (R-I) color in the Cousins system) in the range [0.684;0.816] which also corresponds to $(R\text{-}I)_K$ ((R-I) in the Kron system) in the range [0.503;0.613] according to the transformation formulae of Leggett (1992) (see Leggett 1992 for more information on the Cousin's and Kron photometric systems). According to Kenyon and Hartmann (1995), this range of colors is centered on $(R\text{-}I)_c$=0.75, i.e. the spectral type dK7. However, when we compiled and derived effective temperatures with the PCA-based inversion method (see Paletou et al. 2015 and Sect. 3) for this sample of late K dwarfs, we found in average higher temperatures than what would be expected from the $(R\text{-}I)_C$-T_{eff} tabulation of Kenyon and Hartmann (1995). We give the stellar parameters and spectral types of our late K dwarf sample in Table 1. One can see in this table that most stars are dK5 or dK6 stars, with a few dK4 and dK7 stars. In view of this relatively large range of spectral types, we decided to restrict our sample to the range dK5.7 to dK7.3 in order to obtain a better defined RAC (Houdebine et al. 2016). This restricted sample is centered on the spectral sub-type dK5.9. We shall therefore refer to this sample as the dK6 stars. Our dK6 stellar sample contains stars that have similar (R-I) colours and the same effective temperatures to within $\pm$110 K. We refer to HM for a discussion of corresponding data for our sample of dM3 stars. Values of $(R\text{-}I)_C$ for our samples of stars were taken from the following papers: Veeder (1974), Eggen (1974), Rodgers & Eggen (1974), Eggen (1976a, 1976b),

Eggen (1978), Eggen (1979), Eggen (1980), Weis & Upgren (1982), Upgren & Lu (1986), Eggen (1987), Booth et al. (1988), Leggett & Hawkins (1988), Bessel (1990), Weis (1991a 1991b), Dawson & Forbes (1992), Leggett (1992), Weis (1993).

These papers provided us with a starting list of a large number (419) of late K dwarfs. Searching through databases at the European Southern Observatory (ESO) and Observatoire de Haute Provence (OHP), we identified spectra of 112 different stars which are suitable for our purposes. The final list of 105 stars in our sample late K dwarf sample is provided in Table 1 (note that in Table 1 we also added other stars with known $v \sin i$ and [M/H], see next sections).

The spectra which we use for determining $v \sin i$ came from two different échelle spectrographs; HARPS (High Accuracy Radial velocity Planet Search, ESO) and SOPHIE (OHP). These two high-resolution échelle spectrographs are designed for planet search programs and are very stable in wavelength and resolution. The instrumental stability makes the spectra well suited for the measurement of rotation in M dwarfs (see HM). We included in our sample the SOPHIE observations obtained in the High Efficiency (HE) mode for the purpose of measuring the Ca II and H_α line equivalent widths (Houdebine et al. 2016). For further details of the spectrographs, see HM. For measuring $v \sin i$ with SOPHIE spectra, we used observations in the High Resolution (HR) mode only (R=75000 and an image scrambler).

For comparison, when we were studying dM3 stars (see HM), we started off with a list of 381 dM3 objects based on $(R\text{-}I)_C$ data in the literature. Searching through the same databases as above, we found suitable observations for 86 different dM3 stars.

2.2. Biases in our sample stars

The stars in our sample includes all stars from all observing programs which have been carried out with HARPS and SOPHIE. These programs are mostly planet-search programs, although some programs are dedicated to magnetic activity. Because of requirements of achieving high S/N in the spectra, the selection of stars is brightness limited.

Our initial target list of 419 late K dwarfs (based on broad-band colors) is estimated to be complete down to apparent brightness $m_V \approx 11$. In our sample of 105 stars with sufficiently high S/N spectra for our present purposes, the list is estimated to be complete down to $m_V \approx 10$ for the slow rotators. Assuming an absolute magnitude $M_V \approx 8.5$ as the boundary between normal disk stars and subdwarfs, our sample of 105 late K dwarfs is estimated to be complete out to a distance of 20 pc for our slow rotators. For subdwarfs, we cannot claim that our target list is complete.

As far as the bias towards bright stars at spectral type dM3 is concerned, HM reported that this bias has little effects on the mean rotation period of low-activity M dwarfs. This is due to the fact that the rotation period does not change much with the stellar radius for disk stars (see HM). Analogously, the brightness-limited bias in our late K dwarf sample is expected to have only minor effects in the RAC. The bias may contribute somewhat to the density of sampling at different parts of the RAC, but this is not expected to cause significant discrepancies as regards the overall RAC (Houdebine et al. 2016).

In the planet-search programs, observers tend to avoid stars with high levels of magnetic activity: spot modulation in such stars can mimic the effects of planets and can also add significant noise to the data. Therefore our spectral samples are likely to be biased in general towards low activity stars, i.e. stars which are far removed from "saturated" magnetic effects. Despite this "anti-activity" bias, we found that a small percentage of more active (i.e. dMe) stars did survive in our samples: 2% of our late K dwarf sample are catalogued as dKe, and 10% of our dM3 sample are catalogued as dM3e. We note that the latter figure is not far from the report of West et al (2008) that 10-20% of dM3 stars are dM3e. However, we completed our own samples with $v \sin i$ measures and Ca II and H_α line equivalent width measures from the literature, including notably many new fast rotators. Therefore, the samples of stars studied in this paper do not contain *only* low activity stars (i.e. slow rotators).

3. Stellar parameters

Here, we discuss the methods we use to derive T_{eff} and radius for each of our samples of stars.

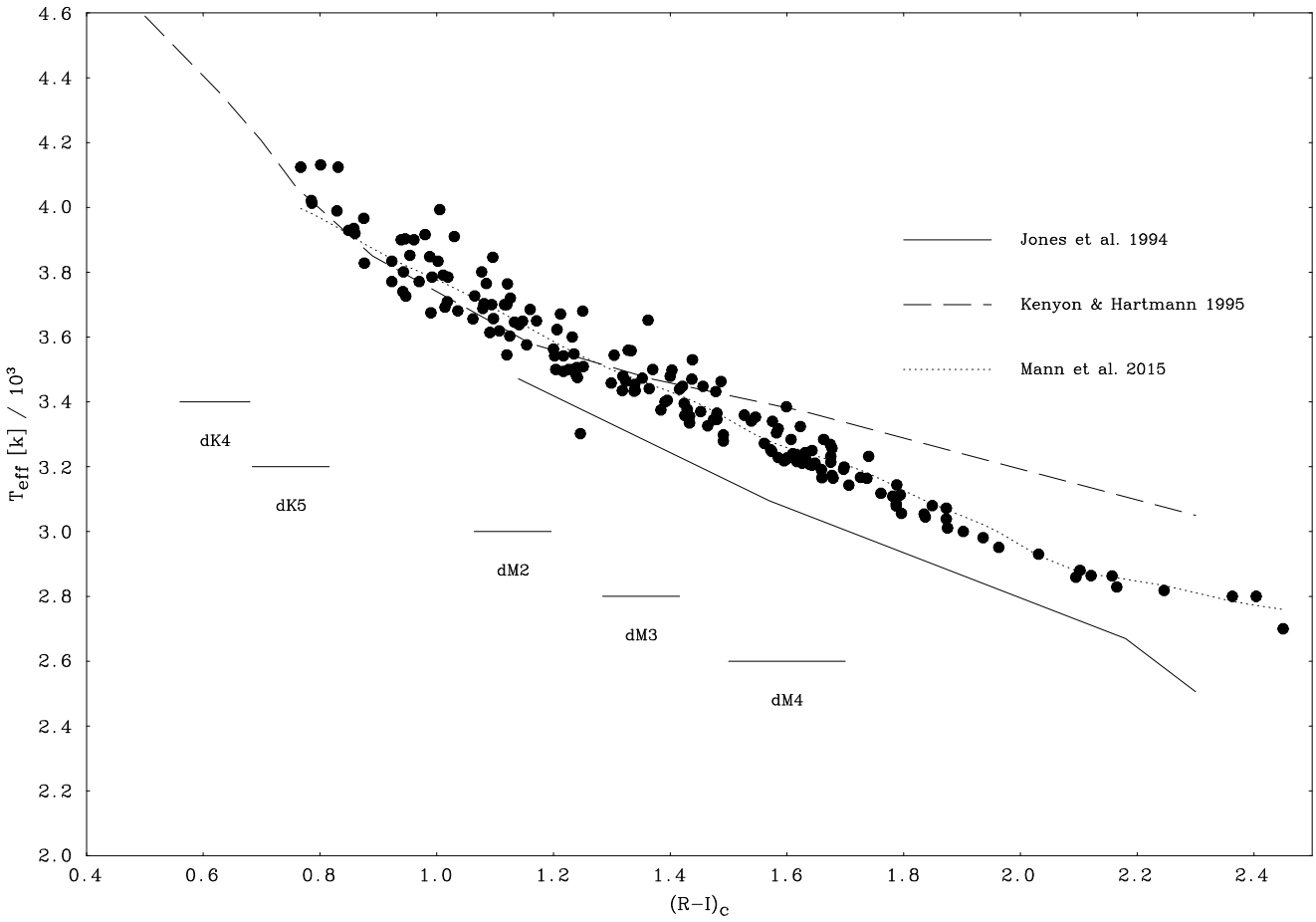

Fig. 1.— Values of T_{eff} as a function of the (R-I)$_C$ color for the data of Mann et al. (2015, filled circles) and a smoothing of this data (dotted line). Also shown for comparison: the values of Jones et al. (1994, solid line) used in some of our previous studies. A difference of about ∼170 K exists between the two correlations. Also shown: the calibration of Kenyon and Hartmann (1995). This later calibration agrees well with the more recent measures of Mann et al. up to (R-I)$_C$=1.3, but tends to overestimate T_{eff} for later spectral types. We overplot the (R-I)$_C$ domains of our samples of stars from dK4 to dM4.

The radius is necessary for the determination of the projected rotation periods, P/sini.

3.1. PCA-based inversion of stellar fundamental parameters for late K dwarfs

In order to derive estimates of effective temperatures (T_{eff}) for our late K dwarfs In Table 1 we used the calibration of Kenyon & Hartmann (1995: hereafter KH). We derived the effective temperature as a function of $(R\text{-}I)_C$ according to this tabulation. We searched the literature for other T_{eff} measurements for our late-K targets (we used the tutorial developed by Paletou & Zolotukhin 2014[2]). We found a relatively good agreement between these temperatures and effective temperatures previously published: The mean difference in only of the order of 75 K.

As an independent method of determining values of T_{eff} for our sample of late K dwarfs, we used the principal component analysis-based (PCA) method to derive Teff and also [Fe/H], $log(g)$ and $v \sin i$ (Paletou et al. 2015b). HARPS and SOPHIE spectra were inverted using the PCA method introduced for stellar fundamental parameters by Paletou et al. (2015a). In the latter paper, stellar spectra of FGK stars were inverted using a so-called "learning database" made from the Elodie stellar spectra library (see Prugniel et al. 2007): the "learning" occurs by using *observed* spectra for which fundamental parameters had already been evaluated. We note that the spectra considered in Paletou et al. (2015a) had typical spectral resolutions $\mathcal{R}$ of 50 000 and 65 000: these are significantly lower than the resolution of HARPS and SOPHIE data which will be analyzed in the present paper.

For the present study, we used the PCA method, but with a difference: the "learning" was achieved by referring to *synthetic* spectra. A grid of 6336 spectra was computed using Synspec-48 synthetic spectra code (Hubeny & Lanz 1992) and Kurucz Atlas-12 model atmospheres (Kurucz 2005). The linelist was built from Kurucz (1992) `gfhyperall.dat`[3]. In order to deal with stars close to dK6, we adopted a grid of parameters such that T_{eff} is in the range 3500–4600 K (with steps of 100 K), log$g$ is in the range 4–5 cgs (with steps of 0.2 dex), metallicity [Fe/H] is in the range from -2 to +0.5 (with steps of 0.25 dex) and, finally, $v$sin$i$ is in the range from 0 to 14 $km\,s^{-1}$ (with steps of 2 $\mathrm{km\,s^{-1}}$). For all models the microturbulent velocity was fixed at $\xi_t = 1\ \mathrm{km\,s^{-1}}$ and [α/Fe] was set to 0. Also, for producing the reference spectra, we adopted the spectral resolution of the HARPS or SOPHIE spectrograph i.e., $\mathcal{R} = 115\,000$ or $\mathcal{R} = 75\,000$. We finally limited the PCA study to a spectral band almost 100 Å wide centred on the Na I D-doublet, ranging from 585.3 to 593.2 nm.

Even though the choice of Atlas-12 for such cool stars, as well as the choice of the synthetic spectral band we considered may be open to debate, we believe that parameters inverted from HARPS and SOPHIE data using our PCA approach are realistic enough for an initial analysis (see Paletou et al. 2015b).

Table 2 provides the results we have obtained from our PCA approach to the sample of 112 late K dwarfs as regards T_{eff}, log$g$, [Fe/H], and $v\ sini$. Typical uncertainties for these four parameters are respectively of order 100 K, 0.2 dex, 0.1 dex, and 1.5 $km\,s^{-1}$. It is important to note that the $v\ sini$ values derived from PCA are only preliminary estimates in order to obtain synthetic spectra to be used for "learning". Later on (Section 4 below), we shall derive more precise $v\ sini$ values based on the cross-correlation analysis: then we shall compare (Section 5) the precise values with the estimates derived from PCA (see Figure 12 below). Note that the spectra of GJ 1248 and Gl 747.1 were not inversed with the PCA method because they were too noisy.

In our sample of 112 stars, the PCA approach indicated that seven stars have significantly lower T_{eff} values than those expected for a late K dwarf: the seven stars are GJ 1248, Gl 17.1, Gl 369, Gl 401, Gl 747.1, Gl 842, and Gl 855 (see Table 2). It appears that our sample of late K dwarfs is polluted by a few cooler stars with spectral types which are actually later than dK7. Confirmation of the unusual coolness of 7 stars in our list of 112 is provided by our PCA determinations of T_{eff} in Table 2. Clearly, some of the $(R\text{-}I)_C$ values in our sample are discrepant: In view of this, we have excluded the 7 discrepant stars from our initial sample of 112 objects (Table 1).

Now let us compare the results for T_{eff} which

[2] http://www.astropy.org/

[3] http://kurucz.harvard.edu

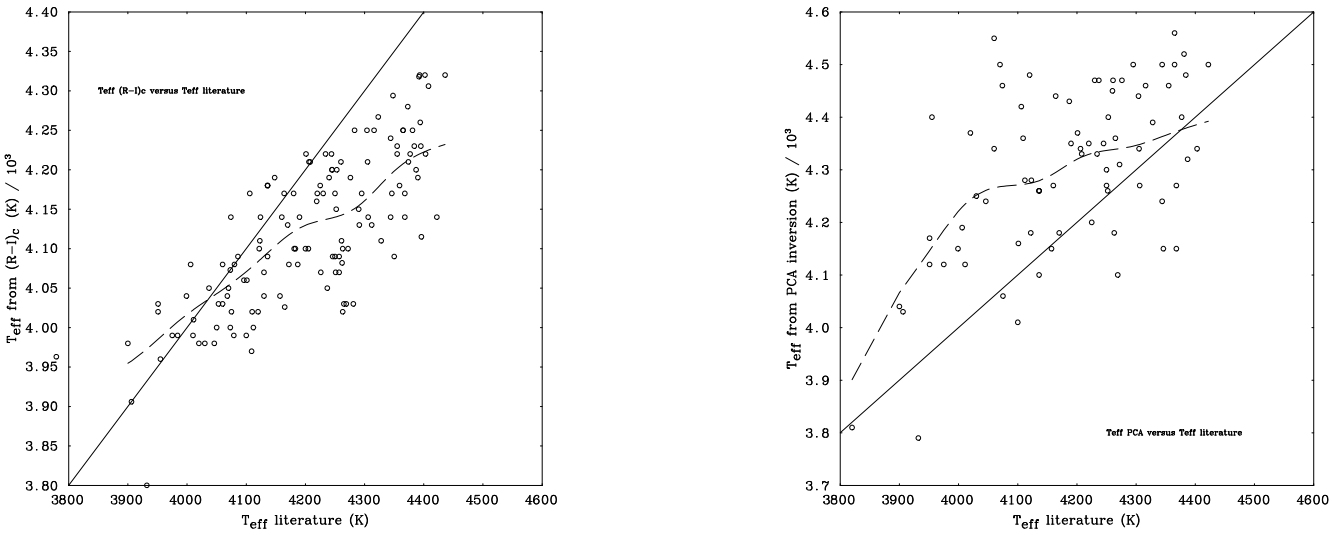
Teff (R−I)c versus Teff literature
T_eff from (R−I)_C (K) / 10^3
T_eff literature (K)
Teff PCA versus Teff literature
T_eff from PCA inversion (K) / 10^3
T_eff literature (K)

Fig. 2.— Values of T_{eff} derived from the (R-I)$_C$ colour as a function of the T_{eff} values compiled from the literature (left panel). The solid line is the one-to-one correlation. The dashed line shows the smoothed data. Right Panel: Values of T_{eff} derived from the PCA inversion method as a function of the T_{eff} values compiled from the literature. Same description as the left panel.

we have derived by means of the two different methods: KH and PCA. For our sample, we obtained a mean effective temperature of 4130 ±100K when we use the (R-I)$_C$ colour calibration method (KH). However, for the same sample of stars we obtained a mean effective temperature of 4270 ±100K when we use the PCA approach. There is a systematic difference of 140 K between PCA and colour calibration. Comparatively, the (R-I)$_C$ colour calibration method (KH) is in better agreement with the values given in the literature (see references therein), with a systematic difference of only 75 K. We show in Fig. 2 the values of T_{eff} derived from the (R-I)$_C$ colour as a function of the T_{eff} values compiled from the literature (left-hand panel). The solid line is the one-to-one correlation. The dashed line shows the smoothed data. There is a significant scatter among the data: typically ±70 K. Our measures inferred from (R-I)$_C$ agree rather well with other published values, typically within 50 K, up to a temperature of 4200 K. For larger values our temperature inferred from (R-I)$_C$ tend to be lower than published values, up to a value of 100 K. However, this latter difference is still reasonable. We can say that globally the temperatures inferred from (R-I)$_C$ are good evaluations. Houdebine et al. (2016, in preparation) show that (R-I)$_C$ is a good effective temperature diagnostic (based on the calibration of Boyajian et al. 2012) from spectral types dK3 to dM7 with typical differences with a large compilation of effective temperatures from the literature of only ±40 K.

We show in Fig. 2 (right-hand Panel) the values of T_{eff} derived from the PCA inversion method as a function of the T_{eff} values compiled from the literature. One can note that the PCA method tends to globally over-estimate T_{eff} at low and large values. The maximum difference in average is of the order of 200 K.

The differences we find between the different approaches are to be compared with systematic difference of typically 200-300 K between the results obtained by various investigators for K dwarfs (e.g. Ramirez & Melendez 2005; Ammons et al. 2006; Morales et al. 2008; Jenkins et al. 2009; Soubiran et al. 2010). We found during the course of our compilation of T_{eff} from the literature for our objects that differences between au-

thors are often different by more than 100-200 K. In some cases, the differences may attain more than 500 K. These systematic differences seem relatively large compared to the precisions which are claimed by the various authors (typically ±100 K). In view of these systematic differences already in the literature, we believe that the T_{eff} differences which we encounter between our two methods are not excessive: in fact, given the scatter in the data, we consider our results reasonable and consistent with values in the literature. In what follows, we have taken the mean of the three different values (KH, PCA and mean of published values) in order to obtain reliable estimates of our effective temperatures for our sample of late K dwarfs (Table 1).

According to our PCA approach, the mean metallicity of our sample is -0.316 dex (excluding dKe stars and subdwarfs). Therefore, on average, our late K dwarfs are metal poor. However, if we compare this value to the average of the metallicities for dM2 stars (-0.154 dex, Paper XIV) we find that the present metallicities for our sample may be underestimated. As a matter of fact, for dM2 stars, we obtained a good RAC after correction from the metallicity effects in Paper XIV, which somewhat confirms a posteriori the accuracy of those metallicities. On the other hand, when we attempt to correct the dK6 star RAC for metallicity effects (Houdebine et al. 2016), we obtain a larger scatter in the RAC. This may arise from the larger uncertainty we have on the metallicity for dK6 stars (0.2 dex).

3.2. Effective temperatures for our samples of M dwarfs and the Stellar radii

In order to derive radii for the stars in our dK6 and other samples, we used the classical formula;

$$M_v + BC = 42.36 - 5 \times log\frac{R_*}{R_\odot} - 10 \times log T_{eff}, \quad (1)$$

where symbols take their usual meaning. We used the BC tabulation as a function of (R-I)$_C$ from KH: these authors compiled data on BC as a function of various colours from the literature. We estimate that their tabulation yields an uncertainty of about 10% in BC at spectral type K6 (see KH). Using Eq. (1), we obtained the radii for our late K dwarfs as listed in Table 1. In this table, we give the mean of the effective temperatures derived from the (R-I)$_C$ colour from KH, the values of the PCA method and values previously published. The sources of the published effective temperature are: Wright et al. (2003), Valenti & Fischer (2005), Ammons et al. (2006), Masana et al. (2006), Sanchez-Blazquez et al. (2006), Sousa et al. (2006), Cenarro et al. (2007), Morales et al. (2008), Jenkins et al. (2009), Lafrasse et al. (2010), Soubiran et al. (2010), Casagrande et al. (2011), Prugniel et al. (2011), McDonald et al. (2012), Chen et al. (2014), Gaidos et al. (2014). We estimate the errors as the σ of these measures. The errors on the radii in Table 1 were computed taking into account the combination of the error on the absolute magnitude, an assumed error of 0.02 magnitudes on the (R-I)$_C$ colour, and a typical 100 K error in T_{eff}. The mean T_{eff} and radius for our dK6 sample are 4226 K and 0.6469 R$_\odot$ respectively. The value of the radius for this T_{eff} given by Boyajian et al. (2012) is 0.6457 R$_\odot$. Therefore the two values agree within 0.19%. We generally considered that in our dK6 sample, stars with [M/H]<-0.5 ($M_V \approx 8.6$) are subdwarfs.

For our samples of dM2 and dM4 stars, we used in previous studies the calibration of Jones et al. (1994). However, a more recent study which should be more precise (Mann et al. 2015) indicates that the values from Jones et al. (1994) may be underestimated by about 170 K. We show the calibrations of T_{eff} as a function of (R-I)$_C$ of Jones et al. (1994), KH and Mann et al. (2015, filled circles) in Fig. 1. We also show a smoothing of the data of Mann et al. (2015, dotted line). The calibration of Kenyon and Hartmann (1995) agrees well with the more recent measures of Mann et al. (2015) up to (R-I)$_c$=1.3, but tends to overestimate T_{eff} for later spectral types. Therefore, the stellar radii have been overestimated in our previous studies of dM2 and dM4 stars by the order of 10-15%.

In the coming sub-sections, our measurements of $v \sin i$ have been compared with, and supplemented by, those from other authors. For comparison between the different spectral sub-types used in this study, we overplot the (R-I)$_C$ domains of our samples of stars from dK4 to dM4. However, we recall that there are systematic differences of the order of 200-300 K in the T_{eff}-radius plane between the interferometric calibrations of Boyajian

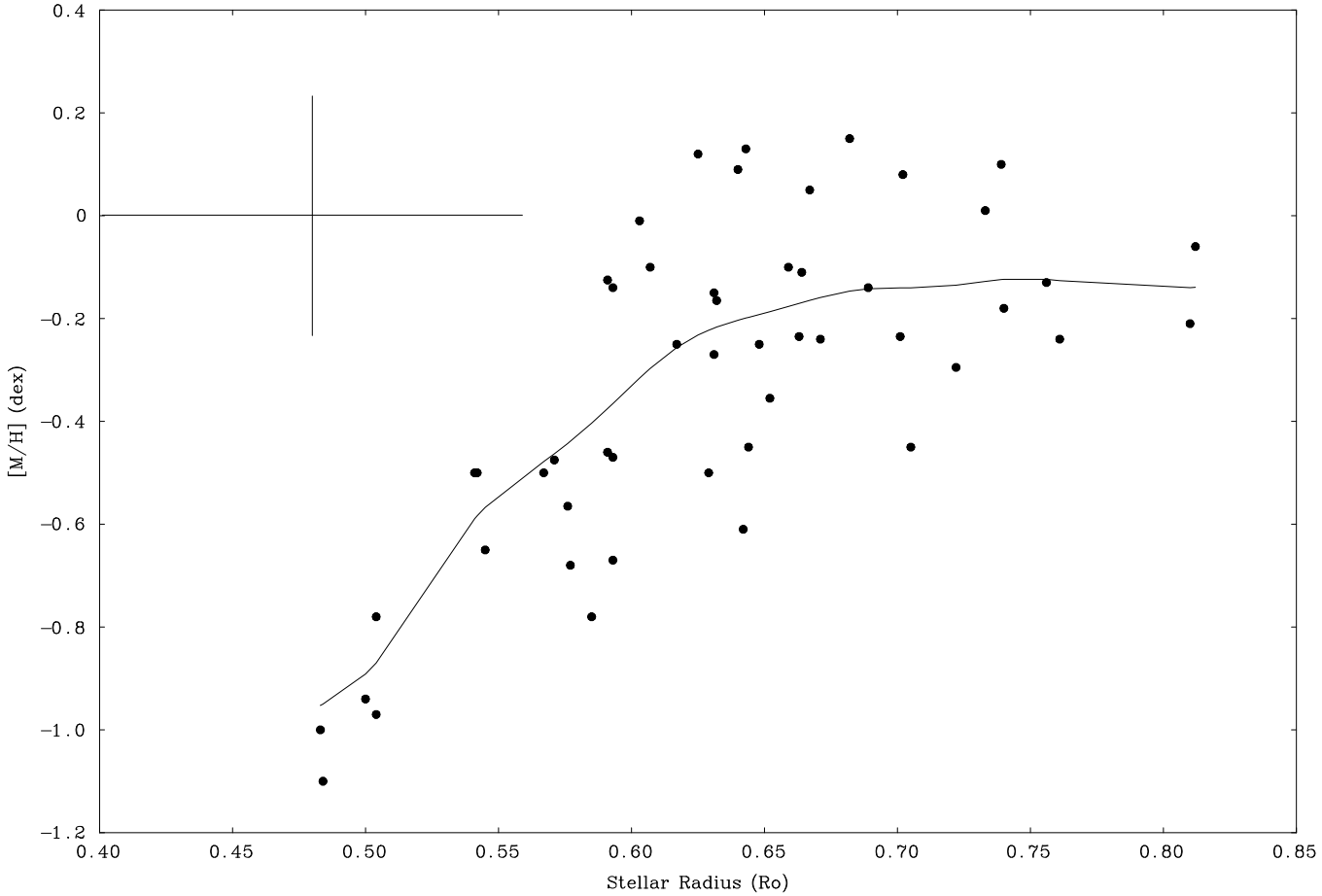

Fig. 3.— Correlation between the metallicity [M/H] and the stellar radius for stars with spectral sub-type dK6. The two parameters do correlate for dK6 stars but the scatter is large. This large scatter is essentially due to the large errors on the stellar radii and [M/H] as indicated by the error box.

et al. (2012) and the Double-Eclipsing Binaries calibrations (see Boyajian et al. 2012 for a comparison) for K and M dwarfs. Therefore, the calibration of Mann et al. (2015) may not be definitive and may still be subject to improvements.

We give in Tables 3, 4 and 5 the stellar parameters for our samples of dM2, dM3 and dM4 stars respectively. The mean T_{eff} and radii for our samples of dK4, dK6, dM2, dM3 and dM4 stars are given in Table 6. We find values of 4600 K, 4226 K, 3658 K, 3462 K and 3317 K for the mean T_{eff} of our samples of dK4, dK6, dM2, dM3 and dM4 stars respectively. The mean radii are 0.6469 $R_{\odot}$, 0.5082 $R_{\odot}$, 0.4090 $R_{\odot}$ and 0.3008 $R_{\odot}$ for the dK6, dM2, dM3 and dM4 samples respectively. These radii agree with those of Boyajian et al. (2012) within 0.19%, 6.3%, 4.3% and 8.2% respectively, which is acceptable for the studies of the $P \sin i$ distributions and the RAC's.

For our sample of dK5 stars (Houdebine 2011a and 2012b, Papers XVI and XVIII), we found that the mean temperature is 4600 K (Table 6). Effective temperatures for these stars were computed from values published in the literature (see Paper XVI). The stars were initially selected with $(R\text{-}I)_C$=[0.56:0.68] which corresponds to the spectral sub-type ∼K5 (KH). However, as in the case of dK6 stars, we found that the published effective temperatures were somewhat higher and rather correspond in average to the spectral sub-type dK4 (KH). Therefore, we shall refer to the dK4 stars for this sample of stars thereafter. We do not repeat the stellar parameters of our dK4 stellar sample here as the effective temperatures have not changed and the data is available in Paper XVI.

3.3. Stellar metallicities

We saw in Paper XV that correction from metallicity effects in dM2 stars is essential in order to obtain a good correlation between the Ca II EW and $P/\sin i$. This is due to the fact that the Ca II line formation depends sensitively on the Ca abundance (Houdebine & Panagi, in preparation). The same applies to dK6 stars and to the Ca II surface fluxes. Therefore, we compiled [M/H] measures from the literature for our dK6 stellar sample in order to obtain a metallicity-radius empirical correlation as in Houdebine (2008, Paper VII), and correct our Ca II surface fluxes from metallicity effects, assuming a proportionality between [M/H] and Ca II surface fluxes. We found several measures of [M/H] from the following authors: Marsakov & Shevelev (1988), Alonso et al. (1996), Valenti & Fischer (2005), Ammons et al. (2006), Sanchez-Blazquez et al. (2006), Sousa et al. (2006), Cenarro et al. (2007), Mishenina et al. (2008), Soubiran et al. (2010), Casagrande et al. (2011), Milone et al. (2011), Prugniel et al. (2011), Wu et al. (2011), Anderson & Francis (2012), Gaidos et al. (2014). We averaged the values from the literature with those from our PCA-based inversion method.

We plot in Fig. 3 these average values of [M/H] as a function of radius for our dK6 stars. One can see in this diagram that the scatter is large. We show the error box in Fig. 3, which gives in [M/H] the mean of the differences between values from the literature and our values from the PCA-based inversion method, and in radius, the mean of the errors on the radii for our stars. Both errors are large and explain the poor correlation between these two parameters for dK6 stars as well as the large scatter at about the running mean (solid line). As a consequence, the corrections from metallicity turn out to be rather poor: in fact, we do not obtain an improved RAC after corrections for [M/H] compared to the RAC without such corrections (see Houdebine et al. 2016).

For our dM2 stellar sample, we used the empirical correlation found by Houdebine (2008, Paper VII) to determine the metallicity for each stars as a function of its radius. These values were computed in Paper XV and are reported in Table 3.

We show the correlation between [M/H] and stellar radius for stars with spectral sub-type dM3 in Fig. 4. The correlation is relatively tight as in dM2 stars (Paper VII) in spite of the relatively large error on the radius (see the error box in Fig. 4). The scatter in this correlation is about three times less than in the same correlation for dK6 stars (Fig. 3). We can see that, as in dM2 and dK6 stars, the metallicity decreases with decreasing radius for a given $(R\text{-}I)_C$. We show some obvious outliers as open circles and the continuous line represents the data smoothed by a Gaussian. We derived the metallicities for dM3 stars according to this mean correlation. We report the values of [M/H] in Table 6.

We decided also to compile all the metallicities

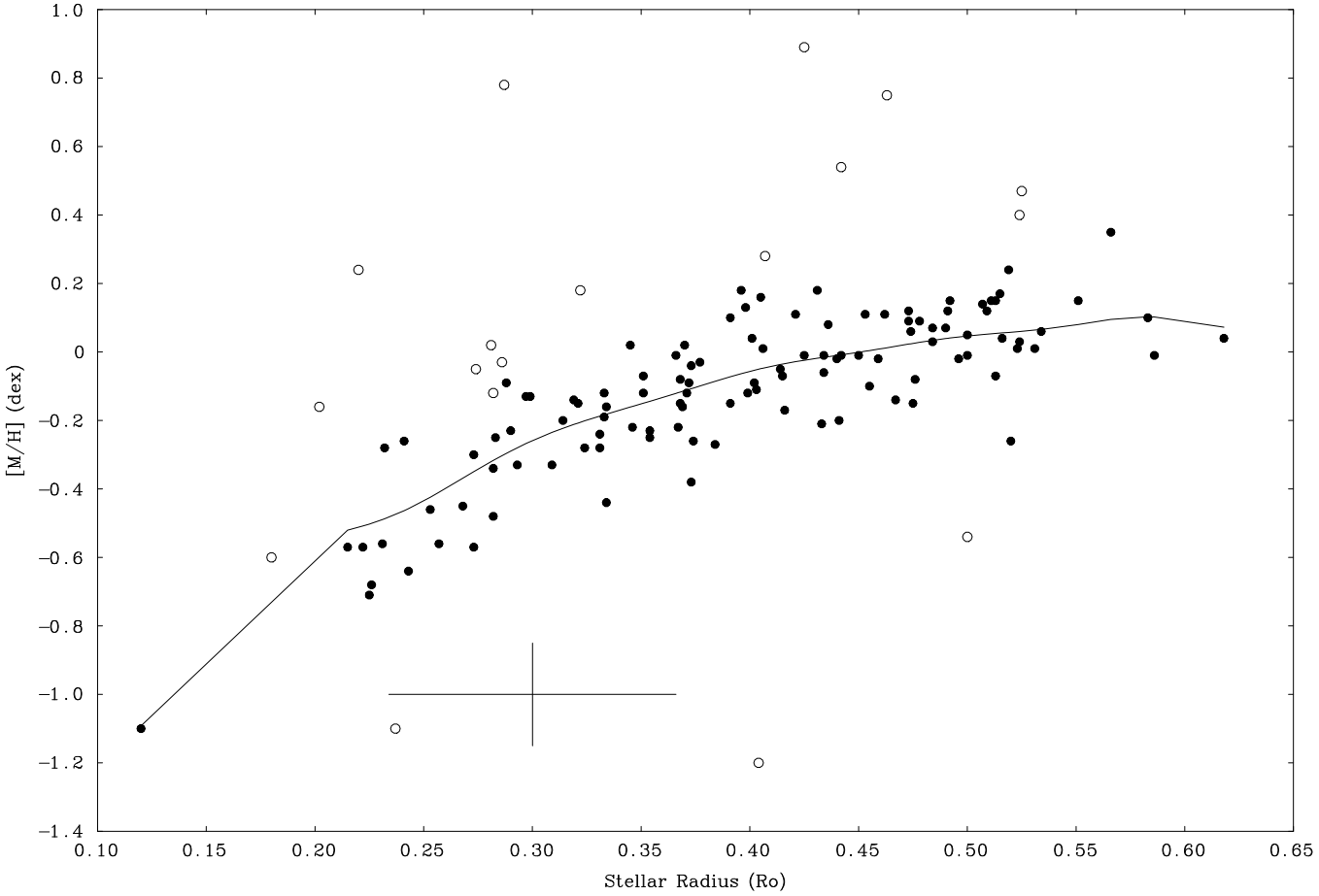

Fig. 4.— Correlation between [M/H] and stellar radius for stars with spectral sub-type dM3. The correlation is relatively tight as in dM2 stars (Paper VII) in spite of the relatively large error on the radius (error box). We can see that, as in dM2 and dK6 stars, the metallicity decreases with decreasing radius for a given $(R\text{-}I)_C$. We show some obvious outliers as open circles and the continuous line represents the data smoothed by a Gaussian.

published for our initial selection list of 395 dM4 stars, and try to obtain a metallicity-radius correlation for these stars. We found metallicities from the literature for 179 dM4 stars. We give these metallicities in Table 5. Our measures of [M/H] for our list of dM4 stars were collected from the following authors: Marsakov & Shevelev (1988), Ivanov et al. (2004), Ammons et al. (2006), Sanchez-Bazquez et al. (2006), Cenarro et al. (2007), Holmberg et al. (2009), Jenkins et al. (2009), Soubiran et al. (2010), Casagrande et al. (2011), Milone et al. (2011), Prugniel et al. (2011), Wu et al. (2011), Anderson & Francis (2012), Koleva & Vazdekis (2012), Rojas-Ayala et al. (2012), Kordopatis et al. (2013), Mann et al. (2013), Pace (2013), Gaidos et al. (2014), Gomez da Silva et al. (2014), Newton et al. (2014), Mann et al. (2015). We show the empirical relationship between [M/H] and stellar radius for stars with spectral sub-type dM4 in Fig. 5.

The correlation is not as tight as in dM2 stars or dM3 stars, particularly for small radii where the scatter is large (about ±0.5 dex). We have no simple explanation for this relatively large scatter at this stage. We also note that the mean of the data (continuous line) is rather flat and stands at [M/H] of about 0 dex over a large range of radii. This was not the case for dK6, dM2 and dM3 stars for which [M/H] starts to diminish more rapidly at small radii. In Fig. 5, we show some obvious outliers as open circles and the continuous line represents the data smoothed by a Gaussian. Also, for dM4 stars, the minimum values of [M/H] do not fall below -0.5 dex for the smoothed curve even for the smallest radii which questions the presence of subdwarfs in our sample, in spite of the fact that individual measures of [M/H] include about ten stars below -0.5 dex (Table 7). We give the [M/H] values from the smoothed data in Table 7.

4. Rotation of the dK6 stars

In view of the inhomogeneity of our sample of 105 late K dwarfs, that include severall K4, K5 and K6 dwarfs and a few K7 dwarfs, we selected a sub-sample of stars from K5.7 to K7.3, i.e. an effective temperature of 4226±110 K. For this sub-sample of K6 dwarfs, it is possible to intercompare the spectra and identify rotational broadening effects in the absorption lines. The profiles of the photospheric lines depend on three main four parameters; rotational broadening, microturbulence, macro-turbulence and Zeeman broadening. Micro and macro turbulence (typically of order 1 $km\ s^{-1}$) are not expected to vary much among our sub-sample of dK6 stars. Metallicity plays a role in the line strengths but not on macro- and/or micro-turbulence. The molecular lines we use for our cross-correlations have Landé factors that are generally lower than those of atomic spectral lines (e.g. Afram & Berdyugina 2015). Only two well defined molecular bands have larger Landé factors (e.g. Reiners & Basri 2006): TiO at 7050Å, and FeH at 9900Å. For high activity stars, the Zeeman broadening effect could be significant even for small Landé factors. But considering the large $v \sin i$ for these stars ($6-18\ km\ s^{-1}$), the Zeeman broadening effect should be completely negligible.

In order to extract rotational information, we carefully selected the spectral domain that we used for the cross-correlations: in Paper XIV, in our study of dM2 stars, we chose a 125Å wide spectral domain between 5460Å and 5585Å. Here, in order to obtain cleaner cross-correlation functions for dK6 stars, trial and error has led us to prefer a 120Å wide spectral domain between 5730Å and 5850Å. In this latter domain there are fewer weak and unsaturated narrow spectral lines that yield clean cross-correlation functions as far as the cross-correlation background is concerned (see Sect. 5). Unfortunately, in the present study, we cannot exploit spectral lines in molecular bands at the red end of the spectrum (such as we could do for dM3 and dM4 stars): in the warmer dK6 stars, the bands are not strong enough to be useful. This is unfortunate, since molecular bands give the bests results for the cross-correlations (see Paper XVII, HM). As we shall see below, the noise in the background is central to reaching the highest precision in the $v \sin i$ measurements. We show in Fig. 6 the spectral domain we have chosen for our rotational analysis of dK6 stars, using as an example the star Gl 798: this star, with $m_V = 8.82$, is neither the brightest nor the faintest star in our sample, which ranges from $m_V = 7.87$ to 11.80. In Fig. 6, the level of the continuum has been normalised to 1.

For each star in our sample, we cross-correlated the spectra with themselves in order to identify at

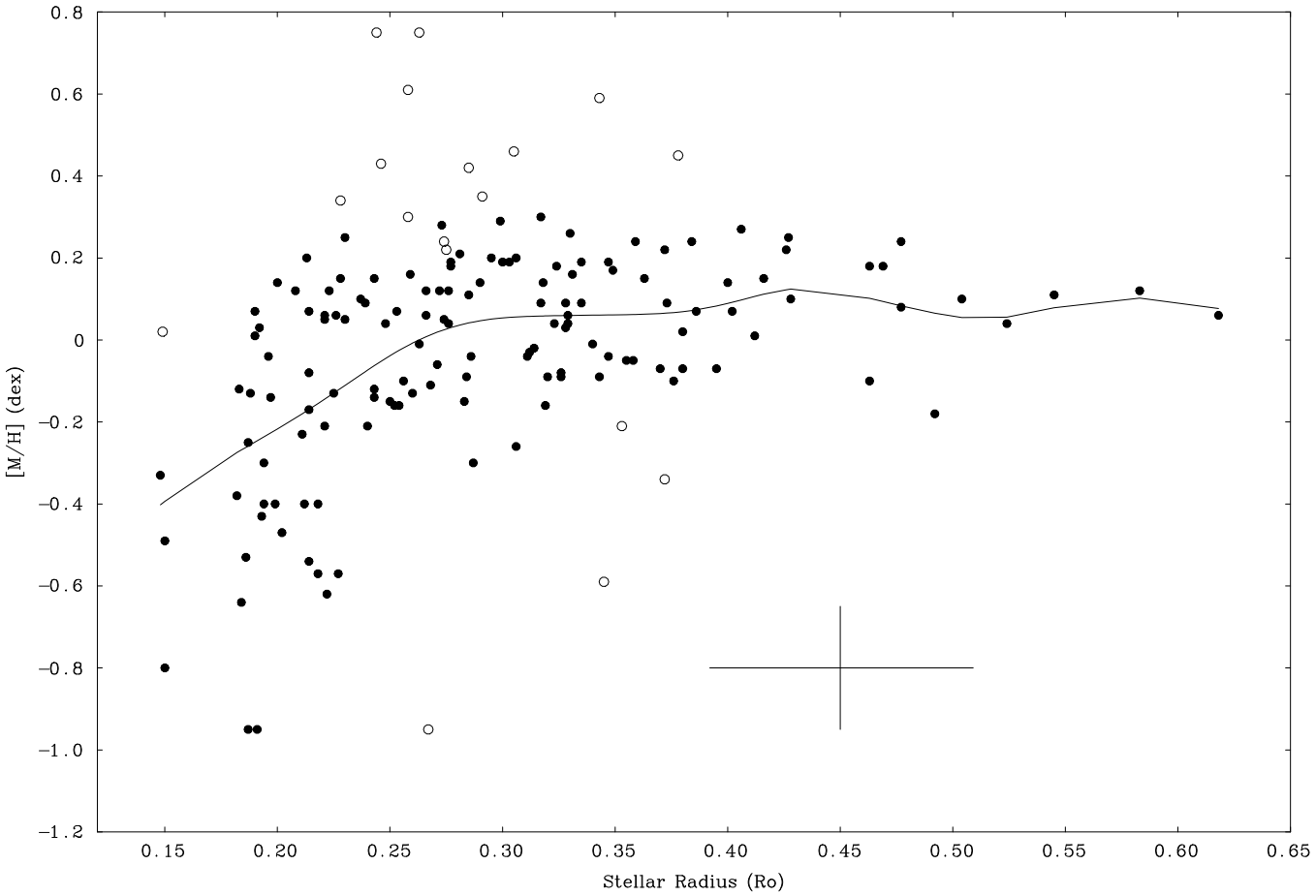

Fig. 5.— Correlation between [M/H] and stellar radius R_* for stars with spectral sub-type dM4. The open circles are outliers that were not included in the smoothing of the data (solid line).

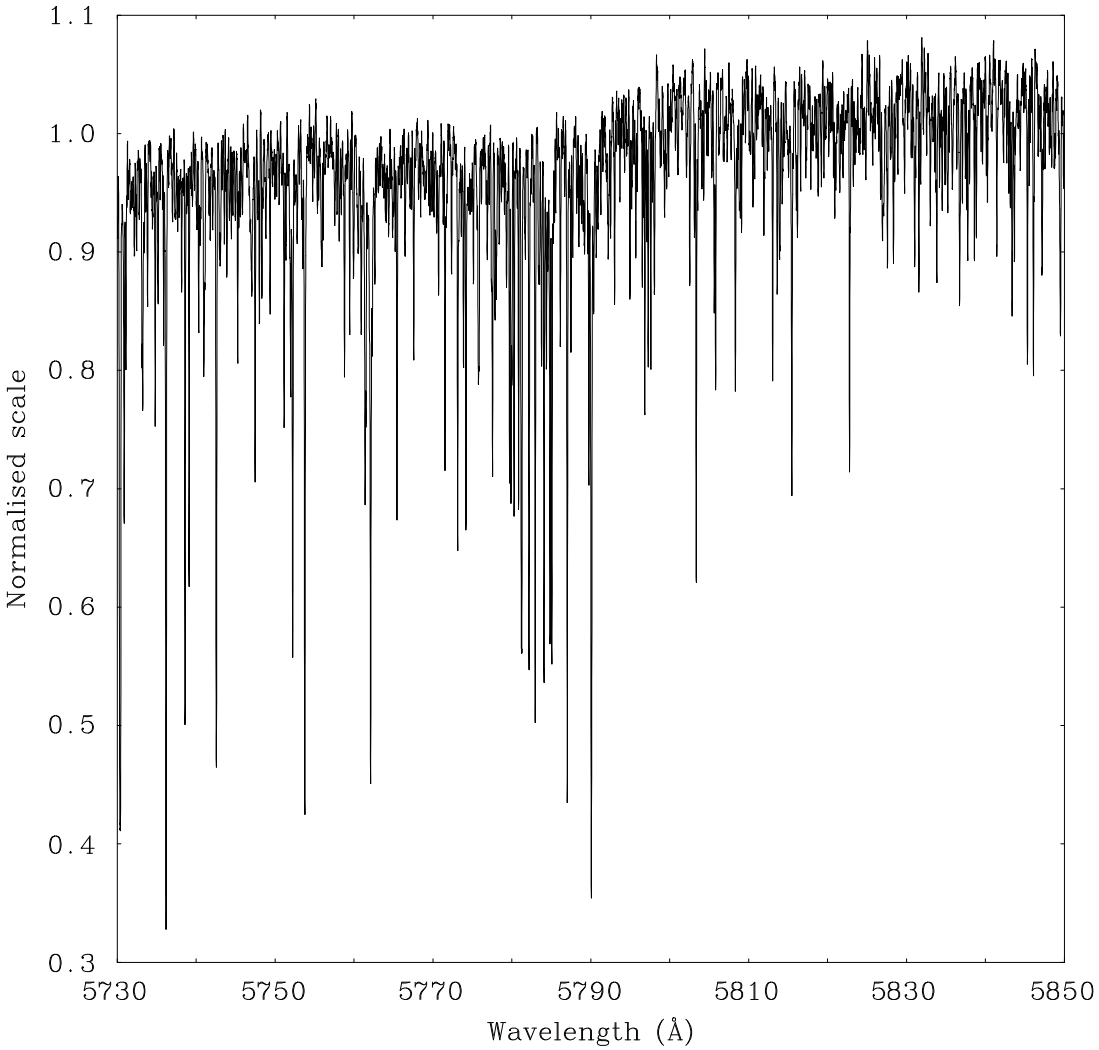

Fig. 6.— A portion of the wavelength range used for our cross-correlation analysis of the late-K dwarf Gl 798: 5730Å-5850Å. This range yields very clean cross-correlation profiles for late-K dwarfs. For Gl 798, the S/N ratio is ≈ 380: the variations in the spectrum near the continuum level are actually numerous blended weak absorption lines, each of which contributes to the cross-correlation function for this star.

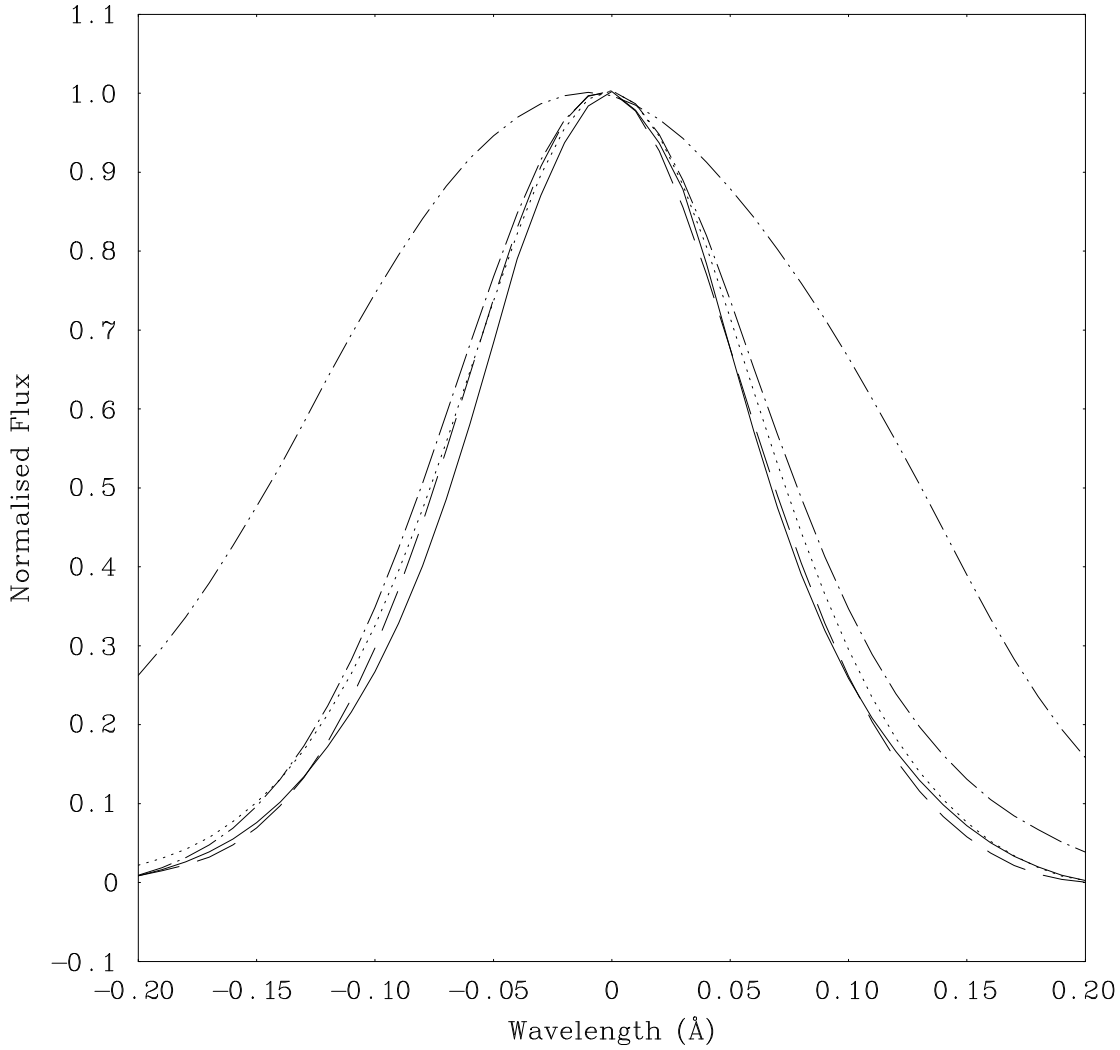

Fig. 7.— Examples of cross-correlation functions obtained from our analysis of HARPS spectra of 5 late-K dwarfs in our sample: Gl 57 (0 $km\ s^{-1}$), GJ 9299 (1.78 $km\ s^{-1}$), GJ 9714 (2.51 $km\ s^{-1}$), Gl 425B (3.35 $km\ s^{-1}$) and Gl 517 (9.77 $km\ s^{-1}$) (from narrowest to broadest). The FWHM of the peak for any particular star (in units of Å) is used to determine the value of $v \sin i$ for that star.

first our "zero-rotation" template stars. For each spectral sub-type, we chose our templates empirically as the star with the lowest FWHM of the cross-correlation peak among the sample of stars at that sub-type. We found that the best template for our dK6 stars in the HARPS database is Gl 57 with a FWHM = 0.1236Å which corresponds to a Gaussian with a width of 6.40 $km\ s^{-1}$. This is slightly broader than the 0.1006Å FWHM (5.40 $km\ s^{-1}$) at 5585Å which we measured in HARPS spectra of dM2 stars, and slightly narrower than the 0.1455Å FWHM (7.54 $km\ s^{-1}$) at 5790Å which we measured for the dK4 stars. This is consistent with a decrease in the widths of photospheric lines as we go to later spectral type among K and M dwarfs. Gl 57 lies at the lower end of our selection range. Our mean effective temperature for this star is 4040 K which implies a spectral type of K7.1. Our PCA based inversion for this star gives a temperature of 4030 K which yields also a spectral type K7.1. We trust more the effective temperatures than the $(R\text{-}I)_C$ colour because for the late K dwarfs, T_{eff} may vary a lot for a given $(R\text{-}I)_C$, because the gradient of T_{eff} versus $(R\text{-}I)_C$ increases a lot in late K dwarfs (see Fig. 1). Therefore, Gl 57 appears to agree with our selection of dK6 stars. We emphasize, that during the course of this study we also investigated the cross-correlation with Gl 847A, a low $v \sin i$ star with a somewhat higher effective temperature ($(R\text{-}I)_C$=0.761 and T_{eff}=4110 K) and earlier spectral type (K6.7). But finally we found little differences in the $v \sin i$ measures between these two templates. We therefore conclude that Gl 57 is a reliable template although it has a bit lower effective temperature than the rest of the sample.

In SOPHIE spectra, we found that Gl 728, has the narrowest cross-correlation function: we used that as our template spectrum in analyzing SOPHIE spectra. Note that the cross-correlation of Gl 116 with Gl 728 yields a FWHM of 0.1583Å that is a bit narrower than the self cross-correlation function of Gl 728 with itself (0.1611Å). The cross-correlation of Gl 116 with itself yields a FWHM of 0.1475Å that is significantly smaller than those of most other dK6 stars. We believe this star has a later spectral type than dK6.

We show in Fig. 7 the cross-correlation profiles obtained with HARPS observations for 5 late-K dwarfs in our sample: Gl 57 (0 kms^{-1}), GJ 9299 (1.78 $km\ s^{-1}$), GJ 9714 (2.51 $km\ s^{-1}$), Gl 425B (3.35 $km\ s^{-1}$) and Gl 517 (9.77 $km\ s^{-1}$) (from narrowest to broadest). The FWHM of the peak for any particular star (in units of Å) is used to determine the value of $v \sin i$ for that star. In order to measure the FWHM of the cross-correlation functions, we measured the background level on each side of the cross-correlation functions: then we subtracted the linear interpolation of this background, and normalized the functions. This ensures that we isolate only the cross-correlation profiles in our results, with little influence of the background. We then measured directly the FWHM from the profiles. We note that we have very high S/N ratios (typically severall hundreds) and a good sampling for the cross-correlation functions (0.01Å).

As in our previous papers, we take into account limb-darkening effects before we can derive significant $v \sin i$ measures for our rotators. We computed synthetic rotational profiles that include limb darkening. The synthetic profiles were computed according to the formulation of Gray (1988) with the center to limb darkening after Claret (2000). We computed synthetic profiles for the following range of $v \sin i$ values (in $km\ s^{-1}$): 0.05, 0.25, 0.50, 0.75, 1.00, 1.50, 2.00, 3.00, 4.0, 5.0, 7.0, and 10.0.

We convolve our cross-correlation functions of our template stars (Gl 57 for HARPS and Gl 728 for SOPHIE) with our rotational profiles. The FWHM of Gl 57 is 0.1236Å (6.40 kms^{-1}) and for Gl 728 it is 0.1611Å (8.35 kms^{-1}). Some of the cross-correlation profiles of Gl 57 convolved with our theoretical rotational profiles are shown in Fig. 8 in order of increasing FWHM: 0, 1.0, 2.0, 3.0,4.0, 5.0, 7.0, and 10.0 kms^{-1}. One can see in this figure that the cross-correlation profile broadened at 1.0 kms^{-1} is clearly distinguishable from the unbroadened cross-correlation profile of Gl 57 (solid line).

We measured the FWHM of the rotational profiles and show these measurements as a function of the theoretical $v \sin i$ in Fig. 9 for HARPS and SOPHIE. We use this diagram to derive $v \sin i$ values from the direct FWHM measures. In general, the correct $v \sin i$ values are smaller than the corresponding FWHM values assuming a Gaussian profile.

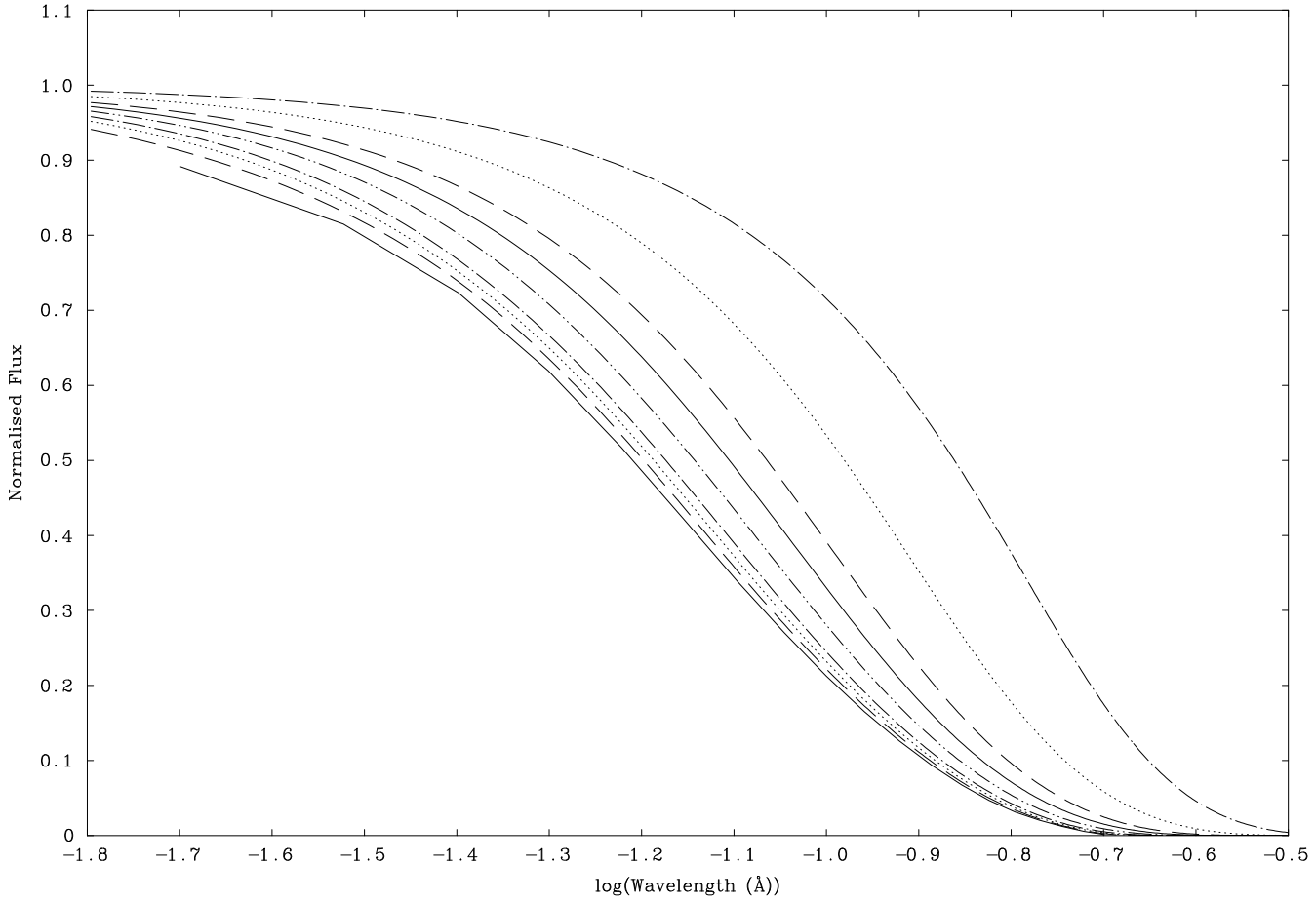

Fig. 8.— The cross-correlation profile of Gl 57 convolved with our theoretical rotational profiles. In order of increasing FWHM: 0, 1.0, 2.0, 3.0, 4.0, 5.0, 7.0, and 10.0 $km\ s^{-1}$. One can see in this figure that the cross-correlation profile broadened at 1.0 kms^{-1} is clearly distinguishable from the unbroadened cross-correlation profile of Gl 57 (solid line).

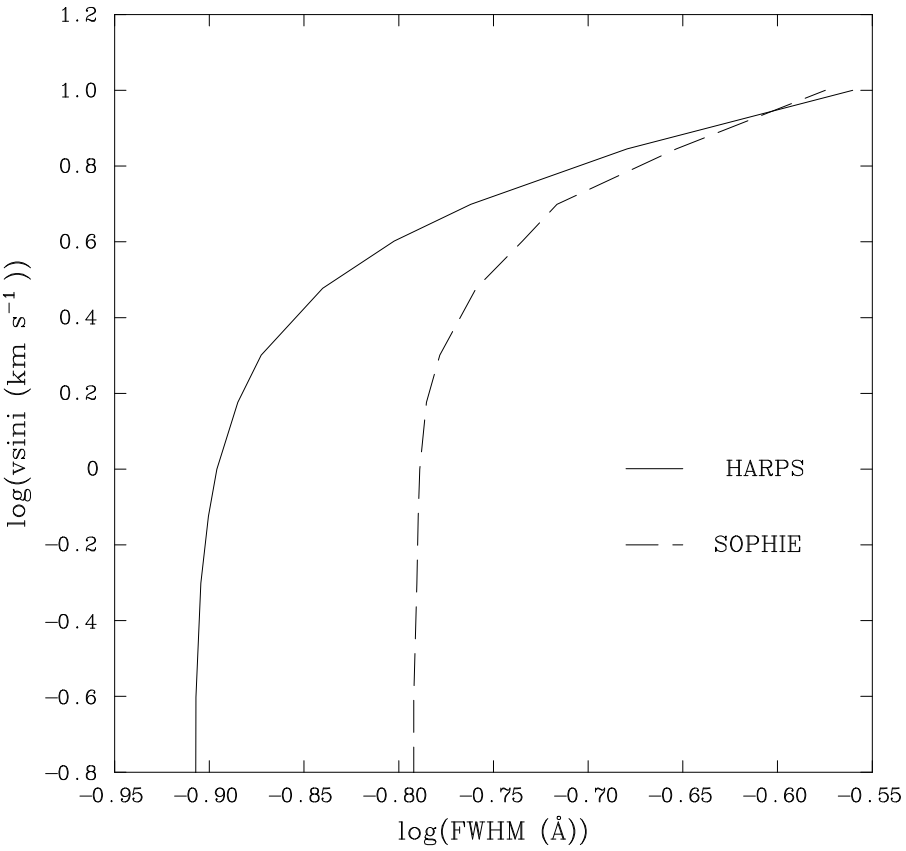

Fig. 9.— The true $v \sin i$ (in $km\ s^{-1}$) as a function of the measured FWHM (in Å) of the cross-correlation peak. These curves are used to compute a star's $v \sin i$ from HARPS (continuous line) and SOPHIE (dashed line) measurements of FWHM. The typical uncertainty on these curves is ±0.005Å on the X-axis.

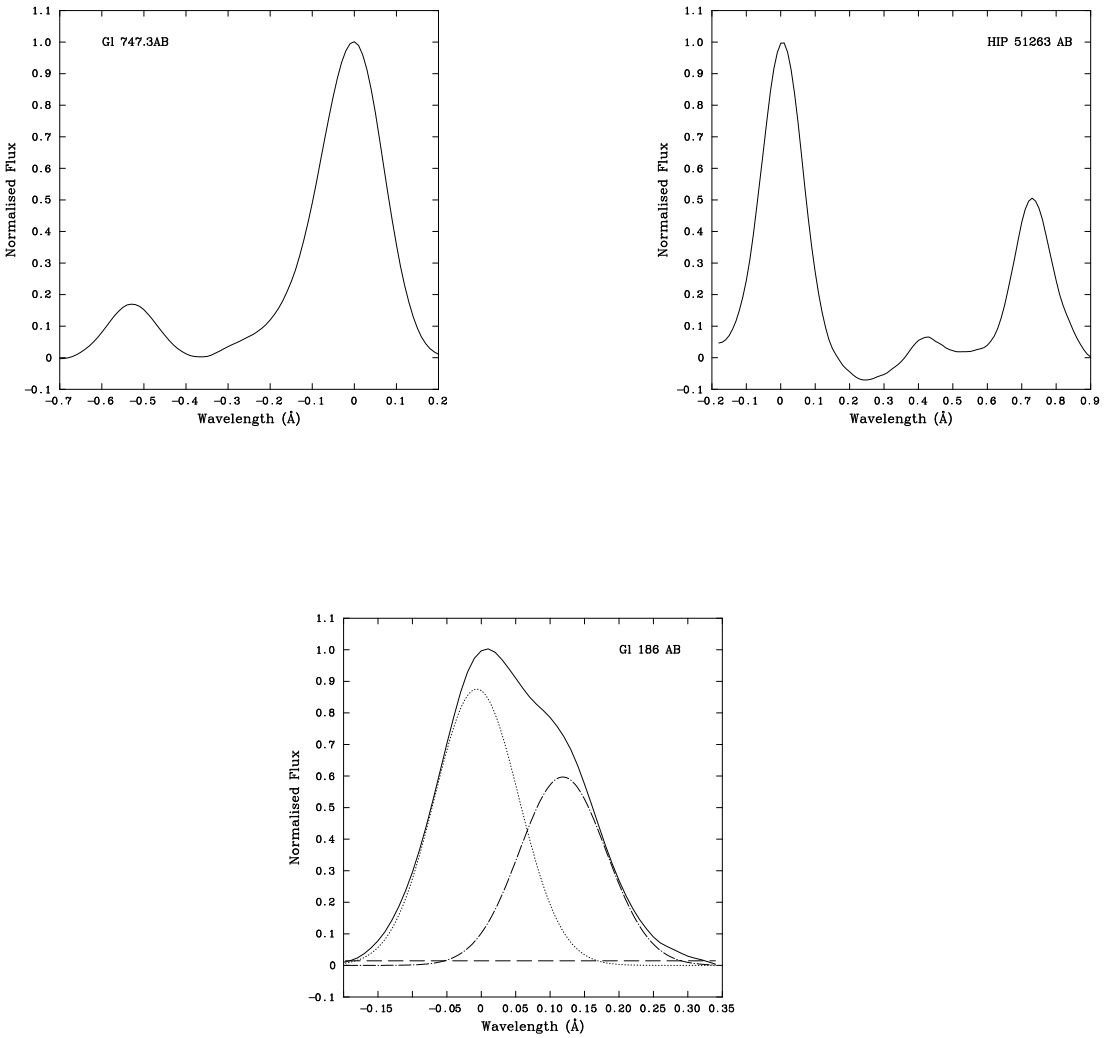

Fig. 10.— Cross-correlation functions for three spectroscopic binaries in our late-K dwarf sample: Gl 186AB, Gl 747.3AB and HIP 51263AB. For two of these binaries, the two components are well separated and we do not need to use multi-Gaussian fits in our analysis. Moreover, in these two cases, the secondary is an M dwarf of later spectral type, and as a result is considerably fainter than the primary. In the case of Gl 186AB we analyzed this system using multi-Gaussian fit to the cross-correlation function. We illustrate the best fit (superposed) as well as the profiles of the individual components.

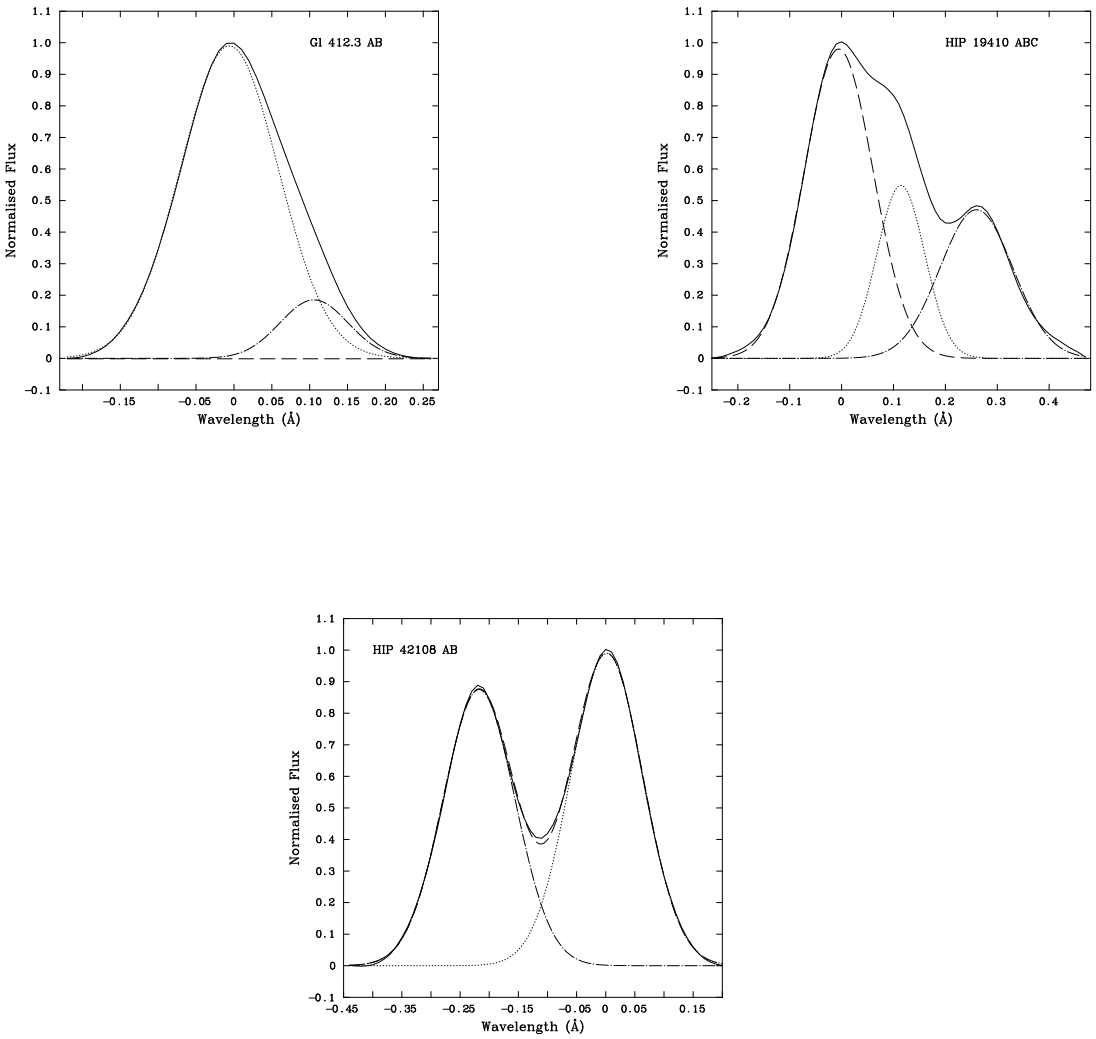

Fig. 11.— Cross-correlation functions for two spectroscopic binaries and one triple system in our late-K dwarf sample: Gl 412.3AB, HIP 19410ABC, and HIP 42108AB. We analyzed these systems using multi-Gaussian fits to the cross-correlation functions. In each figure we illustrate the best fit (superposed) as well as the profiles of the individual components.

In Table 7, we list the values we have derived for $v \sin i$ for our late K dwarfs. Rotation was detected in most of our sample (92 stars), with $v \sin i$ typically in the range 1.0-3.5 $km\ s^{-1}$.

With HARPS, we also observed a few stars of particular interest; five spectroscopic binaries (Gl 186AB, Gl 412.3AB, Gl 747.3AB, HIP 42108AB, HIP 51263AB) and one spectroscopic triple system (HIP 19410ABC). For two of these stars, the components are well separated (Gl 747.3AB and HIP 51263AB). We show their cross-correlation profiles in Fig. 10. One can see that in both cases the secondary peak is much weaker than the primary peak. This indicates that the secondary has a later spectral type than that of the primary. For these two spectroscopic binaries, we proceeded as in the case of single stars, i.e., we measured the FWHM directly from the correlation profiles. For the other stars, the two or three components are blended. In these cases we applied multi-Gaussian fits to the cross-correlation profiles. We show these profiles in Fig. 11 together with the fits and the profiles of each component.

In the case of Gl 186AB, the secondary is significantly weaker than the primary. It is therefore most likely not a late K dwarf. The same applies to the secondary and tertiary components of HIP 19410. On the contrary, the primary and secondary components of HIP 42108AB have almost the same intensity. In this case, we assume that both components are late K dwarfs. Note, the relatively good fits that we obtain with multi-Gaussians. We give the FWHM of the cross-correlation peaks for all these stars in Table 7 together with the uncertainties on the fits.

We would like to emphasize that a few of the active stars in our dK6 stellar sample are candidate young stars that may not yet have contracted to the Main- Sequence (MS). A reliable way to idendify the (few) Pre-Main-Sequence (PMS) stars in our samples is the stellar radius: the fact is, that PMS stars that have not yet contracted to the MS have abnormally large radii. We identified three such stars in our dK6 sample: GJ 1177A, GJ 182 and GJ 425B as possible PMS stars (see Table 1). Of these, Gl 425B is a rather low activity star. As such, the abnormally large radius for this star is probably due to binarity. Nevertheless, we shall find (in Paper II) that these stars *do correlate well with the MS stars in the Rotation-Activity Correlation* (RAC). In our M2 sample (see Table 3), we have identified also two PMS stars: GJ 1264 and GJ 803. But again, as we shall see in Paper II, these PMS stars do correlate very well with the other MS stars in the context of the RAC. In our M3 sample, GJ 277A is a possible PMS star (Table 4). In our M4 sample, GJ 2069A, GJ 3322, GJ 4185A, GJ 4338B, GJ 669A, and GJ 812A are possible PMS stars according to their radii (Table 5). *We emphasize that all these stars do not rotate especially fast. There are many MS stars that rotate faster.* These PMS stars are supposed actually to spin up as they contract to the MS, and young MS stars are supposed to be the fastest rotators (e.g. Barnes 2003). That is what we actually observe in our samples of stars: Young MS stars are the fastest rotators (e.g. among our M4 sample; GJ 3631, GJ 3789, GJ 4020B, GJ 4338B, GJ 431, GJ 630.1, GJ 791.2A) with $v \sin i$ in excess of 15 $km\ s^{-1}$ and up to 56 $km\ s^{-1}$.

All our RACs will turn out (in Paper II) to demonstrate that PMS stars do not depart significantly from the overall RAC's of the MS stars with the same spectral sub-type. Numerous previous studies also found similar results: e.g. Mamajek & Hillebrand (2008), Browning et al. (2010), Christian et al. (2011), West et al. (2015). This finding is rather intriguing since PMS stars may have internal structures which are different from MS stars: some PMS stars may even be fully convective. More investigation is required to confirm this result, but so far, in our samples, we found no evidence that PMS stars obey significantly different RACs from those of MS stars (see Paper II).

5. Sources of uncertainty in the measures

For dM2 stars (Paper XIV), we showed that, by using four different spectrographs and the results from other authors, it was possible to attain a detection limit of 1 $km\ s^{-1}$ in $v \sin i$, with a precision of about 0.3 $km\ s^{-1}$. This empirical analysis includes all sources of uncertainties on the measures.

In the present study, as was the case for our dM2 stars, our cross-correlation profiles have a very high S/N ratio (several hundreds, see Fig. 7). This is due to the fact that many spectral lines enter into our calculation of the cross-correlations. It is therefore in theory possible to measure subtle differences between different cross-correlation

profiles of only a few percent. However, as in the case of dM2 stars (mentioned above) as well in the case of dM3 stars (see HM), the greatest uncertainty arises from the background of the cross-correlation functions. There are secondary peaks in the cross-correlation function backgrounds and this represents a problem in defining the zero level. In fact, these secondary features repeat in all of our cross-correlations because all of our stars have quite similar spectral types. For dK6 stars, we found that the noise in the background is a bit greater than that of dM2 and especially dM3 stars. This is due to the nature of the spectral range we use for the cross-correlations. In dM3 stars, there are hundreds of narrow spectral lines present in the spectrum, and these lines are evenly distributed across the selected wavelength range. However, for dK6 stars, the spectral lines are stronger, and there are fewer of them within our selected wavelength range. This results in a larger background noise when we calculate the cross-correlation functions.

In order to assess the noise in the background from one star to another, we averaged the backgrounds, after normalisation of the cross-correlation peaks, of four stars: Gl 45, Gl 57, Gl 162.2 and Gl 425B. We then subtracted this average background to the raw cross-correlation profiles: the resulting profiles and remaining background fluctuations are shown in Fig. 12. One can notice some differences in the broadenings of the cross-correlation functions, Gl 57, Gl 45, Gl 162.2, Gl 425B, but also some variations in the cross-correlation backgrounds. This gives us a direct estimate of the typical background "noise". This noise (i.e. the secondary peaks) has an amplitude of about $\pm 3\sigma$ =3% of the main peak (Fig. 12). The noise level in the dK6 analysis implies an uncertainty of 3σ=0.0028Å in the FWHM, i.e., $3\sigma = 0.40 km\ s^{-1}$ on $v \sin i$ for HARPS spectra for $v \sin i = 2 km\ s^{-1}$. For SOPHIE spectra we have an uncertainty of about 3σ=0.0034Å. However, these uncertainties on the FWHM yield a variable uncertainty on $v \sin i$ depending on where the data fall relative to the curves in Fig. 9. Indeed, because the curves in Fig. 9 are significantly steeper at small FWHM, the uncertainty in $v \sin i$ increases, the smaller the value of $v \sin i$. The curves in Fig. 9 show that $v \sin i$ is not detected within $\pm 3\sigma$ below 0.88 $km\ s^{-1}$ for HARPS and 1.67 $km\ s^{-1}$ for SOPHIE.

In order to further assess the precision of our measurements from our cross-correlations, we plot in Fig. 13 the values of $v \sin i$ obtained from the PCA-based inversion of the stellar parameters (Sect. 3.1) versus the values of $v \sin i$ measured from our cross-correlations: the agreement between the results from these two independent methods is reasonable if one considers the relatively high uncertainty from the PCA-based inversion method (1.5 $km\ s^{-1}$). We find that the mean of the differences between the two sets of measures is only 0.633 $km\ s^{-1}$. The standard deviation of the differences in this set of measurements compared to the one-to-one relationship (see Fig. 13) is $\sigma = 0.421 km\ s^{-1}$. This means that the typical 3σ uncertainty for these measures is $1.263 km\ s^{-1}$. This is better than the expected uncertainty of the PCA-based inversion method (1.5 $km\ s^{-1}$, see Sect. 3.1).

We searched the literature for other $v \sin i$ or rotational period P measurements for our K6, M2, M3 and M4 targets (we used the tutorial developed by Paletou & Zolotukhin 2014[4]). We found several measurements of $v \sin i$ (Vogt et al. 1983, Marcy & Chen 1992, Tokovinin 1992, Favata et al. 1995, Delfosse et al. 1998, Mohanty & Basri 2003, Nordstrom et al. 2004, Glebocki & Gnacinski 2005, Torres et al. 2006, Schroder et al. 2009, Jenkins et al. 2009, Martínez-Arnáiz et al. 2010) and P (Pizzolato et al. 2003, Kiraga & Stepień 2007, Irwin et al. 2011). In cases where a rotation period P was reported in the above papers, we derived the $v \sin i$ from P assuming $\sin i = 1$.

We show in Fig. 14 our results for $v \sin i$ versus the results from other spectrographs (e.g. SOPHIE as a function of HARPS [Paper XIV, HM], 19 measurements in total) and the measurements from other authors (73 measurements). Filled circles denote results obtained for dK6 stars in this paper. The overall agreement between our measures and those of other authors is good. The agreement goes down to $v \sin i$ as low as 0.5 $km\ s^{-1}$. For results below 1 $km\ s^{-1}$ we have 13 data points. For these points, the mean difference between our results and others is found to be 0.37 $km\ s^{-1}$. The standard deviation of the differences in this set of measurements com-

[4] http://www.astropy.org/

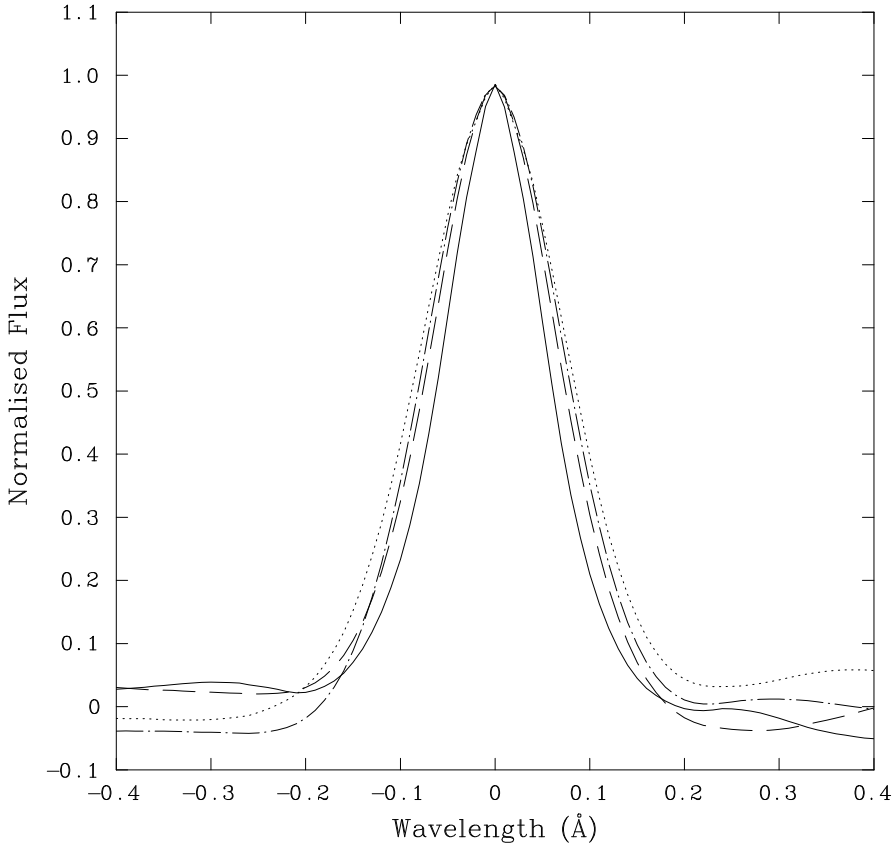

Fig. 12.— The cross-correlation profiles and the variations in the background continuum for four late-K dwarfs: Gl 57 (solid line), Gl 45 (dashed line), Gl 162.2 (dot-dashed line) and Gl 425B (dotted line). This diagram illustrates what are the variations in the background continuum from one star to another, and yields an estimate of the error on the FWHM measurements of the cross-correlation peaks.

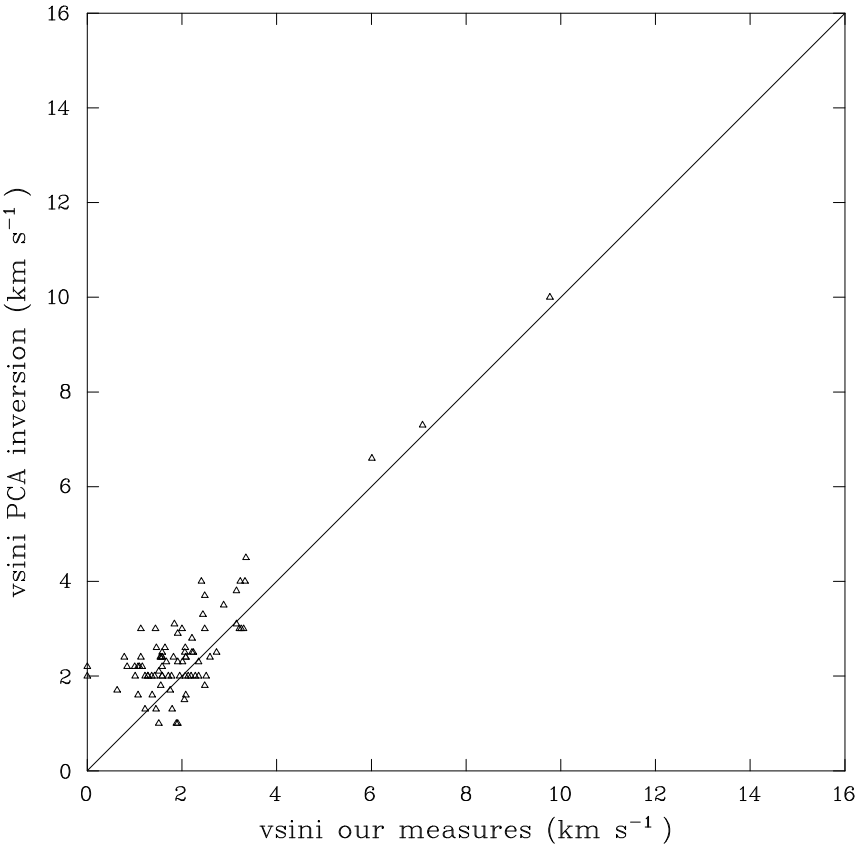

Fig. 13.— Comparison between our cross-correlation results for $v \sin i$ (x-axis) and results from our PCA-based inversion of the stellar parameters (Sect. 3.1) (y-axis). The solid line indicates the one-to-one relation. Differences between the two independent methods do not exceed 0.63 $km\ s^{-1}$ in average.

pared to the one-to-one relationship (see Fig. 14) is $\sigma = 0.27km\ s^{-1}$. This means that the typical 3σ uncertainty for this sub-set of measures is only $0.81km\ s^{-1}$.

For the slow rotators, i.e. for dK6, dM2, dM3 and dM4 stars (with no evidence for emission in H_α), the mean of the differences between our $v \sin i$ results and those reported by other authors is only $0.50\ km\ s^{-1}$. The standard deviation of the differences in this set of measurements compared to the one-to-one relationship is $\sigma = 0.32km\ s^{-1}$. This means that the typical 3σ uncertainty for the slow rotators is only $0.96km\ s^{-1}$. These figures are lower than the ones we derived from the uncertainties arising from features in the background of the cross-correlations (see above and HM). This indicates that the uncertainty on our $v \sin i$ measures when using the cross-correlation technique depends essentially on the S/N ratio in the cross-correlation peaks, and that the effects of the uncertainties on the background continuum have been overestimated. Therefore, the uncertainties on $v \sin i$ and $P/\sin i$ derived in Table 7 are only safe upper limits. These results confirm that both HARPS and SOPHIE are very stable instruments on the long-term: therefore, our spectra are well suited for reliable measurements of small rotational broadenings in K and M dwarfs.

For the fast rotators, i.e. for dK6e, dM2e, dM3e and dM4e stars (with clear evidence for emission in H_α), the mean of the difference between our $v \sin i$ results and those reported by others is $0.99\ km\ s^{-1}$. The standard deviation of the differences in this set of measurements compared to the one-to-one relationship is $\sigma = 0.60km\ s^{-1}$. This means that the typical 3σ uncertainty for the fast rotators is about $1.80km\ s^{-1}$. This uncertainty is about twice larger than for the slow rotators. This is probably due to the presence of large spots on the surface of these stars.

The reason why we can attain precisions in $v \sin i$ as good as those mentioned above is that we have paid attention to several factors in our analysis. (i) The choice of the wavelength interval is crucial in obtaining cross-correlation profiles where the S/N is high, and the background noise is as low as possible. (ii) The method of subtracting the background noise is essential in order to recover with the highest precision the true cross-correlation profiles. (iii) The spectra which we selected for analysis are mostly high S/N ratio spectra, and were all reduced with an identical automated technique. (iv) We use only spectrographs that are very stable in radial velocity and that use image scramblers to avoid seeing effects on the FWHM of the spectral lines. By combining these factors, we have found that it is possible to measure subtle differences between different cross-correlation profiles at the level of as little as a few percent.

6. The distributions of rotational periods among M and K dwarfs

We derived the projected rotation periods $P/\sin i$ for all our dK6 targets according to the $v \sin i$ results in Table 7 and the radii given in Table 1. Values of $P/\sin i$ are given in Table 7 for our dK6 target stars, along with their uncertainties.

We show in Fig. 12 the histogram of $P/\sin i$ values for dK6 stars, together with the analogous results for dM2 stars (upper panel). Also shown are the histograms of $P/\sin i$ values for dM3 and dM4 stars (lower panel). We see that the peak of the distribution for dK6 stars lies at a mean projected period in the range 13-22 days. We also see that the longest $P/\sin i$ that we have detected for dK6 stars is 30-35 days (see Fig. 15): these longest periods overlap with the range of upper limits ($\sim$33-66 days) which were estimated in Sect. 1 above, given the limitations ($0.5\text{-}1km\ s^{-1}$) on measuring $v\ sini$.

The histogram for dK6 stars in Fig. 15 has a different shape from that of dM2 stars, in spite of their relatively close spectral types. In dM2 stars, in addition to a main peak at about 11 days, there may be a second (smaller) peak at shorter periods (4 days): if these two peaks are really distinct, we could refer to them as belonging to slow and fast rotators respectively, with more slow rotators than fast. Among the dK6 sample, there is also an analogue of a short-period peak at about 3-7 days. In dM2 stars the distribution among the slow rotators is compact, extending to periods no larger than 16-20 days, whereas in dK6 stars, the distribution is more spread out, extending to 25 days. The distribution for dM4 stars is not bimodal as in dM2 and dK6 stars. For dM4 stars, there is a hint that there are more fast rotators than slow rotators. For dM3 stars, our dataset suggests that the distribution is also bimodal, with two distinct

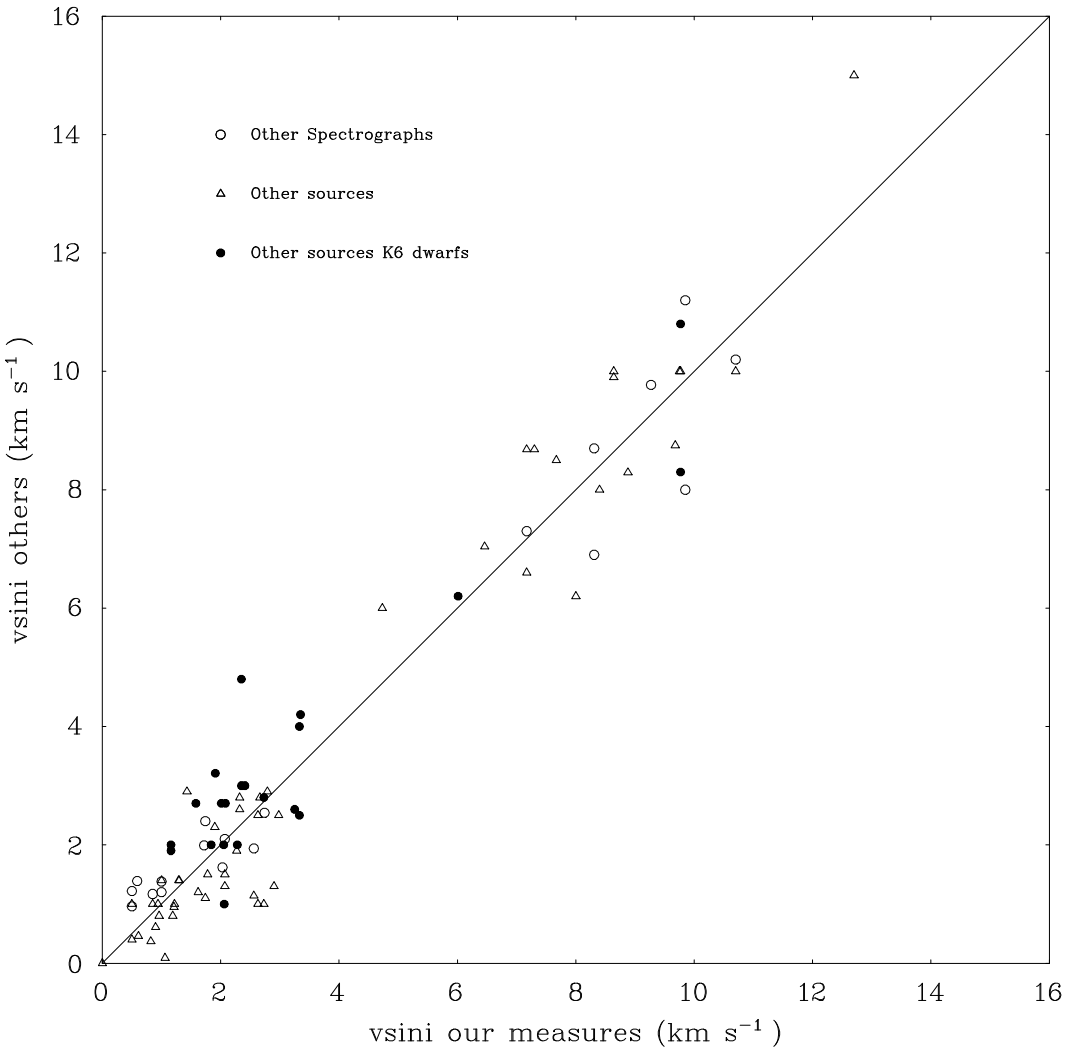

Fig. 14.— Comparison between our results for $v \sin i$ (x-axis) and results from other authors (y-axis). We show the K6 dwarf measurements of other sources as a function of the present measurements as filled circles. Included in the plot are data for all of our samples of M dwarfs (including sub-types K6, M2, M3 and M4). The solid line indicates the one-to-one relation. Differences between our results and the others do not exceed 0.50 $km\ s^{-1}$ in average for the low activity stars.

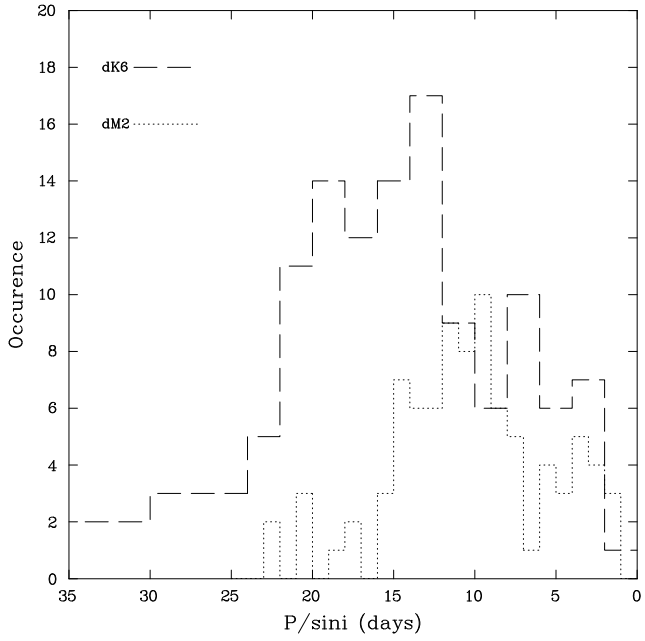

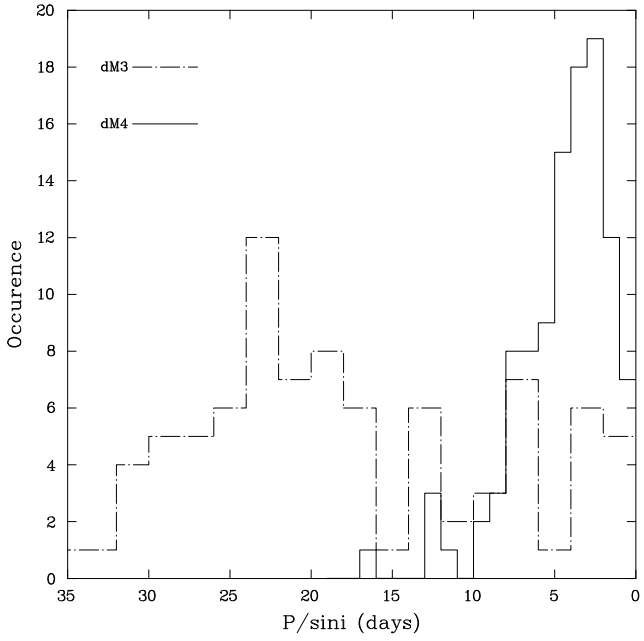

Fig. 15.— Histograms of stars as a function of $P/\sin i$ for dK6 stars, dM2 stars, dM3 stars and dM4 stars. The peak of the distribution shifts from (about) 17 days for dK6 stars, to 10 days for dM2 stars, and to 3

groups of slow and fast rotators.

The principal conclusion which we draw from the two panels in Fig. 15 is that there appears to be a global shift of the distributions from dK6 stars to dM4 stars. Specifically, mid-M dwarfs rotate in general faster than early M dwarfs, a fact already well established among M dwarfs. The differences between the 4 histograms in Fig. 15 indicate the value of selecting stars in narrowly restricted spectral sub-types: this selection suggests that different sub-types among the M dwarfs may exhibit distinctive rotational properties. Finally, we note that the mean period of the dK6 star histogram (17 days) is intermediate between the mean period of the dM2 star histogram (11 days) and that of dK4 stars ($\approx$ 35 days, Paper XVI). This is an indication of the overall trend towards shorter rotation periods as we go from dK4 to dM4 (see HM).

Formally, we have calculated a mean value and a median value for each of the 4 histograms shown in Fig. 15. For dK6 stars, we find a mean of 15.8 days, and a median of 16.0 days. For dM2 stars, the mean and median are 10.8 days and 11.5 days respectively. For dM3 stars, the mean and median are 18.0 days and 20.5 days respectively. For dM4 stars, the mean and median are 4.9 days and 5.0 days respectively. Thus, whether we consider the mean period or the median period, we can state the following: as we go from dK6 to dM2 to dM4, there is a trend towards shorter periods. However, there is an exception to this trend at spectral subtype dM3: there, the mean/median period does not fit the trend, but is definitely longer than the dK6-dM2-dM4 trend would predict. In fact, the dM3 mean/median period is actually longer than the results for dK6. Thus, as already suggested by the smaller data set used by HM, the dM3 stars in our sample have markedly slower rotations than the trend between dK6 and dM4.

In HM, histograms were derived for $P/\sin i$ values among dM2 stars (85 targets), dM3 stars (80 targets), and dM4 stars (21 targets) (see Fig. 9 in HM). In the present paper, we have obtained a fourth histogram, for dK6 stars. Even a casual inspection shows that there are differences between the histograms (see Fig. 15). The question is: can a random distribution of inclination angles produce the 4 distributions, assuming the actual period distribution is the same for all three samples?

To address this, we have applied the Kolmogorov-Smirnov (K-S) two-sided test to each histogram in order to test the null hypothesis that the stars in any one sample are drawn from the same population as the stars in another sample. For any pair of samples, we construct the cumulative distributions F(1) and F(2) for periods ranging from 44 days to 1 day. Extracting numerical values for the K-S statistic $D(1,2)$, we find that when we compare a given distribution to the distribution of any other spectral sub-type, the null hypothesis (namely, that the distributions are drawn from the same population) is rejected at a confidence level which is better than 0.001%. This suggests that the $P/\sin i$ distribution (i.e. the rotational braking mechanism) in dM3 stars is controlled by different factors than in dM2 or dM4 stars. The K-S analysis also indicates that the dK6 stars have a distribution which differs significantly from those of the other dM spectral sub-types.

But in this regard, an anonymous referee has pointed out that histograms can suffer from slight distortions as a result of choices related to binning. In view of this, the referee suggests that, when comparing the rotational period distributions in Fig. 15, it may be more useful to compare smoothed continuous distributions, rather the raw histograms. Different possibilities are available for smoothing, e.g. kernel density estimates, splines, bezier... Here, the software package (gnuplot) which is available to one of the authors (DJM) offers bezier smoothing. Using this, the smoothed rotation distributions were used to construct cumulative distributions for all 4 spectral sub-types. For each pair of spectral sub-types, the K-S statistic $D(1,2)$ was extracted. The maximum value of $D(1,2)$, normalized by a factor which depends on the sizes of the two distributions which are being compared, leads to a coefficient $c(\alpha)$ which was found to have the following numerical values for various sample pairs: 5.067 (K6 versus M4), 4.623 (M3 versus M4), 3.602 (M2 versus M4), 2.901 (M2 versus M3), 2.201 (K6 versus M2), and 1.382 (K6 versus M3). Statistically speaking, values of $c(\alpha)$ in excess of 1.95 correspond to a probability α of less than 0.001 that a pair of distributions has been drawn from the same parent population. The above numerical results indicate that the rotational distributions of K6 and M3 stars (for which $c(\alpha) = 1.382$) *might* originate from the same population. But in the case of all the other

pairs (K6,M2), (K6,M4), (M2,M3), (M2,M4), and (M3,M4), the bezier smoothed distributions have a chance of less than 0.1% of being drawn from the same population. This suggests that the $P/\sin i$ distribution (which is determined by the rotational braking mechanism) in dM3 stars is controlled by different factors from those which operate in dM2 or dM4 stars, but that dK6 stars *might* have a similar braking mechanism to that in dM3 stars.

7. Conclusion

In this paper, we have derived numerical values of various parameters of K and M dwarfs in preparation for a follow-up study of RAC's (in a future Paper II). For M dwarfs, values of T_{eff} have been determined from the $(R\text{-}I)_C$ color using the empirical calibration of Mann et al. (2015). For late-K dwarfs, values of T_{eff} have been determined from the $(R\text{-}I)_C$ color using the calibration of Kenyon & Hartmann (1995). These determinations have led to values of T_{eff} for a total of 612 stars with spectral sub-types dK4, dK6, dM2, dM3 and dM4. In an independent approach, we have also determined several stellar parameters (T_{eff}, $log(g)$ and [M/H]) using the PCA-based inversion technique of Paletou et al. (2015a) for a sample of 105 late-K dwarfs. We also compile all effective temperatures from the literature for this sample of late-K dwarfs. Together with our determinations of T_{eff} from the $(R\text{-}I)_C$ color, this allows us to obtain reliable values of T_{eff} for our sample of late-K dwarfs. With values of T_{eff} available, we then derived the stellar radii for our sample of K-M dwarfs, based on parallax measurements from Hipparcos. We find that our radii agree well with the interferometric radii reported by Boyajian et al. (2012): in the T_{eff}-radius plane, we find that our estimates of radii are within 0.19%, 6.3%, 4.3% and 8.2% of the Boyajian results for our late-K, dM2, dM3 and dM4 stellar samples respectively.

We also propose empirical relationships between radius and metallicity for dK6, dM3 and dM4 stars, similar to that reported for dM2 stars by Houdebine (2011b). This allows us to derive metallicity for all our targets, and these will be used in Paper II to correct the RAC's for metallicity effects.

We present a cross-correlation analysis of HARPS and SOPHIE spectra of 105 late-K dwarfs, which has allowed us to detect $v \sin i$ in 92 of these stars. In combination with our previous $v \sin i$ measurements in M and K dwarfs (Papers VII, XIV, XVI, XVII, HM) and from the compilations of $v \sin i$ measurements from the literature for dK6, dM3 and dM4 stars, we now derive $P/\sin i$ measures for a sample of 418 K and M dwarfs. This allows us to investigate the distributions of $P/\sin i$ for each spectral sub-type separately. We find that the $P/\sin i$ distributions are statistically distinct from one spectral sub-type to another at a 99.9% confidence level. Therefore, if one wants to investigate certain properties of K and M dwarfs which are related to rotation (such as RAC's), it is important to consider the different spectral sub-types separately.

The parameters which we have derived in this paper for stars belonging to various spectral sub-types from dK4 to dM4 will be used as input in Paper II to construct separate RAC's for each spectral sub-type.

acknowledgements

This research has made use of the SIMBAD database, operated at CDS, Strasbourg, France. DJM is supported in part by the NASA Space Grant program. This research was based on data obtained from the ESO Science Archive Facility and the Observatoire de Haute Provence SOPHIE database. This research made use of Astropy[5], a community-developed core Python package for Astronomy (Astropy Collaboration, 2013)). This research has made use of the VizieR catalogue access tool, CDS, Strasbourg, France. The original description of the VizieR service was published in A&AS 143, 23

REFERENCES

Afram, N.; Berdyugina, S. V. 2015, A&A 576, 34

Alonso A., Arribas S., Martinez-Roger C. 1996, Astron. Astrophys. Suppl. Ser. 117, 227

Ammons, S.M., Robinson, S.E., Strader, J., Laughlin, G., Fisher, D., & Wolf, A, 2006, ApJ. 638, 1004

Anderson E., Francis C. 2012, Astron. Letters 38

[5] http://www.astropy.org/ and http://astroquery.readthedocs.org/en/latest/

Bessel, M.S. 1990, A&A Sup. Ser. 83, 357

Booth, J., Caruso, J., Weis, E.W. 1988, PASP 100, 749

Boyajian, T.S.; von Braun, K.; van Belle, G.; McAlister, H.A.; ten Brummelaar, T.A.; Kane, S.R.; Muirhead, P.S.; Jones, J.; White, R.; Schaefer, G.; Ciardi, D.; Henry, T.; Lpez-Morales, M.; Ridgway, S.; Gies, D.; Jao, Wei-Chun; Rojas-Ayala, B.; Parks, J.R.; Sturmann, L.; Sturmann, J.; Turner, N.H.; Farrington, C.; Goldfinger, P.J.; Berger, D.H. 2012, ApJ 757, 112

Browning, M.K., Basri, G., Marcy, G.W., West, A.A. & Zhang, J. 2010, AJ 139, 504

Casagrande L., Schoenrich R., Asplund M., Cassisi S., Ramirez I., Melendez J., Bensby T., Feltzing S. 2011, Astron. Astrophys. 530, A138

Cenarro A.J., Peletier R.F., Sanchez-Blazquez P., Selam S.O., Toloba E., Cardiel N., Falcon-Barroso J., Gorgas J., Jimenez-Vicente J., Vazdekis A. 2007, Mon. Not. R. Astron. Soc., 374, 664

Chen C.H., Mittal T., Kuchner M., Forrest W.J., Lisse C.M., Manoj P., Sargent B.A., Watson D.M. 2014, ApJ. Suppl. Ser., 211, 25

Christian, D.J., Mathioudakis, M., Arias, T., Jardine, M. and Jess, D.B. 2011, ApJ 738, 164

Claret, A. 2000, A&A 363, 1081

Cram, L.E. & Mullan, D.J. 1979, ApJ 234, 579

Dawson, P.C., Forbes, D. 1992, AJ 103, 2063

Delfosse, X., Forveille, T., Perrier, C., Mayor, M., 1998, A&A 331, 581

Eggen, O.J., 1974, PASP 86, 697

Eggen, O.J., 1976a, ApJS 30, 351

Eggen, O.J., 1976b, ApJ 204, 101

Eggen, O.J., 1978, ApJS 37, 251

Eggen, O.J., 1979, ApJS 39, 89

Eggen, O.J., 1980, ApJS 43, 457

Eggen, O.J., 1987, AJ 92, 379

Gaidos E., Mann A.W., Lepine S., Buccino A., James D., Ansdell M., Petrucci R., Mauas P., Hilton E.J. 2014, Mon. Not. R. Astron. Soc., 443, 2561

Glebocki, R. & Gnacinski, P. 2005, Catalog of Stellar Rotational Velocities, VizieR On-line Data Catalog III/244

Gray, D.F. 1988, Lectures on spectral-line analysis: F,G, and K stars, Arva: Ontario

Holmberg J., Nordstrom B., Andersen J. 2009, Astron. Astrophys. 501, 941

Houdebine, E.R. 2008, MNRAS 390, 1081 (Paper VII)

Houdebine, E.R. 2009a, MNRAS 400, 238 (Paper VIII)

Houdebine, E.R. 2009b, MNRAS 397, 2133 (Paper XII)

Houdebine, E.R. 2010a, MNRAS 407, 1657 (Paper XIV)

Houdebine, E.R. 2010b, MNRAS 509, 65 (Paper IX)

Houdebine, E.R. 2011a, MNRAS 416, 2233 (Paper XVI)

Houdebine, E.R. 2011b, MNRAS 411, 2259 (Paper XV)

Houdebine, E.R. 2012a, MNRAS 421, 3180 (Paper XVII)

Houdebine, E.R. 2012b, MNRAS 421, 3189 (Paper XVIII)

Houdebine, E.R. & Doyle, G.J. 1994, in Cool Stars, Stellar Systems and the Sun, Eigth Cambridge Workshop, Proceedings, held in Athens, Georgia, Caillault J.P. ed., ASPCS, Vol. 64, p. 423

Houdebine, E.R. & Stempels, H.C. 1997, A&A (Paper VI)

Houdebine, E.R. & Mullan, D.J. 2015, ApJ 801, 106

Houdebine, E.R., Mullan, D.J., Bercu, B., Paletou, F. & Gebran, M. 2016, Paper II, submitted to ApJ.

Hubeny, I., Lanz, T. 1992, A&A, 262, 501

Irwin, J., Berta, Z.K., Burke, C.J., Charbonneau, D., Nutzman, P., West, A.A. & Falco, E.E. 2011, ApJ 727, 56

Ivanov V.D., Rieke M.J., Engelbracht C.W., Alonso-herrero A., Rieke G.H., Luhman K.L. 2004, Astrophys. J. Suppl. Ser., 151, 387

Jenkins, I.S., Ramsey, L.W., Jones, H.R.A., Pavlenko, Y., Gallardo, I., Barnes, J.R. & Pinfield, D.I. 2009, ApJ, 704, 975

Jones, H.R.A., Longmore, A.J., Jameson, R.F., Mountain, C.M., 1994, MNRAS, 267, 413

Kenyon, S.J. & Hartmann, L. 1995, ApJ Suppl. Ser. 101, 117

Kiraga, M.& Stepien, K. 2007, Acta Astron. 57, 149

Koleva M., Vazdekis A. 2012, Astron. Astrophys. 538, A143

Kordopatis G., Gilmore G., Steinmetz M., Boeche C., Seabroke G. M., Siebert A., Zwitter T., Binney J., de Laverny P., Recio-Blanco A., Williams M.E.K., Piffl T., Enke H., Roeser S., Bijaoui A., Wyse R.F.G., Freeman K., Munari U., Carrillo I., Anguiano B., Burton D., Campbell R., Cass C.J.P., Fiegert K., Hartley M., Parker Q.A., Reid W., Ritter A., Russell K.S., Stupar M., Watson F.G., Bienayme O., Bland-Hawthorn J., Gerhard O., Gibson B.K., Grebel E.K., Helmi A., Navarro J.F., Conrad C., Famaey B., Faure C., Just A., Kos J., Matijevic G., McMillan P.J., Minchev I., Scholz R., Sharma S., Siviero A., Wylie de Boer E., Zerjal, M. 2013, Astron. J., 146, 134

Kurucz, R. L. 1992, Rev. Mex. Astron. Astrofis., 23, 45

Kurucz, R. L. 2005, Mem. Soc. Astron. Ital. Supp., 8, 14

Lafrasse S., Mella G., Bonneau D., Duvert G., Delfosse X., Chelli A. 2010, SPIE Conf. on Astronomical Instrumentation 77344E

Leggett, S.K., 1992, ApJS 82, 351

Leggett, S.K., Hawkins, M.R.S. 1988, MNRAS 234, 1065

Mamajek, E.E. & Hillebrand, L.A. 2008, ApJ 687, 1264

Mann A.W., Brewer J.M., Gaidos E., Lepine S., Hilton E.J. 2013, Astron. J., 145, 52

Mann A.W., Feiden G.A., Gaidos E., Boyajian T., Von Braun K. 2015, Astrophys. J., 804, 64

Marcy, G.W. & Chen, G.H. 1992, ApJ 390, 550

Marsakov V.A., Shevelev Yu.G. 1988, CDS Inf. Bull., 35, 129

Martínez-Arnáiz, R., Maldonado, J., Montes, D., Eiroa, C. & Montesinos, B. 2010, A&A 520, A79

Marsakov V.A., Shevelev Yu.G. 1988, CDS Inf. Bull., 35, 129

Masana E., Jordi C., Ribas I. 2006, Astron. Astrophys. 450, 735

McDonald I., Zijlstra A.A., Boyer M.L. 2012, Mon. Not. R. Astron. Soc., 427, 343

Milone A.DE C., Sansom A.E., Sanchez-Blazquez P. 2011, Mon. Not. R. Astron. Soc., 414, 1227

Mishenina T.V., Soubiran C., Bienayme O., Korotin S.A., Belik S.I., Usenko I.A., Kovtyukh V.V. 2008, Astron. Astrophys., 489, 923

Mohanty, S. & Basri, G. 2003, ApJ 583, 451

Morales J.C., Ribas I., Jordi C. 2008, A&A 478, 507

Mullan, D. J. , Mathioudakis, M., Bloomfield, D.S., & Christian, D.J. 2006, ApJ Suppl. 164, 173

Newton E.R., Charbonneau D., Irwin J., Berta-Thompson Z.K., Rojas-Ayala B., Covey K., Lloyd J.P. 2014, Astron. J., 147, 20

Nielsen, M.B., Gizon, L., Schunker, H. & Karoff, C. 2013, A&A 557, L10

Nordstrom, B., Mayor, M., Andersen, J., Holmberg, J., Pont, F., Jorgensen, B.R., Olsen, E.H., Udry, S., & Mowlavi, N. 2004, A&A 418, 989

Noyes, R.W., Hartmann, L.W., Baliunas, S.L., Duncan, D.K., Vaughan, A.H. 1984, ApJ 279, 763

Pace, G. 2013, A&A 551, L8

Paletou, F. & Zolotukhin, I. 2014, arXiv:1408.7026

Paletou, F., Böhm, T., Watson, V., Trouilhet, J.-F. 2015a, A&A, 573, 67

Paletou, F., Gebran, M., Houdebine, E.R. & Watson, V. 2015b, A&A, 580, A78

Pizzolato, N., Maggio, A., Micela, G., Sciortino, S., Ventura, P. 2003, A&A 397, 147

Prugniel, P., Soubiran, C., Koleva, M., Le Borgne D. 2007, [arXiv:astro-ph/0703658]

Prugniel P., Vauglin, I., Koleva M. 2011, Astron. Astrophys. 531, A165

Ramirez, I., Melendez, J. 2005, ApJ 626, 465

Reiners, A.; Basri, G. 2006, ApJ 644, 497

Rodgers, A.W., Eggen, O.J., 1974, PASP 86, 742

Rojas-Ayala B., Covey K.R., Muirhead P.S., Lloyd J.P. 2012, Astrophys. J., 748, 93

Sanchez-Blazquez P., Peletier R.F., Jimenez-Vicente J., Cardiel N., Cenarro A.J., Falcon-Barroso J., Gorgas J., Selam S., Vazdekis A. 2006, Mon. Not. R. Astron. Soc., 371, 703

Soubiran C., Le Campion J.-F., Cayrel de Strobel G., Caillo A. 2010, Astron. Astrophys. 515, A111

Sousa S.G., Santos N.C., Israelian G., Mayor M., Monteiro M.J.P.F.G. 2006, Astron. Astrophys. 458, 873

Spada, F., Demarque, P., Kim, Y.-C., Sills, A. 2013, ApJ 776, 87

Stepien, K. 1989, A&A 210, 273

Stepien, K. 1993, in the Proceedings of the 157th Symposium of the IAU, The Cosmic Dynamo, Eds. F. Krause, K. H. Radler, and Gunther Rudiger, p. 141

Stepien, K. 1994, A&A 292, 207

Torres, C.A.O., Quast, G.R., da Silva, L., de la Reza, R., Melo, C.H.F., & Sterzik, M. 2006, A&A 460, 695

Upgren, A.R., Lu, P.K. 1986, AJ 92, 903

Valenti J.A., Fischer D.A. 2005, Astrophys. J. Suppl. Ser., 159, 141

Veeder, G.J. 1974, AJ 79, 1056

Vogt, S.S., Soderblom, D.R., Penrod, G.D. 1983, ApJ 269, 250

Weis, E.W. 1991a, AJ 101, 1882

Weis, E.W. 1991b, AJ 102, 1795

Weis, E.W. 1993, AJ 105, 1962

Weis, E.W, Upgren, A.R. 1982, PASP 94, 821

West, A.A., Weisenburger, K.L., Irwin, J., Berta-Thompson, Z.K., Charbonneau, D., Dittmann, J., Pineda, J.S. 2015, ApJ 812, 3

Wu Y., Singh H.P., Prugniel P., Gupta R., Koleva M. 2011, Astron. Astrophys. 525, A71

This 2-column preprint was prepared with the AAS LaTeX macros v5.2.

Table 1:: Stellar parameters (e.g. T_{eff}, π, Mv, $R_\star$) for our sample of late-K dwarfs. We also computed [M/H] derived from the [M/H]/radius correlation (see text).

Star	V (mag)	(R-I)$_C$ or (B-V) (mag)	Teff (K)	Teff$\pm\sigma$ (K)	Spect. Type	π (m")	Distance (pc)	Mv (mag)	$R_\star$ ($R_\odot$)	$R_\star$[1] ($R_\odot$)	[M/H] (dex)	[M/H][2] (dex)
GJ 1056	9.259	0.686	4230 ±100	4365 ±103	dK4.9	46.06±1.08	21.7	7.576±0.055	0.687±0.061	0.660	-	-0.175
GJ 1066	8.847	0.680	4250 ±100	4397 ±107	dK4.8	56.31±0.82	17.8	7.600±0.036	0.667±0.052	0.634	-	-0.215
GJ 1067	9.70	0.680	4250 ±100	4385 ±135	dK4.9	38.26±1.27	26.1	7.614±0.091	0.665±0.071	0.634	-	-0.215
GJ 1177A	8.94	0.731	4130 ±100	4260 ±130	PMS K5.6	69.01±1.35	14.5	8.135±0.062	0.576±0.055	0.569	-	-0.471
GJ 1213	10.18	0.781	4030 ±100	4155 ±125	dK6.4	39.64±1.14	25.2	8.171±0.082	0.624±0.072	0.634	-	-0.236
GJ 1248	12.99	0.790	4010 ±100	4010 ±100	sdK7.3	80.2 ±4.3	12.5	12.51±0.13	0.090±0.012	0.140	-	-
GJ 1267	8.992	0.800	4000 ±100	4107 ±117	dK6.7	73.90±1.21	13.5	8.335±0.040	0.606±0.058	0.629	-	-0.225
GJ 1279	8.39	0.686	4230 ±100	4397 ±121	dK4.8	66.74±0.83	15.0	7.512±0.047	0.697±0.059	0.664	-0.10	-0.169
GJ 3072	9.993	0.778	4030 ±100	4070 ±40	dK6.9	49.06±1.88	20.4	8.447±0.086	0.571±0.068	0.604	-	-0.319
GJ 3411	10.16	0.731	4130 ±100	4130 ±100	dK6.5	36.32±1.65	27.5	7.961±0.116	0.664±0.083	0.683	-	-0.169
GJ 3494	9.748	0.740	4110 ±100	4290 ±180	dK5.4	41.22±1.74	24.3	7.824±0.094	0.660±0.074	0.648	+0.71	-0.192
GJ 3551	9.531	0.728	4140 ±100	4239 ±71	dK5.8	43.13±1.04	23.2	7.705±0.057	0.708±0.066	0.705	-0.40	-0.139
GJ 3996	10.333	0.812	3980 ±100	4088 ±110	dK6.8	36.73±1.84	27.2	8.158±0.12	0.673±0.092	0.701	-0.11	-0.140
GJ 4140	10.168	0.812	3980 ±100	4143 ±117	dK6.4	49.33±1.46	20.3	8.634±0.068	0.526±0.057	0.542	+0.42	-0.583
GJ 9073B	10.49	0.719	4160 ±100	4160 ±100	dK6.3	32±4	31.3	8.016±0.276	0.632±0.133	0.645	-	-0.196
GJ 9250	10.14	0.719	4160 ±100	4268 ±107	dK5.6	34.17±1.89	29.3	7.808±0.137	0.661±0.089	0.653	-	-0.185
GJ 9299	9.742	0.728	4140 ±100	4259 ±93	dK5.6	41.24±1.46	24.2	7.819±0.080	0.665±0.070	0.659	+0.15	-0.176
GJ 9667	9.958	0.698	4210 ±100	4210 ±100	dK6.0	43.28±1.64	23.1	8.139±0.086	0.575±0.061	0.578	-	-0.433
GJ 9714	9.326	0.728	4140 ±100	4333 ±148	dK5.1	49.23±1.45	20.3	7.787±0.068	0.652±0.064	0.631	+0.10	-0.221
GJ 9827	10.39	0.716	4170 ±100	4220 ±50	dK5.9	32.98±1.78	30.3	7.981±0.13	0.623±0.082	0.624	-	-0.236
Gl 14	9.00	0.812	3980 ±100	4175 ±195	dK6.2	66.65±0.91	15.0	8.119±0.049	0.657±0.065	0.667	-	-0.165
Gl 40A	8.930	0.702	4200 ±100	4284 ±85	dK5.5	63.96±1.07	15.6	7.960±0.041	0.604±0.051	0.593	-0.61	-0.365
Gl 45	9.482	0.696	4210 ±100	4252 ±62	dK5.7	50.87±0.98	19.7	8.014±0.047	0.596±0.051	0.591	+0.00	-0.375
Gl 50	10.47	0.684	4240 ±100	4240 ±100	dK5.8	30.55±1.79	32.7	7.895±0.31	0.628±0.142	0.625	+0.56	-0.232
Gl 52	8.97	0.740	4110 ±100	4195 ±85	dK6.1	66.97±1.31	14.9	8.099±0.062	0.608±0.059	0.614	-	-0.278
Gl 57	10.130	0.874	3906 ±100	4040 ±90	dK7.1	59.86±1.54	16.7	9.016±0.060	0.411±0.039	0.448	-	-1.514
GL 105.5	9.509	0.680	4250 ±100	4250 ±100	dK5.7	42.91±1.47	23.3	7.672±0.078	0.692±0.070	0.687	-	-0.149
Gl 112.1	8.574	0.664	4280 ±100	4224 ±56	dK5.8	62.46±1.37	16.0	7.552±0.052	0.731±0.065	0.731	-	-0.128
GL 116	9.608	0.725	4150 ±100	4100 ±50	sdK6.7	68.47±1.43	14.6	8.786±0.049	0.459±0.042	0.484	-	-1.100
Gl 123	9.055	0.783	4020 ±100	4065 ±45	dK7.0	66.94±1.94	14.9	8.183±0.067	0.650±0.071	0.685	-	-0.150
Gl 142	8.367	0.752	4080 ±100	4127 ±47	dK6.5	80.04±0.99	12.5	7.884±0.032	0.700±0.058	0.719	-	-0.133
Gl 143.1	9.991	0.799	4000 ±100	4070 ±113	dK6.9	45.28±1.97	22.1	8.271±0.097	0.634±0.079	0.667	+0.45	-0.165
Gl 146	8.60	0.725	4150 ±100	4220 ±50	dK5.9	73.49±0.71	13.6	7.931±0.041	0.642±0.055	0.643	+0.38	-0.199
Gl 153A	9.35	0.728	4140 ±100	4245 ±105	dK5.7	57.68±3.06	17.3	8.155±0.13	0.574±0.075	0.570	-	-0.467
Gl 156	9.015	0.750	4080 ±100	4135 ±55	dK6.5	64.24±1.08	15.6	8.054±0.041	0.644±0.056	0.662	-	-0.172
Gl 162.2	9.72	0.692	4220 ±100	4377 ±111	dK4.9	38.53±0.83	26.0	7.649±0.066	0.664±0.062	0.635	-	-0.213
Gl 182	10.107	1.37	4073 ±100	4073 ±100	PMS K7	38.64±2.54	25.9	8.042±0.14	0.946±0.109	0.978	-	-0.002
Gl 186A	10.02	0.744	4100 ±100	4244 ±102	dK5.7	40.23±2.08	24.9	8.046±0.13	0.611±0.080	0.607	+0.09	-0.307
Gl 186B	10.02	0.744	4100 ±100	4244 ±102	dK5.7	40.23±2.08	24.9	8.046±0.13	0.611±0.080	0.607	+0.09	-0.307
Gl 208	8.841	0.801	3990 ±100	4055 ±65	dK7.0(e)	88.97±1.02	11.2	8.587±0.030	0.554±0.050	0.591	+0.01	-0.375
Gl 221	9.693	0.744	4100 ±100	4134 ±34	dK6.5	49.23±1.65	20.3	8.154±0.077	0.613±0.064	0.631	+0.19	-0.221
Gl 226.2	9.75	0.645	4320 ±100	4357 ±37	dK5.0	40.87±1.85	24.5	7.807±0.116	0.603±0.072	0.577	-	-0.438
Gl 249	8.96	0.657	4294 ±100	4321 ±27	dK5.2	53.89±0.98	18.6	7.618±0.059	0.675±0.061	0.656	-	-0.180
Gl 256	9.157	0.645	4320 ±100	4361 ±41	dK5.0	46.08±1.23	21.7	7.475±0.062	0.702±0.065	0.676	-	-0.156
Gl 296	9.65	0.765	4050 ±100	4044 ±7	dK7.1	51.00±8.00	19.6	8.188±0.336	0.642±0.164	0.683	-	-0.152
Gl 322	9.28	0.764	4050 ±100	4260 ±210	dK5.6	60.46±1.36	16.5	8.187±0.069	0.578±0.062	0.571	-	-0.463
Gl 369	10.016	0.780	3800 ±100	3866 ±66	sdM1	82.92±1.82	12.1	9.609±0.052	0.371±0.039	0.463	-	-1.341
Gl 389.1	9.99	0.692	4220 ±100	4220 ±188	dK5.9	36.54±2.16	27.4	7.804±0.14	0.664±0.089	0.665	-	-0.168
Gl 397	8.83	0.743	4100 ±100	4140 ±40	dK6.4	63.55±1.09	15.7	7.846±0.057	0.717±0.068	0.734	-	-0.126
Gl 401	11.02	0.775	3810 ±100	3810 ±100	sdM1	49.95±2.26	20.0	9.513±0.12	0.392±0.051	0.500	-	-0.916
Gl 412.3A	9.34	0.695	4220 ±100	4263 ±76	dK5.6	35.46±2.84	28.2	7.842±0.19	0.641±0.102	0.634	-	-0.215
Gl 412.3B	9.34	0.695	4220 ±100	4263 ±76	dK5.6	35.46±2.84	28.2	7.842±0.19	0.641±0.102	0.634	-	-0.215
Gl 414A	8.34	0.776	4030 ±100	4185 ±155	dK6.1	87.23±0.86	11.5	8.043±0.042	0.649±0.062	0.660	-	-0.175
Gl 416	9.038	0.706	4190 ±100	4330 ±140	dK5.1	46.36±1.31	21.6	7.369±0.065	0.778±0.075	0.758	-	-0.116
Gl 421B	10.01	0.788	4020 ±100	4030 ±69	sdK7.1	62.53±29.8	16.0	8.990±0.87	0.459±0.278	0.504	-1.50	-0.870
Gl 425B	8.61	0.820	3960 ±100	4227 ±192	dK5.8	63.5 ±8.2	15.7	7.624±0.28	0.812±0.180	0.812	+0.19	-0.093
Gl 455.1	10.016	0.751	4082 ±100	4172 ±90	dK6.2	45.45±1.39	22.0	8.304±0.070	0.564±0.057	0.575	-	-0.446
Gl 466	10.38	0.686	4230 ±100	4230 ±100	dK5.8	26.74±2.27	37.4	7.516±0.20	0.751±0.124	0.750	-	-0.120
Gl 496.1	9.057	0.783	4020 ±100	4040 ±20	dK7.1	63.03±1.36	15.9	8.055±0.051	0.698±0.071	0.740	-0.11	-0.124
Gl 509.1	9.74	0.764	4050 ±100	4275 ±225	dK5.5	40.35±1.10	24.8	7.769±0.078	0.696±0.078	0.686	-	-0.150
Gl 517	9.348	0.722	4510 ±100	4510 ±100	dK4.4e	49.48±0.72	20.2	7.820±0.037	0.588±0.046	0.552	-0.11	-0.542
Gl 522	9.710	0.712	4180 ±100	4220 ±40	dK5.9	42.30±1.48	23.6	7.842±0.079	0.662±0.069	0.663	-0.22	-0.170
Gl 524.1	10.480	0.742	4100 ±100	4275 ±193	dK5.5	39.84±1.97	25.1	8.482±0.11	0.492±0.059	0.482	-0.22	-1.123
Gl 542.2	9.112	0.711	4180 ±100	4296 ±89	dK5.4	45.97±1.59	21.8	7.424±0.079	0.774±0.080	0.760	-	-0.115
Gl 546	8.610	0.716	4170 ±100	4320 ±150	dK5.2	69.70±0.82	14.3	7.826±0.031	0.638±0.051	0.620	-	-0.253
Gl 558	9.58	0.740	4110 ±100	4250 ±140	dK5.7	49.43±1.07	20.2	8.050±0.066	0.606±0.059	0.601	-	-0.332
Gl 562	9.23	0.716	4170 ±100	4285 ±115	dK5.4	65.8 ±7.2	15.2	8.321±0.25	0.517±0.100	0.505	-	-0.862
Gl 570.2	11.110	0.806	3990 ±100	3987 ±3	dK7.4	25.76±4.32	38.8	8.165±0.342	0.700±0.182	0.757	-	-0.117
Gl 571	10.14	0.716	4170 ±100	4170 ±100	dK6.2	40.79±1.47	24.5	8.193±0.097	0.579±0.065	0.590	-	-0.380
Gl 571.1	9.472	0.805	3990 ±100	4076 ±69	dK6.9	51.70±1.97	19.3	8.039±0.087	0.708±0.085	0.739	+0.37	-0.124

Table 1:: continued.

Star	V (mag)	b(R-I)$_C$ or (B-V) (mag)	Teff (K)	Teff$\pm\sigma$ (K)	Spect. Type	π (m")	Distance (pc)	Mv (mag)	$R_\star$ ($R_\odot$)	$R_\star$[1] ($R_\odot$)	[M/H] (dex)	[M/H][2] (dex)
Gl 576	9.815	0.748	4090 ±100	4197 ±107	dK6.1	53.80±2.80	18.6	8.469±0.115	0.516±0.064	0.522	-	-0.734
Gl 583	9.459	0.721	4160 ±100	4213 ±41	dK5.9	52.92±1.60	18.9	8.077±0.070	0.600±0.060	0.603	+0.37	-0.324
Gl 585.1	10.23	0.743	4100 ±100	4152 ±52	dK6.4	37.96±1.90	26.3	8.127±0.126	0.614±0.080	0.628	-	-0.227
Gl 619	8.98	0.746	4090 ±100	4205 ±115	dK6.0	63.62±0.73	15.7	7.998±0.045	0.637±0.056	0.641	-	-0.202
Gl 626	8.85	0.651	4306 ±100	4306 ±100	dK5.3	57.08±1.26	17.5	7.632±0.067	0.672±0.064	0.656	-	-0.180
Gl 629.1	10.53	0.754	4080 ±100	4120 ±40	dK6.6	30.53±2.51	32.8	7.954±0.19	0.681±0.112	0.702	-	-0.140
Gl 659B	9.36	0.645	4320 ±100	4378 ±58	dK4.9	49.46±4.03	20.2	7.831±0.190	0.591±0.093	0.573	-	-0.454
Gl 673	7.530	0.760	4060 ±100	4078 ±18	dK6.9	129.86±0.73	7.70	8.097±0.017	0.654±0.049	0.685	-	-0.150
Gl 707	8.372	0.675	4260 ±100	4267 ±106	dK5.6	76.31±1.06	13.1	7.785±0.035	0.648±0.052	0.640	+0.34	-0.204
Gl 708	10.020	0.694	4220 ±100	4232 ±12	dK5.8	34.05±1.76	29.4	7.681±0.114	0.700±0.084	0.699	-	-0.142
Gl 710	9.660	0.755	4070 ±100	4120 ±37	dK6.6	51.12±1.63	19.6	8.203±0.073	0.608±0.063	0.629	+0.00	-0.225
Gl 726	8.810	0.700	4210 ±100	4270 ±60	dK5.6	70.04±1.17	14.3	8.037±0.041	0.586±0.048	0.577	-0.97	-0.437
Gl 728	9.155	0.776	4030 ±100	4100 ±70	dK6.7	58.82±1.34	17.0	8.003±0.054	0.689±0.071	0.714	-	-0.135
Gl 747.2	9.73	0.743	4100 ±100	4141 ±41	dK6.4	33.35±1.16	30.0	7.345±0.094	0.885±0.101	0.902	-	-0.005
Gl 747.3	9.342	0.730	4130 ±100	4203 ±70	dK6.0	48.59±1.53	20.6	7.775±0.072	0.698±0.071	0.702	+0.33	-0.140
Gl 757	10.95	0.802	3990 ±100	4069 ±97	sdK6.9	34.11±2.11	29.3	8.614±0.15	0.544±0.083	0.577	-	-0.437
Gl 763	9.326	0.790	4010 ±100	4065 ±55	sdK7.0	69.32±1.55	14.4	8.530±0.053	0.559±0.057	0.594	-	-0.361
Gl 773	9.285	0.737	4115 ±100	4288 ±173	dK5.4	53.54±1.29	18.7	7.928±0.057	0.628±0.058	0.616	-	-0.269
Gl 782	8.890	0.691	4220 ±100	4332 ±80	dK5.1	64.04±1.50	15.6	7.922±0.056	0.597±0.053	0.576	-0.88	-0.442
Gl 786.1	10.16	0.800	4000 ±100	4140 ±140	dK6.4	40.58±1.10	24.6	8.202±0.079	0.634±0.073	0.651	-	-0.187
Gl 795A	9.348	0.707	4190 ±100	4190 ±100	dK6.1	59.80±3.42	16.7	8.232±0.13	0.559±0.072	0.566	-	-0.484
Gl 795B	9.348	0.707	4190 ±100	4190 ±100	dK6.1	59.80±3.42	16.7	8.232±0.13	0.559±0.072	0.566	-	-0.484
Gl 798	8.82	0.748	4090 ±100	4135 ±120	dK6.5	82.31±1.07	12.1	8.397±0.048	0.549±0.050	0.567	-1.50	-0.478
Gl 801	9.88	0.704	4200 ±100	4203 ±118	dK6.0	40.04±1.92	25.0	7.892±0.12	0.648±0.082	0.652	-0.21	-0.186
Gl 818	8.272	0.680	4250 ±100	4342 ±88	dK5.1	66.41±0.95	15.1	7.383±0.036	0.756±0.060	0.733	+0.12	-0.127
Gl 820B	7.40	1.37	4073 ±100	4073 ±100	sdK6.9	285.88±0.54	3.50	9.681±0.024	0.316±0.025	0.348	-	-2.664
Gl 826.1	9.086	0.749	4090 ±100	4243 ±111	dK5.1	61.65±1.13	16.2	8.036±0.044	0.616±0.054	0.613	-	-0.282
Gl 828.1	10.480	0.803	3990 ±100	4212 ±222	dK5.9	36.93±2.28	27.1	8.317±0.135	0.583±0.083	0.586	-	-0.399
Gl 830	9.075	0.728	4140 ±100	4178 ±65	dK6.2	54.33±1.18	18.4	7.750±0.052	0.713±0.065	0.722	-0.21	-0.131
Gl 836.9AB	8.85	0.775	4040 ±100	4140 ±100	dK6.4	52.1±8.5	19.2	7.434±0.348	0.876±0.229	0.893	-	-0.006
Gl 842	9.715	1.039	3780 ±100	3700 ±80	dM1	83.43±1.77	12.0	9.322±0.050	0.446±0.042	0.585	-	-0.404
Gl 847A	10.97	0.761	4060 ±100	4110 ±50	sdK6.7	33.13±1.87	30.2	8.571±0.14	0.518±0.076	0.541	-	-0.591
Gl 857.1	8.770	0.728	4140 ±100	4300 ±160	dK5.3	46.33±1.09	21.6	7.099±0.056	0.909±0.084	0.894	-	-0.058
Gl 884	7.869	0.770	4040 ±100	4063 ±64	dK7.0	121.69±0.69	8.22	8.295±0.017	0.609±0.051	0.644	-1.16	-0.198
Gl 885A	9.57	0.749	4090 ±100	4196 ±106	dK6.1	63±16	15.9	8.567±0.511	0.493±0.172	0.499	-	-0.927
Gl 889A	9.640	0.756	4070 ±100	4241 ±126	dK5.8	47.76±1.82	20.9	8.035±0.087	0.620±0.067	0.617	+0.74	-0.265
Gl 891	9.75	0.820	3963 ±100	3963 ±100	dK7.4	62.17±3.27	16.1	8.718±0.131	0.558±0.081	0.622	-	-0.245
Gl 894	10.38	0.728	4140 ±100	4240 ±73	dK5.8	30.61±1.90	32.7	7.809±0.15	0.674±0.095	0.671	-0.23	-0.159
Gl 895.3	10.19	0.691	4220 ±100	4275 ±55	dK5.5	37.04±1.99	27.0	8.033±0.13	0.582±0.074	0.572	-	-0.459
Gl 898	8.607	0.716	4170 ±100	4258 ±129	dK5.6	65.98±1.96	15.2	7.704±0.069	0.695±0.069	0.689	+0.01	-0.147
Gl 900	9.546	0.814	3970 ±100	4165 ±195	dK6.3	52.56±1.29	19.0	8.149±0.058	0.652±0.068	0.664	-	-0.169
Gl 906	9.91	0.776	4030 ±100	4065 ±35	dK7.0	52.14±1.66	19.2	8.496±0.088	0.558±0.067	0.593	-	-0.365
Gl 907.1	9.63	0.774	4040 ±100	4040 ±100	dK7.1	35.46±2.20	28.2	7.379±0.151	0.943±0.145	0.985	-	-0.002
HIP 3121	10.46	0.742	4100 ±100	4194 ±94	dK6.1	27.72±1.65	36.1	7.674±0.146	0.741±0.104	0.747	-	-0.121
HIP 6290	10.39	0.743	4100 ±100	4192 ±92	sdK6.1	49.77±2.10	20.1	8.875±0.110	0.427±0.052	0.434	-	-1.675
HIP 11437	10.19	0.667	4267 ±100	4180 ±88	dK6.2	25.03±2.25	40.0	7.182±0.207	0.887±0.151	0.896	-	-0.006
HIP 14593A	10.06	0.716	4170 ±100	4260 ±90	dK5.6	31.43±2.52	31.8	7.547±0.19	0.747±0.121	0.740	-	-0.124
HIP 19410A	11.39	0.704	4200 ±100	4302 ±77	dK5.3	22.51±2.20	44.4	8.152±0.22	0.549±0.098	0.761	+0.01	-0.115
HIP 19410B	12.15	0.704	4200 ±100	4302 ±77	dK5.3	22.51±2.20	44.4	8.908±0.23	0.388±0.071	0.373	-	-
HIP 19410C	12.15	0.704	4200 ±100	4302 ±77	dK5.3	22.51±2.20	44.4	8.908±0.23	0.388±0.071	0.373	-	-
HIP 21865	10.03	0.680	4250 ±100	4393 ±103	dK4.8	32.77±1.30	30.5	7.607±0.10	0.665±0.074	0.632	-0.19	-0.219
HIP 40170	10.14	0.706	4190 ±100	4290 ±100	dK5.4	39.18±2.12	25.5	8.105±0.134	0.565±0.075	0.553	-	-0.538
HIP 42108A	11.03	0.716	4170 ±100	4160 ±10	dK6.3	28.19±1.71	35.5	8.283±0.15	0.558±0.079	0.571	-	-0.463
HIP 42108B	11.03	0.716	4170 ±100	4160 ±10	dK6.3	28.19±1.71	35.5	8.283±0.15	0.558±0.079	0.571	-	-0.463
HIP 42910	10.16	0.752	4080 ±100	4299 ±193	dK5.4	27.45±1.91	36.4	7.353±0.17	0.824±0.125	0.810	+0.16	-0.094
HIP 50773	10.69	0.788	4020 ±100	4100 ±80	dK6.7	33.56±1.55	29.8	8.319±0.12	0.604±0.082	0.629	-	-0.225
HIP 51073	10.75	0.697	4210 ±100	4285 ±55	dK5.4	25.43±2.63	39.3	7.777±0.23	0.654±0.118	0.642	-0.72	-0.200
HIP 51263A	10.44	0.692	4220 ±100	4321 ±76	dK5.2	28.09±1.64	35.6	7.686±0.14	0.669±0.089	0.650	-	-0.189
HIP 51263B	10.44	0.692	4220 ±100	4321 ±76	dK5.2	28.09±1.64	35.6	7.686±0.14	0.669±0.089	0.650	-	-0.189
HIP 53175	10.69	0.788	4020 ±100	4250 ±230	dK5.7	25.62±2.02	39.0	7.733±0.18	0.736±0.122	0.731	-	-0.128
HIP 56838	10.03	0.698	4210 ±100	4240 ±160	dK5.7	32.73±1.30	30.6	7.605±0.10	0.724±0.082	0.721	-	-0.132
HIP 58945	11.12	0.752	4080 ±100	4255 ±175	dK5.7	23.76±2.06	42.1	7.999±0.20	0.625±0.105	0.619	-	-0.257
HIP 59247	11.04	0.776	4030 ±100	4195 ±165	dK6.1	23.95±1.91	41.8	7.936±0.20	0.678±0.121	0.684	-	-0.151
HIP 60438A	10.78	0.781	4026 ±100	4095 ±69	dK6.8	22.31±2.06	44.8	8.275±0.212	0.613±0.114	0.639	-	-0.206
HIP 60438B	10.78	0.781	4026 ±100	4095 ±69	dK6.8	22.31±2.06	44.8	8.275±0.212	0.613±0.114	0.639	-	-0.206
HIP 60501	10.58	0.716	4170 ±100	4295 ±125	dK5.4	17.66±2.09	56.6	6.815±0.26	1.029±0.206	1.015	-	-0.007
HIP 72044	9.91	0.680	4250 ±100	4405 ±155	dK4.8	38.54±1.42	25.9	7.840±0.10	0.595±0.066	0.573	-	-0.454
HIP 76550	11.35	0.747	4090 ±100	4095 ±5	sdK6.8	31.45±4.57	31.8	8.838±0.31	0.457±0.105	0.483	-	-1.111
HIP 78395	10.33	0.716	4170 ±100	4322 ±135	dK5.2	32.90±2.05	30.4	7.916±0.15	0.612±0.086	0.593	+0.11	-0.365
HIP 80083	11.4	0.712	4180 ±100	4514 ±314	dK4.3	20.78±2.76	48.1	7.988±0.37	0.541±0.140	0.504	-0.81	-0.870
HIP 95223	9.93	0.645	4318 ±100	4355 ±37	dK5.0	33.73±1.25	29.6	7.570±0.099	0.674±0.075	0.649	-	-0.190
HIP 103150	11.18	0.812	3980 ±100	4149 ±198	sdK6.4	29.22±2.05	34.2	8.508±0.17	0.556±0.090	0.571	-0.20	-0.463
HIP 110245	10.17	0.728	4140 ±100	4387 ±175	dK4.8	26.99±2.23	37.1	7.326±0.19	0.787±0.126	0.756	+0.04	-0.117

Table 1:: continued.

Star	V (mag)	b(R-I)$_C$ or (B-V) (mag)	Teff (K)	Teff$\pm\sigma$ (K)	Spect. Type	π (m")	Distance (pc)	Mv (mag)	$R_\star$ ($R_\odot$)	$R_\star$[1] ($R_\odot$)	[M/H] (dex)	[M/H][2] (dex)
HIP 110714	10.52	0.770	4040 $\pm$100	4116 $\pm$54	dK6.6	32.20$\pm$1.90	31.1	8.059$\pm$0.14	0.661$\pm$0.097	0.682	+0.37	-0.152
HIP 113597	9.65	0.756	4070 $\pm$100	4186 $\pm$116	dK6.1	32.74$\pm$2.03	30.5	7.226$\pm$0.151	0.924$\pm$0.132	0.932	-	-0.004
HIP 116011	11.80	0.704	4200 $\pm$100	4295 $\pm$95	dK5.4	18.41$\pm$3.47	54.3	8.125$\pm$0.40	0.558$\pm$0.156	0.545	-	-0.571
LHS 3060	10.10	0.706	4190 $\pm$100	4190 $\pm$100	dK6.1	39.40$\pm$0.29	25.4	8.077$\pm$0.036	0.600$\pm$0.050	0.607	-	-0.307
STKM 1-607	9.56	0.756	4070 $\pm$100	4070 $\pm$100	dK6.9	-	-	-	-	-	-	-
											-	

[1]Radius corrected from T_{eff} effects.

[2]Computed from the [M/H]-radius relationship.

Table 2:: Inverted stellar parameters $T_{\rm eff}$, log$g$, [Fe/H] and $v$sin$i$ for HARPS and SOPHIE objects, using our Atlas-based PCA method.

Object	$T_{\rm eff}$ [K]	log$g$ [dex]	[Fe/H] [dex]	$v$sin$i$ [km s^{-1}]
GJ 1056	4480	4.8	-0.20	2.4
GJ 1066	4500	5.0	-0.25	1.0
GJ 1067	4520	4.8	-0.22	2.4
GJ 1267	4270	5.0	-0.50	2.5
GJ 1279	4450	4.9	-0.12	2.5
GJ 3072	4110	4.8	-0.50	2.2
GJ 3494	4470	4.9	-0.25	3.3
GJ 3551	4270	4.7	-0.50	1.3
GJ 3996	4240	4.8	-0.36	2.9
GJ 4140	4250	4.9	-0.50	3.0
GJ 9299	4270	4.8	-0.25	2.0
GJ 9714	4500	5.0	-0.25	2.0
GJ 9827	4270	4.9	-0.50	1.3
Gl 14	4370	4.9	-0.25	3.0
Gl 17.1	3810	4.8	-0.72	2.0
Gl 40A	4400	4.9	-0.33	2.3
Gl 45	4340	4.9	-0.25	1.6
Gl 50	4240	4.7	-0.44	2.0
Gl 52	4280	4.9	-0.46	2.0
Gl 57	4030	4.8	-0.75	2.2
Gl 116	4050	4.5	-1.10	2.2
Gl 143.1	3980	4.7	-0.40	2.1
Gl 146	4260	4.8	-0.25	2.4
Gl 153A	4350	4.8	-0.43	2.5
Gl 156	4190	4.8	-0.25	1.6
Gl 162.2	4460	4.8	-0.19	3.0
Gl 186	4310	4.7	-0.19	7.3
Gl 191	$\leq$3500	4.6	-1.00	2.0
Gl 208	4120	4.8	-0.47	3.1
Gl 221	4180	4.8	-0.46	1.7
Gl 322	4470	5.0	-0.25	2.5
Gl 369	3790	4.8	-0.86	2.4
Gl 389.1	4450	4.9	-0.25	2.0
Gl 401	3810	4.9	-0.94	2.2
Gl 412.3	4370	4.8	-0.25	3.5
Gl 414A	4340	4.9	-0.20	2.0
Gl 416	4470	4.8	-0.25	4.0
Gl 421B	4120	4.7	-0.44	2.2
Gl 425B	4400	4.8	-0.25	4.5
Gl 496.1	4060	4.7	-0.25	2.0
Gl 509.1	4500	5.0	-0.25	3.0
Gl 517	4510	4.6	-0.14	10.0
Gl 522	4260	4.8	-0.25	1.8
Gl 524.1	4180	4.8	-0.43	2.4
Gl 546	4470	4.9	-0.21	2.3

Table 2:: continued.

Object	$T_{\rm eff}$ [K]	log$g$ [dex]	[Fe/H] [dex]	$v$sin$i$ [km s^{-1}]
Gl 558	4390	4.9	-0.44	2.2
Gl 562	4400	4.9	-0.39	3.1
Gl 571.1	4160	4.8	-0.27	2.4
Gl 583	4260	4.8	-0.38	2.3
Gl 619	4320	4.8	-0.33	2.4
Gl 629.1	4160	4.7	-0.33	2.3
Gl 707	4400	5.0	-0.25	2.0
Gl 710	4160	4.8	-0.50	2.0
Gl 726	4330	4.9	-0.39	2.6
Gl 728	4170	4.8	-0.50	2.0
Gl 747.3	4180	4.7	-0.25	5.4
Gl 757	4010	4.8	-0.73	2.2
Gl 763	4120	4.9	-0.57	5.9
Gl 782	4400	4.8	-0.25	3.0
Gl 786.1	4280	4.9	-0.21	2.6
Gl 798	4300	5.0	-0.50	2.0
Gl 801	4350	4.9	-0.50	1.0
Gl 818	4460	4.8	-0.12	1.5
Gl 826.1	4290	4.8	-0.28	2.8
Gl 830	4270	4.7	-0.38	1.7
Gl 842	3770	4.8	-0.78	2.5
Gl 847A	4160	4.9	-0.50	2.4
Gl 855	3830	4.8	-0.75	2.8
Gl 857.1	4460	4.7	-0.09	6.6
Gl 884	4150	4.8	-0.45	2.4
Gl 889A	4370	4.8	-0.25	2.6
Gl 894	4270	4.8	-0.25	2.4
Gl 895.5	4330	4.8	-0.25	3.0
Gl 898	4440	4.8	-0.15	4.0
Gl 900	4360	4.8	-0.14	7.4
Gl 906	4100	4.8	-0.67	2.1
HIP 14593A	4350	4.8	-0.28	2.0
HIP 19410	4320	4.8	-0.25	12.4
HIP 21865	4440	4.8	-0.14	2.0
HIP 42108	4150	4.6	-0.37	12.7
HIP 42910	4550	5.0	-0.06	2.0
HIP 50773	4180	4.8	-0.44	2.2
HIP 51073	4340	4.9	-0.50	1.3
HIP 51263	4340	4.9	-0.71	3.4
HIP 53175	4480	4.9	-0.12	3.7
HIP 56838	4450	4.9	-0.25	2.0
HIP 58945	4430	4.9	-0.18	2.5
HIP 59247	4360	4.8	-0.33	1.8
HIP 60501	4420	5.0	-0.10	1.6
HIP 72044	4560	4.9	-0.25	2.4
HIP 76550	4100	4.7	-1.00	2.0
HIP 78395	4500	5.0	-0.25	3.0
HIP 80083	4200	4.8	-0.75	1.0

Table 2:: continued.

Object	$T_{\rm eff}$ [K]	log$g$ [dex]	[Fe/H] [dex]	$v$sin$i$ [km s^{-1}]
HIP 103150	4040	4.7	-0.75	2.6
HIP 110245	4500	4.7	-0.17	4.0
HIP 110714	4150	4.7	-0.22	2.0
HIP 116011	4390	4.7	-0.65	2.9

Table 3:: Stellar parameters (e.g. T_{eff}, π, M_V, $R_\star$) as well as the values of $v \sin i$ from Paper XIV for our dM2 stars. We computed the projected rotational period $P/\sin i$ as well as [M/H] derived from the [M/H]/radius correlation (Paper XVII).

Star	v (mag)	$(R-I)_C$ (mag)	T_{eff} (K)	Spect. Type	π (m")	M_v (mag)	$R_\star$ ($R_\odot$)	$v \sin i$ km/s	$P/\sin i$ (days)	[M/H] (dex)
GJ 1010A	11.31	1.148	3638 ±100	dM2	50.01±2.02	9.805±0.106	0.517 ±0.065	-	-	-0.098
GJ 1062	13.015	1.184	3602 ±100	sdM2	33±3.6	10.608±0.245	0.372 ±0.076	9.8	1.92-0.53+0.65	-0.584
GJ 1114	11.523	1.148	3638 ±100	dM2	54.53±3.60	10.206±0.144	0.430 ±0.063	3.8	5.73-1.50+2.07	-0.339
GJ 1264	9.641	1.112	3674 ±100	PMS M2e	61.29±1.54	8.578±0.059	0.870 ±0.088	6.46	6.82-1.51+2.06	+0.378
GJ 2085	11.185	1.058	3724 ±100	dM2	46.81±2.39	9.537±0.113	0.525 ±0.067	2.46	10.80-3.23+5.31	+0.000
GJ 3084	10.791	1.064	3718 ±100	dM2	48.83±10.7	9.234±0.435	0.608 ±0.187	3.16	9.74-4.07+5.98	+0.023
GJ 3098	11.155	1.088	3696 ±100	dM2	55.98±1.91	9.895±0.078	0.461 ±0.051	2.60	8.97-2.49+3.98	-0.200
GJ 3207	11.51	1.160	3626 ±100	dM2	57±14	10.289±0.497	0.420 ±0.147	-	-	-0.346
GJ 3340	11.542	1.070	3713 ±100	dM2	44.54±4.06	9.786±0.194	0.475 ±0.081	2.67	9.00-2.91+4.59	-0.048
GJ 3215	11.779	1.148	3638 ±100	dM2	46.29±2.98	10.106±0.140	0.450 ±0.065	-	-	-0.314
GJ 3440	11.75	1.148	3638 ±100	dM2	44±8	9.967±0.383	0.479 ±0.127	2.71	8.95-3.56+5.59	-0.165
GJ 3759	10.929	1.090	3694 ±100	dM2	58.94±2.40	9.781±0.092	0.487 ±0.057	2.71	9.10-2.52+3.95	-0.121
GJ 3778	11.9	1.186	3600 ±100	dM2	44±8	10.117±0.463	0.471 ±0.133	1.72	13.86-6.49+13.4	+0.002
GJ 3915	11.65	1.132	3654 ±100	dM2	26±8	8.725±0.603	0.836 ±0.340	1.88	22.51-12.4+24.0	+0.413
GJ 4155	12.10	1.184	3602 ±100	dM2	44±8	10.317±0.383	0.425 ±0.121	-	-	-0.231
GJ 9381	11.56	1.148	3638 ±100	dM2	38.05±2.85	9.462±0.177	0.606 ±0.099	2.19	14.01-4.81+8.44	+0.100
GL 2	9.949	1.112	3674 ±100	dM2	87.0±1.41	9.647±0.040	0.531 ±0.049	2.76	9.74-2.48+3.85	-0.018
Gl 15A	8.13	1.130	3656 ±100	dM2	278.76±0.77	10.356±0.026	0.392 ±0.033	1.43	13.87-4.92+12.0	-0.386
Gl 16	10.864	1.148	3638 ±100	dM2	61.21±2.12	9.798±0.079	0.519 ±0.057	2.34	11.23-3.27+5.53	-0.105
GL 27.1	11.401	1.078	3705 ±100	dM2	43.64±2.59	9.609±0.145	0.520 ±0.075	2.63	10.01-3.03+4.83	-0.016
Gl 29.1A	11.11	1.136	3650 ±100	dM2e	42.0±2.0	9.226±0.121	0.661 ±0.084	10.6	3.16-0.64+0.77	+0.101
Gl 29.1B	11.11	1.136	3650 ±100	dM2e	42.0±2.0	9.226±0.121	0.661 ±0.084	9.5	3.52-0.74+0.91	+0.101
Gl 49	9.564	1.148	3638 ±100	dM2	99.4±1.4	9.551±0.035	0.582 ±0.051	2.49	11.83-3.13+5.12	+0.026
Gl 63	11.22	1.10	3685 ±100	dM2	61.0±8	10.167±0.288	0.413 ±0.092	< 1	> 20.90	-0.309
Gl 87	10.042	1.112	3674 ±100	dM2	96.02±1.66	9.954±0.042	0.462 ±0.043	3.99	5.86-1.24+1.68	-0.027
Gl 91	10.324	1.175	3611 ±100	dM2	79.68±1.69	9.831±0.051	0.525 ±0.053	1.68	15.82-5.34+11.3	-0.090
GL 114.1A	10.717	1.181	3605 ±100	dM2	77.19±1.64	10.155±0.051	0.456 ±0.046	1.82	12.68-4.11+8.14	-0.242
Gl 130	11.51	1.160	3626 ±100	sdM2	70±7	10.735±0.227	0.341 ±0.060	1.27	13.59-5.98+16.7	-0.766
Gl 133	11.21	1.208	3579 ±100	dM2	71.21±1.56	10.473±0.067	0.409 ±0.045	< 1	> 20.70	-0.466
Gl 134	10.29	1.124	3662 ±100	dM2	57.8±2.20	9.100±0.101	0.695 ±0.078	2.53	13.90-3.93+6.37	+0.128
Gl 140AB	10.422	1.160	3626 ±100	dM2	51.31±4.66	9.726±0.194	0.544 ±0.094	9.4	2.93-0.74+0.92	-0.002
Gl 150.1B	10.763	1.112	3674 ±100	dM2	59.92±2.39	9.651±0.090	0.531 ±0.062	3.7	7.26-1.74+2.42	-0.084
Gl 153B	10.79	1.16	3626 ±100	dM2	57.5±2.68	9.588±0.119	0.580 ±0.077	1.4	20.97-8.24+20.6	+0.017
Gl 155.1	11.044	1.063	3719 ±100	dM2	59.36±2.42	9.911±0.092	0.444 ±0.052	2.93	7.67-2.05+3.10	+0.175
Gl 162	10.17	1.076	3707 ±100	dM2	74.37±2.71	9.527±0.098	0.539 ±0.065	2.35	11.61-3.48+5.86	+0.019
Gl 173	10.331	1.196	3590 ±100	dM2	90.10±1.74	10.105±0.047	0.477 ±0.048	2.35	10.27-2.91+4.91	-0.225
Gl 191	8.853	1.058	3724 ±100	sdM2	255.66±0.91	10.891±0.013	0.281 ±0.022	9.15	1.55-0.26+0.33	-1.024
Gl 205	7.967	1.100	3685 ±100	dM2	176.77±1.18	9.204±0.019	0.643 ±0.052	2.73	11.92-2.94+4.59	+0.101
Gl 212	9.779	1.052	3729 ±100	dM2	80.40±1.69	9.298±0.051	0.581 ±0.056	1.98	14.85-4.55+8.51	+0.067
Gl 218	10.736	1.151	3635 ±100	dM2	66.54±1.43	9.851±0.051	0.508 ±0.049	1.66	15.49-5.21+11.1	-0.099
Gl 229	8.125	1.064	3718 ±100	dM2	173.81±0.99	9.325±0.017	0.583 ±0.046	2.63	11.22-2.80+4.46	+0.060
Gl 250B	10.05	1.268	3526 ±100	dM2	108.9±5.4	10.235±0.125	0.495 ±0.070	-	-	-0.247
Gl 275.1	10.84	1.076	3707 ±100	dM2	39.75±2.28	8.837±0.141	0.740 ±0.106	2.7	13.87-4.14+6.51	+0.172
Gl 289	11.418	1.148	3638 ±100	sdM2	67.69±2.65	10.571±0.088	0.363 ±0.042	< 1	> 18.37	-0.741
Gl 330	10.593	1.100	3685 ±100	dM2	58.79±2.72	9.440±0.103	0.580 ±0.071	3.05	9.62-2.57+3.82	+0.023
Gl 361	10.370	1.208	3579 ±100	dM2	88.81±1.68	10.112±0.046	0.483 ±0.048	1.95	12.54-3.90+7.37	-0.212
Gl 366	10.635	1.112	3674 ±100	dM2	61.68±1.42	9.586±0.054	0.547 ±0.054	< 1	> 27.69	-0.014
Gl 378	10.11	1.256	3537 ±100	dM2	67.1±1.7	9.244±0.074	0.769 ±0.088	2.25	17.30-5.20+8.99	+0.096
Gl 382	9.264	1.184	3602 ±100	dM2	127.08±1.90	9.784±0.037	0.544 ±0.051	2.9	9.49-2.37+3.60	-0.059
Gl 390	10.139	1.112	3674 ±100	dM2	81.00±1.91	9.681±0.056	0.524 ±0.052	2.46	10.78-2.97+4.89	-0.030
Gl 411	7.508	1.184	3602 ±100	dM2	392.64±0.67	10.478±0.0087	0.395 ±0.032	0.61	32.77-11.9+30.8	-0.442
Gl 412A	8.798	1.076	3707 ±100	dM2	206.27±1.00	10.370±0.015	0.365 ±0.029	1.6	11.55-3.82+8.40	-0.435
Gl 430.1	10.270	1.060	3722 ±100	dM2	62.92±1.45	9.264±0.054	0.597 ±0.058	0.46	65.7-28.3+108	+0.089
Gl 433	9.813	1.160	3626 ±100	dM2	112.58±1.44	10.070±0.032	0.465 ±0.041	< 1	> 23.54	-0.199
Gl 450	9.762	1.136	3650 ±100	dM2	116.48±1.19	10.093±0.027	0.446 ±0.038	2.47	9.14-2.41+3.96	-0.247
Gl 477	11.092	1.190	3596 ±100	dM2	52.67±3.05	9.700±0.127	0.570 ±0.080	1.95	14.79-5.07+9.57	-0.057
Gl 490A	10.57	1.088	3696 ±100	dM2e	51.93±3.00	9.178±0.142	0.642 ±0.092	8.4	3.87-0.91+1.15	+0.078
Gl 494AB	9.757	1.112	3674 ±100	dM2e	85.54±1.53	10.171±0.043	0.418 ±0.039	9.75	2.17-0.39+0.47	-0.339
Gl 507.1	10.617	1.160	3626 ±100	dM2	58.86±1.49	9.466±0.059	0.614 ±0.062	2.32	13.39-3.83+6.49	+0.065
Gl 508.2	10.66	1.100	3685 ±100	dM2	62.33±1.76	9.633±0.080	0.528 ±0.058	1.78	15.01-5.01+10.1	-0.002
Gl 510	11.015	1.172	3614 ±100	dM2	59.72±2.43	9.896±0.092	0.508 ±0.062	2.49	10.33-3.02+4.93	-0.162
Gl 514	9.039	1.076	3707 ±100	dM2	130.62±1.05	9.619±0.022	0.516 ±0.042	2.07	12.62-3.63+6.59	-0.030
Gl 521	10.243	1.100	3685 ±100	dM2	76.87±1.61	9.672±0.050	0.518 ±0.050	0.85	30.84-9.69+18.7	-0.017
Gl 526	8.464	1.124	3662 ±100	dM2	185.49±1.10	9.806±0.018	0.502 ±0.040	1.00	25.41-6.99+12.1	-0.086
Gl 536	9.707	1.112	3674 ±100	dM2	99.72±1.57	9.701±0.039	0.519 ±0.047	< 1	> 26.27	-0.032
Gl 537AB	9.16	1.076	3707 ±100	dM2	89.1±4.3	9.662±0.122	0.506 ±0.067	3.6	7.11-1.82+2.55	-0.046
Gl 540	10.37	1.076	3707 ±100	dM2	59.10±1.18	9.228±0.063	0.618 ±0.063	2.09	14.97-4.52+8.16	+0.073
Gl 552	10.676	1.208	3579 ±100	dM2	71.39±2.10	9.944±0.068	0.522 ±0.058	0.58	45.55-17.9+49.1	-0.100
Gl 563.2A	11.656	1.124	3662 ±100	sdM2	235.2±22.4	13.513±0.202	0.091 ±0.016	2.24	2.06-0.72+1.24	-1.742
Gl 563.2B	12.066	1.196	3590 ±100	sdM2	221.8±22.4	13.796±0.214	0.087 ±0.016	1.82	2.42-0.93+1.85	-1.754

Table 3:: continued.

Star	v (mag)	$(R-I)_C$ (mag)	T_{eff} (K)	Spect. Type	π (m")	M_v (mag)	$R_\star$ ($R_\odot$)	$v \sin i$ km/s	$P/\sin i$ (days)	[M/H] (dex)
Gl 618.4	11.783	1.156	3630 ±100	dM2	41.77±3.59	9.887±0.184	0.503 ±0.084	1.45	17.56-7.21+17.4	-0.119
Gl 634	11.58	1.184	3602 ±100	dM2	54±5	10.242±0.212	0.440 ±0.082	< 0.6	> 37.12	-0.303
Gl 637	11.326	1.105	3681 ±100	dM2	62.97±1.99	10.322±0.073	0.387 ±0.042	2.19	8.94-2.68+4.71	-0.415
Gl 645	11.44	1.122	3664 ±100	dM2	55±6	10.142±0.245	0.429 ±0.086	2.80	7.75-2.64+4.09	-0.257
Gl 649	9.676	1.088	3696 ±100	dM2	96.67±1.39	9.602±0.036	0.528 ±0.047	2.27	11.77-3.29+5.65	-0.020
Gl 654AB	10.071	1.172	3614 ±100	dM2	94.59±1.85	9.950±0.047	0.495 ±0.049	5.7	4.40-1.02+1.46	-0.090
Gl 672.1	11.635	1.119	3667 ±100	dM2	41.78±4.12	9.740±0.209	0.514 ±0.092	2.99	8.70-2.75+4.13	-0.086
Gl 686	9.599	1.112	3674 ±100	dM2	123.67±1.61	10.060±0.033	0.440 ±0.038	2.49	8.94-2.35+3.85	-0.245
Gl 701	9.367	1.100	3685 ±100	dM2	128.89±1.43	9.918±0.029	0.463 ±0.040	1.6	14.65-4.91+10.8	-0.169
Gl 724	10.630	1.088	3696 ±100	dM2	61.15±2.07	9.562±0.077	0.538 ±0.059	2.97	9.17-2.37+3.58	-0.005
Gl 737B	10.13	1.094	3691 ±100	dM2	69±8	9.324±0.258	0.604 ±0.125	-	-	+0.134
Gl 745A	10.774	1.196	3590 ±100	sdM2	117.45±2.28	11.123±0.047	0.298 ±0.030	3.0	5.03-1.25+1.89	-1.03
Gl 745B	10.771	1.196	3590 ±100	sdM2	114.25±2.30	11.060±0.048	0.307 ±0.031	2.8	5.55-1.44+2.22	-1.07
Gl 767A	9.760	1.148	3638 ±100	dM2	74.9±2.9	9.132±0.087	0.705 ±0.082	2.9	12.30-3.29+5.01	+0.126
Gl 781	11.975	1.064	3718 ±100	sdM2e	63.17±3.82	10.978±0.132	0.272 ±0.038	12.7	1.08-0.22+0.25	-1.10
Gl 800A	10.735	1.100	3685 ±100	dM2	55.72±2.38	9.465±0.096	0.570 ±0.068	2.34	12.33-3.68+6.22	-0.113
Gl 803	8.794	1.100	3685 ±100	PMS M2e	100.91±1.06	8.814±0.028	0.770 ±0.065	9.68	4.03-0.68+0.84	+0.154
Gl 806	10.79	1.196	3590 ±100	dM2	81.17±1.73	10.305±0.063	0.435 ±0.047	0.46	47.86-20.9+80.5	-0.336
Gl 808	11.86	1.184	3602 ±100	sdM2	56±8	10.591±0.310	0.375 ±0.090	1.27	14.94-7.23+20.1	-0.882
Gl 809	8.575	1.064	3718 ±100	dM2	141.87±0.64	9.336±0.022	0.580 ±0.047	2.66	11.04-2.76+4.36	+0.067
Gl 815AB	10.12	1.184	3602 ±100	dM2e	65.40±1.84	9.951±0.080	0.503 ±0.059	7.61	3.35-0.73+0.95	-0.167
Gl 821	10.869	1.112	3674 ±100	sdM2	82.18±2.17	10.443±0.059	0.369 ±0.037	2.63	7.10-1.89+3.02	-0.484
Gl 832	8.663	1.196	3590 ±100	dM2	201.87±1.01	10.195±0.019	0.458 ±0.039	-	-	-0.268
Gl 842	9.737	1.039	3741 ±100	dM2	84.26±1.74	9.365±0.049	0.556 ±0.053	2.80	10.05-2.56+3.96	+0.050
Gl 855	10.708	1.052	3729 ±100	dM2	51.57±1.98	9.270±0.087	0.589 ±0.067	2.99	9.97-2.61+3.92	+0.049
Gl 863	10.373	1.076	3707 ±100	dM2	78.68±2.69	9.852±0.078	0.464 ±0.051	2.64	8.90-2.44+3.88	-0.132
Gl 867A	9.074	1.196	3590 ±100	dM2e	115.01±1.32	9.378±0.030	0.667 ±0.061	7.02	4.81-0.98+1.31	+0.080
Gl 880	8.657	1.124	3662 ±100	dM2	146.09±1.00	9.480±0.020	0.583 ±0.047	2.07	14.25-4.09+7.43	+0.040
Gl 887	7.351	1.088	3696 ±100	dM2	305.26±0.70	9.765±0.011	0.490 ±0.037	-	-	-0.092
Gl 895	10.033	1.112	3674 ±100	dM2	77.15±1.29	9.470±0.041	0.577 ±0.053	0.52	56.16-22.6+71.4	+0.049
Gl 908	8.993	1.100	3685 ±100	dM2	167.29±1.23	10.110±0.017	0.424 ±0.033	2.25	9.54-2.59+4.48	-0.271
St 497	10.59	1.112	3674 ±100	dM2e	68±12	9.753±0.373	0.507 ±0.138	6.5	3.95-1.45+1.98	-0.027
St 928	10.85	1.136	3650 ±100	dM2	68±12	10.013±0.373	0.463 ±0.127	2.1	11.16-4.86+8.74	-0.176
G192-11A	10.255	1.076	3707 ±100	dM2	73.89±1.64	9.598±0.053	0.521 ±0.051	2.6	10.14-2.71+4.33	-0.009
MCC 354A	10.91	1.184	3602 ±100	dM2	51.05±1.75	9.450±0.093	0.634 ±0.078	2.47	12.99-3.82+6.27	+0.109
MCC 452	10.264	1.064	3718 ±100	dM2	50.80±3.74	9.793±0.159	0.470 ±0.071	-	-	+0.360
MCC 488	11.20	1.076	3707 ±100	dM2	37.21±2.45	9.053±0.158	0.670 ±0.102	3.2	10.60-3.03+4.43	+0.113
LHS 1155	12.65	1.196	3590 ±100	dM2	-	-	-		-	-

Table 4:: Stellar parameters (e.g. T_{eff}, π, M_V, $R_\star$) as well as the values of $v \sin i$ from HM and [M/H] compiled from the literature for our targets in our list of dM3 stars. We computed the projected rotational period $P/\sin i$ as well as [M/H] derived from the [M/H]/radius correlation.

Star	v (mag)	$(R-I)_C$ (mag)	Teff (K)	Spect. Type	π (m")	Mv (mag)	$R_\star$ ($R_\odot$)	$v \sin i$ (km/s)	$P/\sin i$ (days)	[M/H] (dex)	[M/H][1] (dex)
GJ 1046	11.595	1.292	3506 ±100	dM3	71.06±3.23	10.85±0.101	0.385±0.050	2.63	7.41-1.1+1.2	-	-0.078
GJ 1050	11.730	1.322	3484 ±100	dM3	66±13	10.83±0.435	0.404±0.128	0.59	34.4-18+310	-1.20	-0.035
GJ 1054B	13.095	1.363	3456 ±100	dM3e	52.08±2.13	11.68±0.091	0.288±0.036	32.13	0.45-0.07+0.08	-0.09	-0.323
GJ 1077AB	11.91	1.38	3444 ±100	dM3	77.5±11	12.11±0.308	0.243±0.060	-	-	-0.64	-0.499
GJ 1080	12.81	1.344	3469 ±100	dM3	50±3	11.30±0.150	0.334±0.052	-	-	-0.44	-0.187
GJ 1097	11.456	1.400	3431 ±100	dM3	81.38±2.49	11.01±0.068	0.415±0.048	<0.5	>41.91	-0.05	-0.033
GJ 1110AB	13.08	1.324	3482 ±100	dM3	45.2±3.2	12.11±0.168	0.225±0.037	-	-	-0.71	-0.579
GJ 1125	11.710	1.125	3661 ±100	sdM3	103.46±3.94	11.78±0.085	0.202±0.023	0.99	10.3-2.9+8.3	-0.16	-0.691
GJ 1146	13.57	1.388	3439 ±100	sdM3	54.2±4.2	12.24±0.189	0.231±0.041	-	-	-0.56	-0.552
GJ 1197	13.25	1.304	3496 ±100	dM3	45.9±3.7	11.56±0.195	0.282±0.051	-	-	-0.12	-0.342
GJ 1200AB	12.93	1.419	3415 ±100	dM3	55.9±3.3	12.42±0.148	0.222±0.035	-	-	-0.57	-0.592
GJ 1202	12.76	1.401	3430 ±100	dM3	53.5±2.9	11.40±0.138	0.346±0.053	-	-	-0.22	-0.166
GJ 1203	12.158	1.352	3463 ±100	dM3	59.63±3.55	11.04±0.131	0.381±0.056	0.82	23.5-7.1+18	-	-0.087
GJ 1209	12.25	1.300	3499 ±100	dM3	58.2±3.2	11.07±0.140	0.351±0.052	-	-	-0.12	-0.157
GJ 1212A	12.032	1.403	3428 ±100	dM3	53.41±4.76	11.42±0.196	0.344±0.063	0.69	25.3-9.6+57	-	-0.170
GJ 1212B	12.032	1.403	3428 ±100	dM3	53.41±4.76	11.42±0.196	0.344±0.063	0.90	19.3-7.1+13	-	-0.170
GJ 1271	11.704	1.298	3500 ±100	dM3	47.52±2.82	10.09±0.131	0.552±0.080	1.39	20.0-5.1+7.7	0.15	+0.127
GJ 1292	11.72	1.425	3410 ±100	dM3	72.8±2.7	11.03±0.101	0.425±0.056	-	-	0.89	-0.030
GJ 2121	12.280	1.386	3440 ±100	dM3	44.58±5.36	10.53±0.264	0.508±0.112	2.06	12.5-3.1+4.2	0.14	+0.059
GJ 3139	11.770	1.333	3476 ±100	dM3	50.68±2.53	10.29±0.110	0.524±0.071	0.90	29.4-7.8+14	0.47	+0.084
GJ 3160A	12.01	1.292	3506 ±100	dM3	38.45±3.15	10.69±0.198	0.415±0.071	0.95	22.0-6.2+9.9	-0.07	-0.033
GJ 3160B	12.01	1.292	3506 ±100	dM3	38.45±3.15	10.69±0.198	0.415±0.071	1.06	19.8-5.3+7.4	-0.07	-0.033
GJ 3189	12.67	1.318	3487 ±100	sdM3	95.5±10.9	12.57±0.269	0.180±0.040	1.42	6.43-1.8+1.6	-0.60	-0.801
GJ 3242	12.70	1.336	3474 ±100	dM3	54±10	11.36±0.427	0.322±0.101	-	-	0.18	-0.212
GJ 3279	11.8	1.324	3482 ±100	dM3	65±13	10.86±0.640	0.399±0.179	0.85	23.7-13+26	-	-0.045
GJ 3293	12.0	1.308	3493 ±100	dM3	55±9	10.70±0.559	0.421±0.166	0.85	25.0-12+25	0.11	-0.031
GJ 3404A	11.73	1.412	3421 ±100	dM3	64±9	10.76±0.327	0.473±0.122	0.90	26.5-9.8+17	0.12	-0.005
GJ 3412A	11.028	1.393	3435 ±100	sdM3	95.43±2.36	11.68±0.056	0.301±0.033	-	-	-	-0.280
GJ 3412B	11.028	1.393	3435 ±100	sdM3	95.43±2.36	11.68±0.056	0.301±0.033	-	-	-	-0.280
GJ 3447B	13.48	1.288	3509 ±100	dM3	30.57±3.72	10.92±0.286	0.372±0.085	-	-	-0.09	-0.108
GJ 3459	11.712	1.390	3437 ±100	sdM3	94.31±3.31	11.58±0.078	0.314±0.038	0.69	23.1-7.7+48	-0.20	-0.238
GJ 3501B	12.36	1.313	3490 ±100	dM3	37.95±2.70	10.26±0.175	0.520±0.088	-	-	-0.26	+0.078
GJ 3508	11.749	1.319	3486 ±100	dM3	52.74±3.69	10.36±0.154	0.500±0.079	-	-	-0.01	+0.047
GJ 3528	11.728	1.300	3499 ±100	dM3	51.25±3.72	10.28±0.160	0.507±0.081	0.90	28.4-8.1+15	-	+0.057
GJ 3553	13.335	1.394	3435 ±100	sdM3	60.8±4.2	12.25±0.152	0.232±0.037	-	-	-0.28	-0.548
GJ 3563	11.953	1.311	3491 ±100	dM3	63.47±3.54	10.97±0.123	0.374±0.053	0.85	22.2-6.3+14	-	-0.104
GJ 3598	12.46	1.292	3506 ±100	dM3	45±9	10.73±0.460	0.408±0.136	0.69	30.0-15+80	-	-0.035
GJ 3634	11.95	1.291	3507 ±100	dM3	56±11	10.69±0.452	0.414±0.136	0.85	24.6-11+22	-0.15	-0.033
GJ 3643	12.369	1.346	3467 ±100	dM3	50.90±4.58	10.90±0.198	0.403±0.073	1.00	20.4-5.7+9.0	-0.11	-0.036
GJ 3708A	11.709	1.376	3447 ±100	dM3	79.43±2.36	11.21±0.067	0.366±0.042	0.50	37.0-17+∞	-0.01	-0.122
GJ 3747	12.600	1.401	3430 ±100	dM3	52±13	11.18±0.557	0.384±0.152	-	-	-0.27	-0.080
GJ 3795	12.5	1.367	3453 ±100	dM3	50±12	10.99±0.732	0.396±0.202	-	-	0.18	-0.052
GJ 3810	12.730	1.413	3420 ±100	dM3	48±11	11.14±0.509	0.398±0.146	-	-	0.13	-0.047
GJ 3836	11.82	1.347	3467 ±100	dM3	61.3±4.6	10.76±0.183	0.431±0.075	-	-	0.18	-0.029
GJ 3842	11.79	1.313	3490 ±100	dM3e	49±10	10.24±0.469	0.524±0.177	-	-	0.03	+0.084
GJ 3846	12.257	1.399	3431 ±100	sdM3	70.03±4.89	11.48±0.154	0.333±0.053	0.82	20.5-6.4+16	-0.12	-0.189
GJ 3892	11.473	1.340	3472 ±100	dM3	69.19±2.60	10.67±0.084	0.444±0.054	0.82	27.4-7.6+20	-	-0.026
GJ 3895	13.45	1.427	3408 ±100	dM3	42.3±3.1	11.58±0.179	0.331±0.058	-	-	-0.24	-0.193
GJ 3916A	11.279	1.306	3495 ±100	dM3	66.21±3.18	11.13±0.106	0.345±0.045	1.24	14.1-3.1+3.8	0.02	-0.168
GJ 3916B	11.279	1.306	3495 ±100	dM3	66.21±3.18	11.13±0.106	0.345±0.045	3.51	4.97-0.7+0.7	0.02	-0.168
GJ 4004	12.1	1.455	3384 ±100	sdM3	81±16	11.64±0.635	0.335±0.151	0.59	28.6-18+290	-	-0.186
GJ 4026	12.67	1.408	3424 ±100	dM3	69.2±2.4	11.87±0.095	0.282±0.037	-	-	-0.34	-0.342
GJ 4048A	11.87	1.363	3456 ±100	dM3	88.0±3.6	11.59±0.109	0.299±0.040	-	-	-0.13	-0.287
GJ 4117	12.20	1.291	3507 ±100	dM3	72.1±7.3	11.49±0.241	0.287±0.058	-	-	0.78	-0.326
GJ 4129	11.95	1.304	3496 ±100	dM3	63.1±3.8	10.95±0.151	0.374±0.058	0.50	37.9-18+∞	-0.26	-0.104
GJ 4149	11.96	1.288	3509 ±100	dM3	37.20±10.98	9.81±0.681	0.618±0.293	-	-	0.04	+0.229
GJ 4176A	12.29	1.376	3447 ±100	dM3	59±8	11.14±0.316	0.377±0.094	-	-	-0.03	-0.096
GJ 4231	12.11	1.388	3439 ±100	dM3e	64±13	11.14±0.467	0.384±0.131	80.00	0.24-0.08+0.09	-	-0.080
GJ 4282AB	12.41	1.401	3430 ±100	dM3e	59±12	11.26±0.468	0.369±0.126	15.00	1.25-0.48+0.54	-0.16	-0.115
GJ 4368	11.50	1.362	3457 ±100	dM3	77±16	10.93±0.478	0.405±0.139	-	-	0.16	-0.035
GJ 9801B	13.52	1.407	3425 ±100	dM3	37.25±0.76	11.37±0.064	0.354±0.040	-	-	-0.23	-0.150
Gl 12	12.61	1.415	3418 ±100	sdM3	84±11	12.23±0.306	0.241±0.059	0.95	12.8-4.4+6.9	-0.26	-0.508
GL 48	9.99	1.363	3456 ±100	dM3e	121.41±1.25	10.41±0.042	0.516±0.052	2.45	10.7-2.9+4.9	0.04	+0.071
Gl 70	10.915	1.274	3521 ±100	dM3	87.62±2.00	10.63±0.052	0.416±0.043	1.01	20.8-5.4+10	-0.17	-0.033
GL 84	10.189	1.290	3507 ±100	dM3	109.38±1.92	10.38±0.040	0.476±0.047	-	-	-0.08	-0.094
GL 100C	12.84	1.351	3464 ±100	dM3	51.16±1.33	11.38±0.076	0.324±0.038	-	-	-0.28	-0.205
Gl 109	10.563	1.376	3447 ±100	dM3	133.16±2.26	11.18±0.039	0.370±0.037	1.34	13.9-3.2+4.8	-0.12	-0.113
GL 118.1B	12.97	1.357	3460 ±100	dM3	34.58±0.85	10.66±0.073	0.455±0.053	-	-	-0.10	-0.023
Gl 119B	11.65	1.313	3490 ±100	dM3	44.8±3.9	9.91±0.201	0.610±0.111	4.00	7.72-2.2+3.0	-	+0.217
GL 120AB	13.04	1.407	3425 ±100	sdM3	54±12	12.45±0.456	0.215±0.052	-	-	-0.57	-0.626

Table 4:: continued.

Star	v (mag)	$(R-I)_C$ (mag)	Teff (K)	Spect. Type	π (m")	Mv (mag)	$R_\star$ ($R_\odot$)	$v \sin i$ (km/s)	$P/\sin i$ (days)	[M/H] (dex)	[M/H][1] (dex)
GL 121.1	11.792	1.304	3496 ±100	dM3e	51.08±3.99	10.33±0.172	0.496±0.083	-	-	-0.02	+0.040
Gl 140C	11.89	1.288	3509 ±100	dM3	60±8	10.78±0.292	0.396±0.092	6.70	2.99-1.0+1.3	-	-0.052
Gl 145	11.47	1.339	3472 ±100	sdM3	93.11±1.94	11.31±0.065	0.330±0.037	0.85	19.6-5.1+12	-0.28	-0.194
Gl 163	11.811	1.416	3417 ±100	dM3	66.69±1.82	10.93±0.061	0.439±0.049	0.85	26.0-6.8+16	-0.02	-0.027
GL 173.1B	14.19	1.401	3430 ±100	dM3	32.69±1.51	11.76±0.120	0.293±0.042	-	-	-0.33	-0.307
Gl 204.2	12.010	1.343	3470 ±100	dM3	49±5	10.46±0.224	0.491±0.096	0.69	36.1-14+83	-	+0.033
Gl 207.1	11.53	1.335	3475 ±100	dM3e	62.75±4.02	10.52±0.159	0.474±0.076	9.52	2.51-0.4+0.4	0.09	+0.006
Gl 226	10.50	1.309	3493 ±100	dM3	106.69±1.31	10.64±0.047	0.434±0.044	1.12	19.6-5.1+9.0	-	-0.028
GL 228AB	10.42	1.313	3490 ±100	dM3	91.65±3.50	10.98±0.103	0.373±0.049	-	-	-0.04	-0.106
Gl 238	11.592	1.331	3478 ±100	dM3	60.77±1.94	10.51±0.071	0.473±0.054	0.85	28.0-7.3+17	-	+0.005
Gl 251AB	10.01	1.425	3410 ±100	sdM3	179.01±1.60	12.03±0.039	0.268±0.038	1.14	16.9-4.4+7.5	-0.45	-0.388
GL 257AB	10.846	1.420	3414 ±100	dM3e	124.85±2.13	11.33±0.039	0.368±0.037	-	-	-0.15	-0.118
GL 268.3	10.87	1.388	3439 ±100	dM3	93.09±2.84	10.71±0.086	0.467±0.058	-	-	-0.14	-0.005
GL 277A	10.57	1.376	3447 ±100	PMS M3e	84.26±3.45	10.20±0.109	0.583±0.080	8.00	3.69-0.86+1.1	0.10	+0.175
GL 298	11.745	1.398	3432 ±100	dM3	60.68±2.48	10.66±0.091	0.485±0.062	1.00	24.6-5.7+9.2	-	+0.023
GL 319C	11.76	1.338	3473 ±100	dM3	66.96±3.91	10.89±0.147	0.401±0.062	-	-	0.04	-0.040
GL 326AB	11.89	1.390	3437 ±100	dM3	77±11	11.32±0.332	0.354±0.092	-	-	-0.25	-0.150
GL 333.2A	12.36	1.380	3444 ±100	dM3	40.77±6.57	10.41±0.373	0.531±0.151	-	-	0.01	+0.095
GL 333.2B	12.688	1.410	3422 ±100	dM3	47.75±7.95	11.08±0.367	0.406±0.114	-	-	0.01	-0.035
GL 347A	12.104	1.333	3476 ±100	dM3e	61.58±3.98	11.05±0.143	0.370±0.056	-	-	0.02	-0.113
GL 350B	14.27	1.338	3473 ±100	dM3	29.51±2.39	11.62±0.196	0.286±0.052	-	-	-0.03	-0.329
GL 352	10.067	1.336	3474 ±100	dM3	99.88±3.60	10.06±0.080	0.585±0.070	0.90	7.6-1.0+1.0	-0.01	+0.178
Gl 357	10.906	1.280	3516 ±100	sdM3	110.82±1.92	11.13±0.040	0.333±0.032	1.21	18.7-4.3+8.2	-0.19	-0.189
Gl 358	10.694	1.356	3461 ±100	dM3e	105.63±1.64	10.81±0.036	0.425±0.041	1.10	17.7-3.3+4.2	-0.01	-0.030
Gl 377	11.440	1.364	3455 ±100	dM3	61.39±2.55	10.38±0.092	0.524±0.066	-	24.1-5.4+7.2	0.40	+0.084
GL 381	10.629	1.274	3521 ±100	dM3e	81.08±2.87	10.17±0.079	0.513±0.060	-	-	-0.07	+0.067
Gl 386	10.998	1.329	3479 ±100	dM3	73.30±2.62	10.32±0.080	0.514±0.061	0.69	37.8-12+79	0.17	+0.068
Gl 388	9.32	1.420	3414 ±100	dM3e	213.00±4.00	10.96±0.061	0.436±0.049	2.63	8.38-1.1+1.2	0.08	-0.028
Gl 399	11.281	1.280	3516 ±100	dM3	60.80±3.14	10.20±0.114	0.511±0.069	0.59	43.6-17+330	0.15	+0.064
Gl 408	10.020	1.338	3473 ±100	dM3	150.10±1.70	10.90±0.027	0.399±0.037	1.12	18.1-4.6+8.1	-0.12	-0.045
GL 414.1AB	10.88	1.351	3464 ±100	dM3	59.16±2.54	10.49±0.113	0.490±0.067	-	-	0.07	+0.031
Gl 422	11.516	1.395	3434 ±100	dM3	78.91±2.60	11.00±0.074	0.413±0.049	0.90	23.1-5.8+11	-	-0.033
Gl 436	10.66	1.351	3464 ±100	dM3	98.8±2.9	10.63±0.084	0.458±0.055	0.86	27.0-9.0+26	-0.02	-0.019
Gl 443	11.700	1.360	3458 ±100	dM3	50.02±3.10	10.20±0.137	0.567±0.084	0.90	31.8-8.7+16	0.35	+0.150
Gl 452A	11.894	1.363	3456 ±100	dM3	51.10±3.58	10.44±0.154	0.510±0.081	0.95	27.1-7.3+12	0.12	+0.062
Gl 452.1	12.74	1.424	3410 ±100	sdM3e	92±12	12.56±0.305	0.210±0.051	1.60	6.66-1.9+2.2	-	-0.651
GL 455AB	12.83	1.419	3415 ±100	dM3	55±12	11.53±0.502	0.237±0.084	-	-	-1.10	-0.526
Gl 463	11.58	1.338	3473 ±100	dM3	54.54±2.03	10.26±0.101	0.535±0.069	1.17	23.1-6.4+10	-	+0.101
Gl 479	10.663	1.357	3460 ±100	dM3	103.18±2.31	10.73±0.051	0.442±0.046	1.06	21.1-4.4+6.3	0.54	-0.026
Gl 480	11.502	1.423	3411 ±100	dM3	69.59±2.79	10.71±0.089	0.491±0.062	0.73	34.0-12+53	0.15	+0.033
GL 507B	12.12	1.376	3447 ±100	dM3	75.38±1.54	11.51±0.064	0.319±0.036	-	-	-0.14	-0.221
GL 512A	11.336	1.394	3435 ±100	dM3e	72.00±2.83	10.62±0.087	0.491±0.062	-	-	0.12	+0.033
Gl 513	11.92	1.412	3421 ±100	dM3	62.9±6.7	10.91±0.252	0.441±0.094	0.77	29.0-11+39	-0.20	-0.027
GL 581	10.56	1.409	3423 ±100	dM3e	160.91±2.62	11.59±0.055	0.321±0.035	-	-	-0.15	-0.215
Gl 588	9.311	1.326	3481 ±100	dM3	168.66±1.30	10.45±0.019	0.484±0.042	0.77	31.8-8.3+35	0.07	+0.022
GL 589A	12.37	1.308	3493 ±100	dM3	69±3	11.56±0.114	0.283±0.039	-	-	-0.25	-0.339
Gl 595AB	11.855	1.410	3422 ±100	sdM3	95.90±5.59	11.76±0.129	0.297±0.044	1.62	9.25-2.1+2.8	-0.13	-0.293
Gl 617B	10.69	1.376	3447 ±100	dM3	93.09±1.48	10.53±0.055	0.499±0.054	1.12	22.6-6.0+11	-0.54	+0.045
Gl 618A	10.586	1.370	3451 ±100	dM3	130.0±8.2	11.16±0.139	0.369±0.055	0.82	22.8-6.9+18	-0.08	-0.115
Gl 623	10.26	1.300	3499 ±100	dM3	124.12±1.16	10.73±0.040	0.412±0.040	0.94	22.3-6.4+16	-	-0.034
Gl 634	12.73	1.376	3447 ±100	sdM3	54±5	11.39±0.222	0.337±0.066	1.00	17.1-5.0+7.8	-	-0.182
Gl 644A	9.023	1.370	3451 ±100	dM3e	161.41±5.64	10.81±0.078	0.433±0.051	1.79	12.2-2.0+2.2	-0.21	-0.029
Gl 644B	9.023	1.370	3451 ±100	dM3e	161.41±5.64	10.81±0.078	0.433±0.051	2.78	7.88-1.1+1.1	-0.21	-0.029
Gl 655	11.677	1.376	3447 ±100	dM3	74.84±3.07	11.05±0.091	0.394±0.050	<0.5	>39.88	-	-0.057
Gl 660A	11.393	1.425	3410 ±100	dM3	98.19±12.09	11.35±0.271	0.367±0.083	0.82	22.6-8.3+20	-0.22	-0.120
GL 661AB	9.40	1.410	3422 ±100	dM3	167.29±5.02	11.27±0.084	0.373±0.066	-	-	-0.38	-0.106
Gl 671	11.37	1.326	3481 ±100	dM3	80.77±1.66	10.91±0.065	0.392±0.043	0.94	21.2-6.3+15	-0.15	-0.061
Gl 674	9.407	1.330	3478 ±100	dM3	220.24±1.42	11.12±0.019	0.357±0.031	0.90	20.0-4.5+8.6	-0.46	-0.143
Gl 687AB	9.22	1.410	3422 ±100	dM3	220.84±0.94	11.69±0.029	0.434±0.042	0.73	30.3-11+130	-0.01	-0.028
Gl 693	10.783	1.412	3421 ±100	sdM3	171.48±2.31	11.95±0.031	0.273±0.026	0.82	16.8-4.3+12	-0.30	-0.372
Gl 694	10.45	1.313	3490 ±100	dM3	105.50±1.18	10.57±0.044	0.451±0.045	1.29	17.7-4.2+6.2	-0.01	-0.024
GL 712	12.60	1.413	3420 ±100	dM3	72±3	11.89±0.111	0.282±0.039		-	-0.48	-0.342
Gl 725AB	8.90	1.390	3437 ±100	sdM3	280.18±2.18	11.89±0.037	0.273±0.027	0.85	22.5-7.0+18.4	-0.57	-0.372
Gl 735A	10.194	1.368	3452 ±100	dM3e	84.94±1.72	10.59±0.046	0.478±0.048	1.86	13.0-2.0+2.4	0.09	+0.012
Gl 735B	10.194	1.368	3452 ±100	dM3e	84.94±1.72	10.59±0.046	0.478±0.048	1.83	13.2-2.1+3.1	0.09	+0.012
Gl 739	11.142	1.298	3500 ±100	dM3	70.95±2.56	10.40±0.080	0.478±0.057	3.19	7.59-1.0+1.0	-	+0.012
Gl 752A	9.115	1.287	3510 ±100	dM3	170.36±1.00	10.27±0.015	0.499±0.043	1.19	21.2-4.3+6.7	0.05	+0.045
GL 781.1A	12.22	1.395	3434 ±100	dM3e	67.08±5.02	11.35±0.183	0.351±0.062	9.20	1.93-0.50+0.62	-0.07	-0.157
GL 791	11.433	1.357	3460 ±100	dM3e	67.38±3.01	10.58±0.099	0.474±0.061	-	-	0.06	+0.062
Gl 793	10.55	1.388	3439 ±100	dM3	125.07±1.08	11.04±0.039	0.403±0.040	1.26	16.2-4.0+5.9	-0.09	-0.036
GL 811.1	11.487	1.331	3478 ±100	dM3e	65.29±3.11	10.56±0.106	0.462±0.061	-	-	0.11	-0.012
GL 813	12.013	1.288	3509 ±100	dM3	72.58±3.16	11.32±0.097	0.309±0.039	-	-	-0.33	-0.254
GL 816	11.219	1.319	3486 ±100	dM3	69.53±2.93	10.43±0.094	0.484±0.061	-	-	0.03	+0.022

Table 4:: continued.

Star	v (mag)	$(R-I)_C$ (mag)	Teff (K)	Spect. Type	π (m")	Mv (mag)	$R_\star$ ($R_\odot$)	$v \sin i$ (km/s)	$P/\sin i$ (days)	[M/H] (dex)	[M/H][1] (dex)
GL 836.4	12.83	1.395	3434 ±100	dM3	41±8	10.89±0.449	0.434±0.143	-	-	-0.06	-0.028
GL 843	12.03	1.394	3435 ±100	dM3	77±10	11.46±0.304	0.334±0.081	-	-	-0.16	-0.187
Gl 844	10.653	1.288	3509 ±100	dM3	61.79±2.23	9.61±0.080	0.679±0.080	3.46	9.92-1.4+1.4	1.30	+0.324
Gl 849	10.366	1.416	3417 ±100	dM3	109.94±2.07	10.57±0.043	0.519±0.053	0.85	30.8-7.8+18	0.24	+0.076
GL 856AB	10.75	1.401	3430 ±100	dM3e	64.47±6.49	10.55±0.228	0.513±0.103	11.00	2.36-0.63+0.76	0.15	+0.067
GL 875.1	11.63	1.401	3430 ±100	dM3e	68.78±2.77	10.82±0.107	0.453±0.062	11.00	2.08-0.44+0.52	0.11	-0.024
Gl 877	10.377	1.346	3467 ±100	dM3	116.07±1.19	10.70±0.024	0.442±0.040	0.95	23.5-5.0+8.2	-0.01	-0.026
Gl 896A	10.165	1.424	3410 ±100	dM3e	161.76±1.66	11.21±0.024	0.391±0.037	14.03	1.41-0.14+0.14	0.10	-0.064
Gl 897AB	10.395	1.315	3489 ±100	dM3e	77.5±9	10.59±0.244	0.447±0.092	7.10	3.18-0.97+1.29	-	-0.025
GL 898BC	10.43	1.326	3481 ±100	dM3	65.98±1.96	10.28±0.084	0.523±0.063	-	-	0.01	+0.082
GL 905.2A	11.70	1.388	3439 ±100	dM3	55.6±1.7	10.43±0.086	0.534±0.067	-	-	0.06	+0.099
L 977-17	13.45	1.401	3430 ±100	dM3	46.42±3.24	11.78±0.172	0.290±0.049	-	-	-0.23	-0.316
LP 24-330	13.93	1.376	3447 ±100	dM3	25.72±1.17	10.98±0.119	0.407±0.058	-	-	0.28	-0.035
LHS 218	14.835	1.331	3478 ±100	sdM3	29.4±3.5	12.18±0.262	0.220±0.048	-	-	0.24	-0.601
LHS 375	15.68	1.425	3410 ±100	sdM3	41.7±1	13.78±0.072	0.120±0.014	-	-	-1.10	-1.100
LHS 1104	12.56	1.288	3509 ±100	dM3	62.1±9.1	11.53±0.341	0.281±0.073	-	-	0.02	-0.346
LHS 1384	14.35	1.285	3512 ±100	dM3	-	-	-	14.00	-	-	-
LHS 2942	14.27	1.401	3430 ±100	dM3	-	-	-	5.33	-	-	-
LHS 3375AB	13.74	1.412	3421 ±100	dM3	33±4	12.08±0.268	0.257±0.057	-	-	-0.56	-0.437
LHS 3673	13.60	1.358	3459 ±100	dM3	43.0±9.4	11.77±0.502	0.274±0.099	-	-	-0.05	-0.369
G 212-26	13.42	1.376	3447 ±100	dM3	-	-	-	5.40	-	-	-
G 247-35	12.71	1.275	3520 ±100	dM3	34.54±1.67	10.40±0.125	0.463±0.065	-	-	0.75	-0.011
HIP 28940BC	15.08	1.363	3456 ±100	dM3	18.77±3.21	12.20±0.363	0.226±0.062	-	-	-0.68	-0.574

[1]Metallicity from the radius-metallicity relation

Table 5:: Stellar parameters (e.g. T_{eff}, π, M_V, $R_\star$) as well as the values of $v \sin i$ and [M/H] compiled from the literature for our targets in our list of dM4 stars. We computed the projected rotational period $P/\sin i$ as well as [M/H] derived from the [M/H]/radius correlation.

Star	v (mag)	$(R-I)_C$ (mag)	T_{eff} (K)	Spect. Type	π (m")	Mv (mag)	$R_\star$ ($R_\odot$)	$v \sin i$ (km/s)	$P/\sin i$ (days)	[M/H] (dex)	[M/H][1] (dex)
GJ 1001A	12.84	1.556	3297 ±100	dM4	76.86±3.97	12.27±0.132	0.291±0.044	1.15	12.81-5.66+18.02	-	+0.047
GJ 1005AB	11.483	1.535	3315 ±100	dM4	200.53±9.41	12.99±0.104	0.202±0.028	3.00	3.41-0.96+1.44	-0.47	-0.210
GJ 1010B	14.10	1.535	3315 ±100	dM4	63.7±5.3	13.12±0.201	0.190±0.036	-	-	0.01	-0.249
GJ 1013	12.75	1.548	3304 ±100	dM4	62.3±4.2	11.72±0.167	0.370±0.063	-	-	-0.07	+0.064
GJ 1034	15.05	1.613	3250 ±100	dM4	48.1±4.5	13.46±0.224	0.182±0.037	4.50	2.05-0.61+0.79	-0.38	-0.275
GJ 1045	14.47	1.672	3211 ±100	dM4	48.8±3.4	12.91±0.172	0.258±0.047	-	-	0.30	-0.018
GJ 1065	12.79	1.535	3315 ±100	dM4	104±3	12.88±0.083	0.213±0.027	4.00	2.70-0.65+0.88	0.20	-0.172
GJ 1068	13.58	1.643	3231 ±100	dM4	80±22	13.10±0.633	0.226±0.104	-	-	0.06	-0.126
GJ 1092	13.775	1.584	3273 ±100	dM4	71.321± -	13.04±0.628	0.212±0.095	-	-	-0.40	-0.176
GJ 1105	12.01	1.535	3315 ±100	dM4	116.06±3.67	12.33±0.089	0.274±0.035	2.00	6.93-2.28+4.24	0.24	+0.022
GJ 1122A	14.51	1.689	3200 ±100	dM4e	49±4	12.96±0.198	0.259±0.051	-	-	0.16	-0.015
GJ 1129	12.60	1.607	3254 ±100	dM4	98±17	12.56±0.401	0.274±0.083	3.00	4.62-1.94+2.91	0.05	+0.022
GJ 1134	12.97	1.654	3223 ±100	dM4	96.7±2.3	12.90±0.072	0.252±0.032	4.10	3.11-0.74+1.00	-0.16	-0.036
GJ 1138AB	13.01	1.640	3233 ±100	dM4	102.9±3.2	13.07±0.088	0.227±0.031	3.24	3.55-0.96+1.40	-0.57	-0.122
GJ 1157	13.63	1.649	3227 ±100	dM4	69±11	12.82±0.369	0.258±0.076	-	-	0.61	-0.018
GJ 1174	12.763	1.533	3317 ±100	dM4	60±4	11.65±0.147	0.373±0.059	-	-	0.09	+0.068
GJ 1193	13.825	1.535	3315 ±100	dM4	48.5±3.4	12.25±0.154	0.284±0.046	-	-	-0.09	+0.037
GJ 1204	13.77	1.610	3252 ±100	dM4e	64±4	12.80±0.156	0.246±0.041	-	-	0.43	-0.054
GJ 1207	12.315	1.566	3288 ±100	dM4e	115.39±1.51	12.63±0.030	0.250±0.025	10.70	1.18-0.21+0.25	-0.15	-0.042
GJ 1215	13.68	1.493	3351 ±100	dM4	73±6	13.00±0.199	0.190±0.035	-	-	0.07	-0.249
GJ 1216	14.42	1.572	3283 ±100	dM4	57±5	13.20±0.211	0.194±0.038	-	-	-0.40	-0.236
GJ 1218AB	12.73	1.548	3304 ±100	dM4	61.56±1.62	12.43±0.077	0.267±0.033	-	-	-0.95	+0.010
GJ 1222	13.13	1.563	3291 ±100	dM4	60±3.7	12.02±0.154	0.329±0.054	-	-	0.06	+0.055
GJ 1225	15.39	1.697	3195 ±100	dM4	57±4	14.17±0.173	0.150±0.028	-	-	-0.49	-0.395
GJ 1235	13.36	1.643	3231 ±100	dM4	100.1±3.5	13.36±0.096	0.200±0.028	-	-	0.14	-0.217
GJ 1254	12.55	1.568	3287 ±100	dM4	61±3	11.48±0.127	0.426±0.064	4.00	5.39-1.41+1.90	0.22	+0.122
GJ 1263	12.74	1.511	3336 ±100	dM4	79.8±4.5	12.25±0.143	0.275±0.043	-	-	0.22	+0.023
GJ 1265	13.64	1.643	3231 ±100	dM4	96.0±1.73	13.55±0.059	0.183±0.022	-	-	-0.12	-0.271
GJ 1270	13.245	1.607	3254 ±100	dM4	72.5±2.9	12.55±0.089	0.276±0.036	-	-	0.04	+0.025
GJ 1289	12.62	1.631	3239 ±100	dM4	123.5±2.9	13.08±0.071	0.223±0.029	2.60	4.34-1.27+2.04	0.12	-0.137
GJ 2036B	13.92	1.625	3242 ±100	sdM4e	89.4±1.98	13.68±0.067	0.168±0.020	19.8	0.429-0.07+0.08	-	-0.327
GJ 2043B	14.68	1.619	3246 ±100	dM4	46±6	12.99±0.305	0.228±0.057	-	-	0.34	-0.118
GJ 2069A	11.89	1.595	3263 ±100	PMS M4e	90.37±8.22	11.67±0.218	0.406±0.081	6.43	3.20-0.98+1.34	0.27	+0.102
GJ 3078B	13.90	1.582	3274 ±100	dM4	64.6±2.7	12.95±0.111	0.221±0.031	-	-	0.05	-0.144
GJ 3092B	14.85	1.769	3148 ±100	dM4	33.83±1.00	12.50±0.083	0.366±0.050	3.80	4.87-1.24+1.70	-	+0.064
GJ 3142	13.62	1.572	3283 ±100	dM4e	60±11	12.51±0.423	0.266±0.084	-	-	0.12	+0.006
GJ 3149B	13.10	1.595	3263 ±100	dM4e	88±17	12.82±0.445	0.239±0.079	4.00	3.02-1.26+1.71	0.09	-0.078
GJ 3198	12.35	1.508	3338 ±100	dM4	65±13	11.41±0.460	0.402±0.136	-	-	0.07	+0.098
GJ 3235	13.010	1.550	3302 ±100	dM4	66±12	12.11±0.401	0.311±0.094	-	-	-0.04	+0.051
GJ 3263	12.38	1.506	3340 ±100	dM4	81±16	11.92±0.455	0.317±0.106	-	-	0.09	+0.053
GJ 3283B	14.97	1.654	3223 ±100	dM4e	42±5	13.09±0.264	0.230±0.054	6.00	1.94-0.67+0.93	-	-0.111
GJ 3322	11.520	1.572	3283 ±100	PMS M4e	30.12±9.56	8.914±0.604	1.396±0.602	7.68	9.20-4.57+5.94	-	-
GJ 3372B	13.57	1.654	3223 ±100	dM4e	76±9	12.97±0.278	0.243±0.059	-	-	0.15	-0.063
GJ 3386C	13.13	1.535	3315 ±100	dM4	39.78±1.31	11.13±0.092	0.477±0.062	-	-	0.24	+0.175
GJ 3398	14.22	1.643	3231 ±100	dM4	54.7±2.4	12.91±0.113	0.246±0.037	4.00	3.11-0.81+1.10	-	-0.054
GJ 3405B	13.33	1.548	3304 ±100	dM4	64±9	12.36±0.327	0.276±0.072	-	-	0.12	+0.025
GJ 3466AB	12.85	1.678	3208 ±100	dM4	80±13	12.37±0.376	0.335±0.100	-	-	0.09	+0.057
GJ 3522	10.895	1.607	3254 ±100	dM4e	224±36	12.65±0.354	0.263±0.073	-	-	-0.01	-0.003
GJ 3573	14.2	1.674	3210 ±100	dM4	62±10	13.16±0.553	0.230±0.094	-	-	0.25	-0.111
GJ 3577A	13.89	1.548	3304 ±100	dM4e	45±6	12.16±0.311	0.303±0.076	-	-	0.19	+0.050
GJ 3577B	14.16	1.572	3283 ±100	dM4e	45±6	12.43±0.311	0.277±0.070	-	-	0.19	+0.027
GJ 3599	13.17	1.537	3313 ±100	dM4	59±11	12.02±0.430	0.317±0.101	-	-	0.30	+0.053
GJ 3631AB	14.40	1.619	3246 ±100	dM4e	46±8	13.46±0.402	0.184±0.056	19.10	0.49-0.16+0.18	-0.64	-0.268
GJ 3637	14.06	1.619	3246 ±100	dM4	71.9±3.1	13.34±0.114	0.194±0.028	-	-	-0.30	-0.236
GJ 3666	12.56	1.523	3325 ±100	dM4	63.8±8.5	11.58±0.311	0.380±0.095	-	-	-0.07	+0.075
GJ 3707	12.06	1.568	3287 ±100	dM4	112±21	12.31±0.432	0.291±0.094	2.0	7.36-3.53+6.55	0.35	+0.047
GJ 3764	12.86	1.493	3351 ±100	dM4	62±16	11.82±0.593	0.326±0.138	-	-	-0.09	+0.055
GJ 3779	12.93	1.578	3278 ±100	dM4	72.5±2.6	12.23±0.098	0.306±0.041	-	-	-0.26	+0.050
GJ 3780	12.90	1.566	3288 ±100	dM4e	62.5±14.4	11.88±0.529	0.353±0.135	-	-	-0.21	+0.061
GJ 3789	12.19	1.595	3263 ±100	dM4e	126±22	12.69±0.403	0.253±0.077	56.50	0.227-0.07+0.07	0.07	-0.033
GJ 3800	13.5	1.666	3216 ±100	dM4e	82±13	13.07±0.547	0.237±0.096	-	-	0.10	-0.085
GJ 3801	11.97	1.511	3336 ±100	dM4	107.77±3.22	12.13±0.085	0.290±0.037	4.00	3.67-0.88+1.20	0.14	+0.047
GJ 3804	11.872	1.497	3348 ±100	dM4	97.62±5.03	11.82±0.114	0.328±0.046	2.50	6.64-2.04+3.32	0.09	+0.055
GJ 3832C	13.95	1.572	3283 ±100	dM4e	40±6	11.96±0.348	0.343±0.094	-	-	0.59	+0.059
GJ 3843	13.04	1.491	3353 ±100	dM4	59±14	11.89±0.545	0.314±0.123	-	-	-0.02	+0.052
GJ 3873	12.355	1.585	3272 ±100	dM4	53.5±10.8	11.00±0.446	0.545±0.181	4.00	6.90-2.89+3.91	0.11	+0.245
GJ 3900	12.840	1.572	3283 ±100	dM4	75±23	12.22±0.690	0.305±0.149	3.00	5.15-2.95+4.43	0.46	+0.050
GJ 3907	14.19	1.641	3232 ±100	dM4	51.1±4.4	12.73±0.207	0.266±0.053	2.50	5.39-1.91+3.11	0.06	+0.006
GJ 3908	13.70	1.500	3345 ±100	dM4	43±8	11.87±0.429	0.323±0.103	-	-	0.04	+0.054
GJ 3919	13.21	1.588	3269 ±100	dM4	56.6±3.9	11.97±0.170	0.349±0.060	-	-	0.17	+0.060

Table 5:: continued.

Star	v (mag)	(R-I)$_c$ (mag)	T_{eff} (K)	Spect. Type	π (m")	Mv (mag)	R$_\star$ (R$_\odot$)	$v \sin i$ (km/s)	$P/\sin i$ (days)	[M/H] (dex)	[M/H][1] (dex)
GJ 4020B	14.70	1.631	3239 ±100	dM4e	30.19±2.00	12.10±0.159	0.350±0.061	16.16	1.10-0.24+0.27	-	+0.060
GJ 4030	13.50	1.515	3332 ±100	dM4	44.8±4.1	11.76±0.219	0.347±0.069	4.50	3.90-1.14+1.49	-0.04	+0.059
GJ 4049B	13.54	1.572	3283 ±100	dM4	88.0±3.6	13.26±0.109	0.188±0.026	2.50	3.81-1.16+1.89	-0.13	-0.255
GJ 4063AB	11.42	1.535	3315 ±100	dM4	138±40	12.87±0.668	0.214±0.101	2.17	4.99-2.93+5.16	-0.54	-0.169
GJ 4108	15.35	1.690	3200 ±100	dM4	47.6±4.1	13.74±0.199	0.181±0.036	4.50	2.04-0.60+0.78	-	-0.278
GJ 4169	13.975	1.660	3219 ±100	dM4	72.2±2.9	13.27±0.089	0.214±0.030	-	-	0.07	-0.169
GJ 4177B	13.12	1.511	3336 ±100	dM4	59±8	11.97±0.316	0.312±0.079	-	-	-0.03	+0.052
GJ 4178AB	13.1	1.497	3348 ±100	dM4	57±11	12.63±0.624	0.237±0.105	-	-	-1.65	-0.085
GJ 4185A	12.68	1.548	3304 ±100	PMS M4e	50.7±6	11.21±0.278	0.469±0.109	-	-	0.18	+0.166
GJ 4186A	12.68	1.548	3304 ±100	dM4	51.4±9	11.23±0.404	0.463±0.141	-	-	0.18	+0.160
GJ 4186B	13.49	1.560	3293 ±100	dM4	51.4±9	12.04±0.404	0.324±0.099	-	-	0.18	+0.054
GJ 4207	12.57	1.505	3341 ±100	dM4	57±21	11.35±0.859	0.412±0.251	-	-	0.01	+0.108
GJ 4214A	13.65	1.584	3273 ±100	dM4	57±6	12.43±0.249	0.281±0.061	-	-	0.21	+0.033
GJ 4232AB	14.06	1.517	3330 ±100	dM4	39±7	12.77±0.414	0.218±0.068	-	-	-0.40	-0.155
GJ 4248	11.80	1.484	3359 ±100	dM4	134.29±1.31	12.44±0.041	0.242±0.025	1.58	7.75-2.71+6.04	-	-0.066
GJ 4277A	13.68	1.548	3304 ±100	dM4	39.1±3.3	11.64±0.204	0.384±0.073	-	-	0.24	+0.079
GJ 4333	11.710	1.578	3278 ±100	dM4	91.00±2.89	11.51±0.071	0.427±0.051	2.50	8.64-2.51+4.09	0.25	+0.123
GJ 4338B	12.43	1.619	3246 ±100	PMS M4e	67.5±2.5	11.58±0.099	0.437±0.059	14.50	1.53-0.29+0.33	-	+0.134
GJ 4367	13.45	1.601	3258 ±100	dM4	66±12	12.55±0.419	0.273±0.086	-	-	0.28	+0.020
GJ 4378A	12.93	1.560	3293 ±100	dM4	56±8	11.67±0.310	0.386±0.096	4.00	4.88-1.69+2.29	-	+0.081
GJ 4387AB	12.6	1.542	3309 ±100	dM4	78±14	12.81±0.594	0.222±0.094	-	-	-0.62	-0.140
GJ 9652B	13.27	1.542	3309 ±100	dM4e	52.40±2.94	11.87±0.142	0.343±0.054	-	-	-0.09	+0.059
Gl 15B	11.07	1.580	3276 ±100	dM4	278.76±0.77	13.30±0.026	0.188±0.018	1.90	5.01-1.57+3.01	-0.95	-0.255
Gl 46	11.801	1.508	3338 ±100	dM4	80.95±3.21	11.34±0.088	0.416±0.053	1.29	16.32-6.60+18.1	0.15	+0.112
Gl 54.1	12.074	1.708	3188 ±100	dM4e	271.01±8.36	14.24±0.069	0.148±0.019	2.50	3.00-0.89+1.45	-0.33	-0.402
Gl 73	14.12	1.624	3243 ±100	dM4	60±12	13.01±0.460	0.228±0.078	-	-	0.15	-0.118
Gl 84.1B	12.77	1.497	3348 ±100	dM4	43.03 ±2.08	10.94±0.125	0.492±0.072	2.00	12.45-4.27+7.94	-0.18	+0.190
Gl 102	12.96	1.66	3219 ±100	dM4e	129±12	13.51±0.223	0.192±0.040	-	-	0.03	-0.243
Gl 105B	11.660	1.607	3254 ±100	dM4	129.4±4.3	12.22±0.074	0.320±0.039	2.45	6.61-1.95+3.21	-0.09	+0.053
Gl 166C	11.19	1.63	3239 ±100	dM4e	207.1±2.5	12.77±0.046	0.256±0.028	2.90	4.47-1.17+1.78	-0.10	-0.024
GL 169.1A	11.07	1.60	3259 ±100	dM4	180±0.8	12.35±0.030	0.299±0.030	1.94	7.80-2.44+4.62	0.29	+0.049
GL 179	11.98	1.492	3352 ±100	dM4	81.38±4.04	11.53±0.128	0.372±0.055	2.50	7.53-2.35+3.84	0.22	+0.065
GL 190	10.29	1.50	3345 ±100	dM4	107.85±2.10	10.45±0.062	0.618±0.071	-	-	0.06	+0.320
GL 203	12.49	1.492	3352 ±100	dM4	113.50±5.01	12.76±0.116	0.211±0.030	4.00	2.67-0.68+0.92	-0.23	-0.179
Gl 206A	12.28	1.510	3336 ±100	dM4e	78.16±3.70	12.49±0.123	0.246±0.051	6.37	1.95-0.62+0.84	0.19	-0.054
Gl 206B	12.28	1.510	3336 ±100	dM4e	78.16±3.70	12.49±0.123	0.246±0.051	6.11	2.04-0.65+0.90	0.19	-0.054
GL 213	11.550	1.608	3254 ±100	dM4e	171.55±3.99	12.72±0.053	0.254±0.028	2.70	4.76-1.29+2.03	-0.16	-0.030
GL 232	13.06	1.63	3239 ±100	dM4	120±2.3	13.46±0.062	0.187±0.022	3.10	3.05-0.80+1.18	-0.25	-0.259
GL 234A	11.12	1.700	3193 ±100	dM4e	242.1±1.7	13.04±0.035	0.254±0.028	4.73	2.72-0.57+0.74	-	-0.030
GL 268A	11.47	1.701	3192 ±100	dM4e	158.87±3.35	12.48±0.066	0.331±0.042	10.65	1.57-0.32+0.38	0.16	+0.056
GL 268B	11.47	1.701	3192 ±100	dM4e	158.87±3.35	12.48±0.066	0.331±0.042	10.65	1.57-0.32+0.38	0.16	+0.056
GL 273	9.850	1.533	3317 ±100	dM4	262.98±1.39	11.95±0.013	0.326±0.029	2.36	6.99-1.91+3.22	-0.08	+0.055
Gl 277B	11.78	1.550	3302 ±100	dM4e	84.26±3.45	11.41±0.109	0.429±0.060	6.40	3.39-0.87+1.19	0.10	+0.125
GL 285	11.15	1.696	3196 ±100	dM4e	167.88±2.31	12.27±0.050	0.359±0.042	6.16	2.95-0.71+0.98	0.24	+0.062
GL 299	12.83	1.71	3187 ±100	dM4	148±2.6	13.68±0.058	0.193±0.024	2.96	3.30-0.90+1.35	-0.43	-0.239
GL 300	12.07	1.68	3206 ±100	dM4	125.60±0.97	12.56±0.037	0.306±0.034	3.00	5.16-1.34+2.01	0.20	+0.050
GL 317	12.00	1.497	3348 ±100	dM4	65.3±0.4	11.07±0.033	0.463±0.046	2.50	9.37-2.56+4.18	-0.10	+0.160
GL 319B	11.83	1.523	3325 ±100	dM4	64.80±2.35	10.89±0.099	0.524±0.070	3.70	7.17-1.82+2.53	0.04	+0.223
GL 324B	13.15	1.640	3233 ±100	dM4	76.8±2.4	12.58±0.088	0.285±0.039	2.36	6.11-1.90+3.20	0.42	+0.039
GL 347B	15.01	1.619	3246 ±100	dM4	60.5±4.1	13.92±0.167	0.149±0.026	-	-	0.02	-0.398
GL 375A	11.28	1.501	3344 ±100	dM4e	64.70±1.75	11.08±0.078	0.464±0.057	10.0	2.35-0.48+0.58	-	+0.161
GL 375B	11.28	1.501	3344 ±100	dM4e	64.70±1.75	11.08±0.078	0.464±0.057	10.0	2.35-0.48+0.58	-	+0.161
GL 398	12.636	1.520	3328 ±100	dM4e	71±10	11.89±0.310	0.328±0.082	-	-	0.03	+0.055
GL 402	11.650	1.582	3274 ±100	dM4e	147.92±3.52	12.50±0.054	0.272±0.030	2.40	5.74-1.65+2.75	0.12	+0.019
Gl 431	11.52	1.490	3354 ±100	dM4e	96.56±2.39	11.44±0.074	0.386±0.046	20.36	0.960-0.15+0.17	-	+0.081
Gl 445	10.82	1.520	3328 ±100	dM4	186.86±1.70	12.18±0.040	0.288±0.030	2.25	6.48-1.90+3.28	-0.30	+0.044
Gl 447	11.160	1.678	3208 ±100	dM4	298.04±2.30	13.53±0.019	0.196±0.020	2.20	4.51-1.33+2.32	-0.04	-0.230
GL 458BC	13.33	1.523	3325 ±100	sdM4	64.43±1.43	13.13±0.068	0.186±0.022	5.40	1.74-0.45+0.65	-0.53	-0.262
Gl 469	12.06	1.519	3329 ±100	dM4	75.85±3.99	11.46±0.134	0.400±0.057	1.58	12.81-4.94+11.0	0.14	+0.095
GL 486	11.390	1.537	3313 ±100	dM4	119.47±2.69	11.78±0.051	0.355±0.039	2.25	7.99-2.37+4.10	-0.05	+0.061
Gl 487A	12.10	1.475	3367 ±100	dM4	97.91±1.83	12.05±0.061	0.285±0.032	1.65	8.74-3.05+6.54	-0.04	+0.039
Gl 487B	12.10	1.475	3367 ±100	dM4	97.91±1.83	12.05±0.061	0.285±0.032	1.22	11.87-4.79+14.05	-0.04	+0.039
Gl 487C	12.10	1.475	3367 ±100	dM4e	97.91±1.83	12.05±0.061	0.285±0.032	2.60	5.55-1.55+2.47	-0.04	+0.039
GL 490B	13.20	1.595	3263 ±100	dM4	51.93±3.00	11.78±0.146	0.386±0.062	8.60	2.27-0.56+0.71	0.07	+0.081
GL 512B	13.69	1.652	3225 ±100	dM4	83.8±11.2	13.31±0.312	0.208±0.054	4.00	2.63-0.94+1.27	0.12	-0.190
GL 520C	14.47	1.584	3273 ±100	dM4e	45.17±1.84	12.74±0.109	0.243±0.034	8.20	1.50-0.35+0.45	-0.14	-0.063
GL 540.2AB	13.86	1.726	3176 ±100	dM4e	86±18	14.28±0.481	0.150±0.055	-	-	-0.80	-0.395
GL 544B	14.50	1.643	3231 ±100	dM4	52.6±6.2	13.10±0.277	0.225±0.054	4.66	2.44-0.80+1.03	-0.13	-0.129
GL 545	12.84	1.517	3330 ±100	dM4	87±12	12.54±0.321	0.243±0.062	4.00	3.07-1.08+1.46	-0.12	-0.063
Gl 553.1	11.95	1.488	3355 ±100	dM4	92.44±3.94	11.78±0.113	0.330±0.046	2.50	6.68-2.04+3.33	0.26	+0.056
GL 555	11.320	1.609	3253 ±100	dM4	164.99±3.29	12.41±0.045	0.295±0.032	2.60	5.74-1.58+2.53	0.20	+0.048
GL 568AB	11.680	1.538	3312 ±100	dM4	98.40±4.42	11.64±0.100	0.378±0.051	4.00	4.78-1.18+1.60	0.45	+0.073
GL 592	12.720	1.561	3293 ±100	dM4	74.9±3.8	12.09±0.112	0.318±0.045	3.00	5.36-1.53+2.29	0.14	+0.053

Table 5:: continued.

Star	v (mag)	(R-I)$_c$ (mag)	T_{eff} (K)	Spect. Type	π (m")	Mv (mag)	$R_\star$ ($R_\odot$)	$v \sin i$ (km/s)	$P/\sin i$ (days)	[M/H] (dex)	[M/H][1] (dex)
GL 609	12.570	1.595	3263 ±100	dM4	99±4	12.55±0.090	0.271±0.035	3.00	4.57-1.25+1.88	-0.06	+0.017
GL 630.1AB	12.995	1.684	3204 ±100	dM4e	68±4	12.91±0.130	0.263±0.042	27.50	0.484-0.09+0.10	-0.34	-0.003
GL 643AB	11.79	1.546	3305 ±100	dM4	148.92±4.00	12.65±0.078	0.240±0.030	2.73	4.45-1.26+1.97	-0.21	-0.074
GL 644B	11.74	1.529	3320 ±100	dM4	161.41±5.64	12.78±0.096	0.221±0.029	2.73	4.10-1.18+1.84	-0.21	-0.144
Gl 669A	11.43	1.530	3319 ±100	PMS M4e	86.27±4.10	11.11±0.123	0.478±0.070	6.30	3.84-1.01+1.39	0.08	+0.176
GL 682	10.95	1.59	3268 ±100	dM4	196.90±2.15	12.42±0.044	0.285±0.030	3.00	4.80-1.22+1.83	0.11	+0.039
GL 695B	10.8	-	3345 ±100	dM4	120.33±0.16	11.20±0.103	0.439±0.059	7.33	3.03-0.72+0.95	-	+0.136
Gl 699	9.511	1.592	3266 ±100	dM4	548.31±1.51	13.21±0.008	0.199±0.018	2.02	4.99-1.49+2.75	-0.40	-0.220
GL 720B	13.00	1.548	3304 ±100	dM4	64.32±0.95	12.04±0.052	0.319±0.035	2.30	7.02-2.06+3.52	-0.16	+0.053
GL 725B	9.69	1.51	3336 ±100	dM4	289.48±3.21	11.25±0.044	0.435±0.086	5.09	4.33-1.42+2.12	-0.57	-0.155
GL 729	10.455	1.550	3302 ±100	dM4e	336.72±2.03	13.09±0.015	0.197±0.018	4.72	2.11-0.41+0.53	-0.14	-0.227
GL 732A	12.70	1.560	3293 ±100	dM4e	72±7	11.99±0.232	0.333±0.069	-	-	-0.01	+0.056
GL 747AB	11.260	1.487	3356 ±100	dM4	123±4	11.71±0.073	0.340±0.041	-	-	-0.08	+0.058
GL 754	12.23	1.687	3202 ±100	dM4	169±8	13.37±0.123	0.214±0.033	-	-	-0.17	-0.169
GL 766AB	12.380	1.654	3223 ±100	dM4	97±6	12.31±0.136	0.329±0.054	-	-	0.04	+0.055
GL 781.1B	12.51	1.582	3274 ±100	dM4e	68.5±5.2	11.69±0.185	0.395±0.071	9.20	2.17-0.56+0.70	-0.07	+0.090
GL 783.2B	13.94	1.603	3257 ±100	dM4	51.0±6.0	12.48±0.277	0.283±0.066	1.76	8.14-3.48+7.09	-0.15	+0.036
GL 791.2A	13.04	1.672	3212 ±100	dM4e	110±1.9	13.25±0.058	0.221±0.027	31.90	0.351-0.05+0.05	0.06	-0.144
GL 792	13.49	1.559	3294 ±100	dM4	62±11	12.45±0.409	0.268±0.083	-	-	-0.11	+0.013
GL 810A	12.47	1.615	3249 ±100	dM4	76±11	11.87±0.337	0.380±0.101	-	-	0.02	+0.075
GL 812A	11.916	1.530	3319 ±100	PMS M4e	56.54±3.92	10.68±0.153	0.583±0.096	10.00	2.95-0.71+0.87	0.12	+0.284
GL 838.1B	14.93	1.625	3242 ±100	dM4	41.00±7.00	12.99±0.394	0.230±0.069	-	-	0.05	-0.111
GL 860B	10.30	1.49	3354 ±100	dM4e	251.9±2.3	12.31±0.040	0.260±0.027	4.05	3.25-0.71+0.96	-0.13	-0.012
Gl 865A	12.23	1.530	3319 ±100	dM4e	75.87±5.83	12.38±0.187	0.266±0.048	7.09	1.90-0.53+0.71	-0.10	+0.006
Gl 865B	12.23	1.530	3319 ±100	dM4e	75.87±5.83	12.38±0.187	0.266±0.048	6.20	2.17-0.64+0.88	-0.10	+0.006
Gl 867B	11.45	1.511	3336 ±100	dM4e	115.01±1.32	11.75±0.045	0.345±0.036	7.01	2.48-0.54+0.72	0.15	+0.059
GL 873A	10.26	1.523	3325 ±100	dM4e	195.22±1.87	11.71±0.041	0.358±0.037	5.99	3.02-0.70+0.98	-0.05	+0.062
GL 876A	10.14	1.548	3304 ±100	dM4	213.28±2.12	11.78±0.041	0.360±0.038	2.57	7.09-1.95+3.13	-	+0.062
GL 896B	12.4	1.62	3246 ±100	dM4e	161.76±1.66	13.44±0.122	0.207±0.031	15.81	1.14-0.18+0.21	0.10	+0.062
LHS 1655	15.32	1.562	3292 ±100	dM4	26±4	12.39±0.357	0.277±0.077	-	-	0.18	+0.027
LHS 2795	15.0	1.612	3251 ±100	dM4	-	-	(0.301)	6.40	(2.38)	-	-
LHS 3279	14.04	1.567	3287 ±100	dM4e	-	-	(0.301)	30.0	(0.508)	-	-
LDS 1751	15.71	1.560	3293 ±100	dM4	22.79±1.12	12.50±0.127	0.263±0.039	-	-	0.75	-0.003
MCC 85B	11.01	1.572	3283 ±100	dM4e	278.76±0.77	13.24±0.026	0.191±0.019	-	-	-0.95	-0.246
MCC 475B	14.88	1.511	3336 ±100	dM4	33.00±1.82	12.47±0.140	0.248±0.038	-	-	0.04	-0.047
G 32-37	14.12	1.523	3325 ±100	dM4	35.3±1.8	11.86±0.131	0.335±0.050	-	-	0.19	+0.057
G 32-38	14.36	1.523	3325 ±100	dM4	35.3±1.8	12.10±0.131	0.300±0.045	-	-	0.19	+0.049
G 97-52B	13.62	1.535	3315 ±100	dM4	-	-	(0.301)	4.00	(3.81)	-	-
G 255-12	15.71	1.560	3293 ±100	dM4	24.6±4.7	12.66±0.440	0.244±0.080	-	-	0.75	-0.060

[1]Metalicity from the radius-metallicity relation

Table 7:: Values of $v \sin i$ which we have derived for the stars in our late-K stellar sample. Also listed: FWHM of the cross-correlation profile, and $P/\sin i$.

Star	FWHM (Å±3σ) HARPS	FWHM (Å±3σ) SOPHIE	V_{rad} km s^{-1}	$v \sin i$ km s^{-1} ± 3σ HARPS	$v \sin i$ km s^{-1} ± 3σ SOPHIE	$v \sin i$ km s^{-1} Others	$P/\sin i$ (days±3σ)
GJ 1056	0.1327 0.0028	-	+5.05	1.82-0.38+0.32	-	-	19.1+7.2-4.3
GJ 1066	0.1334 0.0028	-	+26.08	1.91-0.37+0.29	-	-	17.7+6.0-3.5
GJ 1067	-	0.1672 0.0034	-10.10	-	2.08-0.62+0.45	-	16.2+9.3-4.3
GJ 1177A	-	-	-	-	-	6.1	4.78+1.5-1.1
GJ 1213	-	-	-	-	-	0.0	>31.6
GJ 1267	0.1366 0.0028	-	-5.18	2.24-0.28+0.27	-	-	13.7+3.4-2.6
GJ 1279	0.1347 0.0028	-	+4.81	2.06-0.35+0.27	-	1.0	17.1+5.2-3.3
GJ 3072	0.1277 0.0028	-	+9.22	1.10-0.53+0.42	-	-	26.3+31-9.6
GJ 3411	-	-	-	-	-	6.0	5.60+2.0-1.4
GJ 3494	0.1387 0.0028	-	+7.35	2.44-0.27+0.27	-	-	13.7+3.4-2.7
GJ 3551	0.1285 0.0028	-	+58.98	1.22-0.48+0.41	-	2.85	29.3+23-9.4
GJ 3996	0.1334 0.0028	-	+5.70	1.91-0.37+0.29	-	-	17.8+7.3-4.5
GJ 4140	0.1279 0.0028	-	+7.29	1.13-0.52+0.42	-	-	23.6+25-8.2
GJ 9073B	-	-	-	-	-	2.70	11.8+6.6-4.2
GJ 9250	-	-	-	-	-	0.0	>33.5
GJ 9299	0.1324 0.0028	-	+27.90	1.78-0.39+0.33	-	-	18.9+7.8-4.6
GJ 9667	-	-	-12.01	-	-	-	-
GJ 9714	0.1394 0.0028	-	-14.75	2.51-0.27+0.27	-	-	13.1+3.0-2.4
GJ 9827	0.1300 0.0028	-	+31.99	1.45-0.43+0.38	-	-	21.7+13-6.8
Gl 14	-	0.1766 0.0034	+2.67	-	3.25-0.37+0.34	2.6	10.2+2.4-1.8
Gl 40A	0.1316 0.0028	-	+14.73	1.67-0.40+0.36	-	-	18.3+7.8-4.5
Gl 45	0.1295 0.0028	-	+6.68	1.37-0.44+0.39	-	-	21.9+13-6.3
Gl 50	0.1285 0.0028	-	-0.59	1.22-0.48+0.41	-	-	26.0+27-11
Gl 52	-	0.1687 0.0034	-40.77	-	2.28-0.52+0.45	2.0	13.5+5.7-3.3
Gl 57	0.12361 0.0028	-	+26.67	0	-	-	>38
Gl 105.5	-	-	+73.02	-	-	2.72	12.9+5.3-3.4
Gl 112.1	-	-	-	-	-	5.48	6.75+2.2-1.5
Gl 116	-	0.1583 0.0034	-49.71	-	<1	2.4	9.68+4.4-2.6
Gl 123	-	-	-	-	-	0.90	36.6+21-11
Gl 142	-	-	-	-	-	2.70	13.1+5.1-3.3
Gl 143.1	0.1304 0.0028	-	+13.64	1.51-0.43+0.37	-	-	21.2+12-6.3
Gl 146	0.1306 0.0028	-	+21.63	1.54-0.42+0.37	-	-	21.1+11-5.6
Gl 153A	-	0.1721 0.0034	+2.54	-	2.73-0.45+0.41	2.8	10.6+3.8-2.6
Gl 156	0.1275 0.0028	-	+62.31	1.07-0.55+0.43	-	-	30.5+37-11
Gl 162.2	0.1472 0.0028	-	-4.22	3.21-0.22+0.22	-	-	10.5+1.8-1.6
Gl 182	-	-	-	-	-	-	1.86[1]
Gl 186A	0.133 0.0020	-	+113.5	1.86-0.37+0.31	-	-	16.7+6.9-4.2
Gl 186B	0.137 0.0040	-	+113.5	2.28-0.27+0.27	-	-	13.6+3.8-3.0
Gl 191	0.1309 0.0028	-	+244.89	1.58-0.42+0.37	-	-	7.9+3.7-2.0
Gl 208	0.1355 0.0028	0.1756 0.0034	+21.83	2.14-0.32+0.27	3.15-0.40+0.34	-	8.91+2.2-1.6
Gl 221	0.1252 0.0028	-	+23.18	(0.63)	-	-	(49.1)
Gl 226.2	-	-	-	-	-	0.53	57.6+74-24
Gl 249	-	-	-	-	-	10.46	3.27+0.7-0.5
Gl 256	-	-	-	-	-	7.97	4.46+1.1-0.9
Gl 296	-	-	-	-	-	3.8	8.55+4.2-3.0
Gl 322	-	0.1643 0.0034	-22.02	-	(1.58)	-	(18.6)
Gl 389.1	0.1354 0.0028	-	-3.47	2.13-0.32+0.27	-	-	15.8+5.3-3.6
Gl 397	-	-	-	-	-	2.34	15.5+7.3-4.3
Gl 412.3A	0.142 0.001	-	+18.17	2.76-0.27+0.26	-	-	11.8+3.3-2.7
Gl 412.3B	0.0901 0.002	-	+18.17	<1	-	-	-
Gl 414A	-	0.1643 0.0034	-16.12	-	(1.58)	2.7,3.0	(20.8)
Gl 416	-	0.1697 0.0034	-11.70	-	2.41-0.47+0.45	2.85	16.3+5.9-3.9
Gl 421B	0.1281 0.0028	-	+8.10	1.16-0.51+0.42	-	1.90,2.00	20.0+37-14
Gl 425B	0.1491 0.0028	-	-1.28	3.35-0.21+0.21	-	4.20	12.3+3.7-3.3
Gl 455.1	-	-	-	-	-	3.68	7.76+2.4-1.8
Gl 466	-	0.1677 0.0034	-	-	2.15-0.57+0.45	-	17.7+10-5.5
Gl 496.1	0.1289 0.0028	-	+39.29	1.28-0.46+0.40	-	-	27.5+20-8.7
Gl 509.1	-	0.1771 0.0034	-6.26	-	3.30-0.35+0.34	-	10.7+2.6-2.1
Gl 517	0.2702 0.0028	-	-22.50	9.77±0.13	-	8.3,10.8	3.05±0.28
Gl 522	0.1307 0.0028	-	+46.29	1.55-0.42+0.37	-	-	21.6+11-6.0
Gl 524.1	0.1279 0.0028	-	+6.16	1.13-0.52+0.42	-	-	22.0+24-7.9
Gl 542.2	-	-	-	-	-	3.21	12.2+4.3-3.0
Gl 546	-	0.1692 0.0034	-36.85	-	2.35-0.49+0.45	3.0	13.8+5.4-3.4

Table 6: Mean parameters of our stellar samples. Notably, we give the mean effective temperature and the convective overturning time τ_c according to Noyes et al. (1984) and Spada et al. (2013).

Spectral Type	$(R-I)_c$ domain (mag)	$(R-I)_c$ (mag)	T_{eff} (K)	$R_\star$ ($R_\odot$)	(B-V) (mag)	τ_c[1] (days)	τ_c[2] (days)
dK4	[0.560;0.680]	0.617	4600	0.815	1.151	24.16	51.3
dK6	[0.684:0.816]	0.738	4226	0.6469	1.340	25.68	76.5
dM2	[1.064:1.196]	1.128	3658	0.5082	1.511	27.14	119
dM3	[1.284:1.416]	1.354	3462	0.4090	1.548	27.46	175
dM4	[1.500:1.700]	1.532	3317	0.3008	1.581	27.75	454

Table 7:: continued.

Star	FWHM (Å±3σ) HARPS	FWHM (Å±3σ) SOPHIE	V_{rad} km s^{-1}	$v \sin i$ km s^{-1} ± 3σ HARPS	$v \sin i$ km s^{-1} ± 3σ SOPHIE	$v \sin i$ km s^{-1} Others	P/sini (days±3σ)
Gl 558	-	0.1643 0.0034	-55.14	-	(1.58)	-	(19.5)
Gl 562	-	0.1657 0.0034	+42.68	-	1.84-1.09+0.50	1.90	14.3+28-5.2
Gl 570.2	-	-	-	-	-	2.63	13.5+8.5-5.3
Gl 571	0.1307 0.0028	-	+3.86	1.55-0.42+0.37	-	-	18.9+9.9-5.4
Gl 571.1	0.1271 0.0028	-	+15.86	1.01-0.61+0.43	-	-	35.6+66-14
Gl 576	-	-	-	-	-	6.43	4.06+1.3-1.0
Gl 583	0.1334 0.0028	-	-17.83	1.91-0.37+0.29	-	-	15.9+5.8-3.5
Gl 585.1	-	-	-	-	-	0.0	>31.1
Gl 619	-	0.1672 0.0034	+7.19	-	2.08-0.62+0.45	2.7	15.5+8.5-3.9
Gl 626	-	-	-	-	-	6.4	5.31+1.6-1.1
Gl 629.1	0.1342 0.0028	-	-76.44	2.01-0.37+0.27	-	2.7	17.1+7.3-4.5
Gl 659B	-	-	-	-	-	3.53	8.47+3.3-2.4
Gl 673	-	-	-	-	-	3.67	9.02+2.6-1.8
Gl 707	0.1377 0.0028	-	-2.26	2.35-0.27+0.27	-	-	14.0+3.1-2.4
Gl 708	-	-	-	-	-	5.3	6.68+2.5-1.7
Gl 710	0.1348 0.0028	-	-13.24	2.07-0.34+0.27	-	-	14.9+4.8-3.1
Gl 726	0.1314 0.0028	-	+16.82	1.64-0.41+0.37	-	-	18.0+7.9-4.5
Gl 728	-	0.1611 0.0034	-21.78	-	0	-	>35
Gl 747.2	-	-	-	-	-	14.10	3.18+0.6-0.5
Gl 747.3A	0.1398 0.0027	-	-15.81	2.55±0.27	-	-	13.9+3.2-2.6
Gl 747.3B	0.1263 0.0023	-	+11.44	(0.86)	-	-	(41)
Gl 757	0.1262 0.0028	-	+53.68	(0.84)	-	-	(33)
Gl 763	-	-	-58.54	-	-	2.1	13.5
GL 773	-	-	-	-	-	6.5	4.89+1.4-1.0
Gl 782	0.1341 0.0028	-	+23.12	2.00-0.37+0.27	-	-	15.1+5.1-3.0
Gl 786.1	-	0.1638 0.0034	+13.56	-	(1.46)	-	(22.0)
Gl 795A	-	-	-43.51	-	-	-	-
Gl 795B	-	-	-32.16	-	-	-	-
Gl 798	0.1289 0.0028	-	-45.71	1.28-0.46+0.40	-	-	21.7+15-6.6
Gl 801	0.1332 0.0028	-	-72.45	1.88-0.37+0.30	-	-	17.4+7.0-4.3
Gl 818	0.1346 0.0028	-	-65.45	2.05-0.35+0.27	-	2.00	18.7+5.7-3.5
Gl 820B	-	-	-	-	-	-	48.0
Gl 826.1	0.1362 0.0028	-	+19.01	2.21-0.29+0.27	-	-	14.2+3.6-2.6
Gl 828.1	-	-	-	-	-	1.40	21.1+21-8.4
Gl 830	0.1322 0.0028	-	-83.43	1.75-0.39+0.34	-	3.68	20.6+8.3-4.9
Gl 836.9	-	-	-	-	-	6.65	6.67+3.2-2.4
Gl 847A	0.1259 0.0028	-	-30.55	(0.78)	-	-	(34)
Gl 857.1	-	0.2072 0.0034	-6.85	-	6.01-0.23+0.23	6.2	7.66+1.0-0.96
Gl 884	0.1309 0.0028	-	+17.16	1.58-0.42+0.37	-	3.00,3.21	19.5+9.2-5.1
Gl 885A	-	-	-	-	-	6.27	3.98+2.4-1.7
Gl 889A	0.1348 0.0028	-	+16.35	2.07-0.35+0.27	-	-	15.2+5.0-3.2
Gl 891	-	-	-	-	-	2.5	11.3+5.7-3.5
Gl 894	0.1402 0.0028	-	+0.09	2.59-0.27+0.27	-	-	13.2+3.6-2.9
Gl 895.5	0.1391 0.0028	-	+2.18	2.48-0.27+0.27	-	-	11.9+3.1-2.5
Gl 898	0.1488 0.0028	-	+0.25	3.33±0.21	-	3.37	10.6+1.8-1.6
Gl 900	-	-	-10.41	-	-	13.0	2.54+0.5-0.4
Gl 906	-	0.1618 0.0034	-20.49	-	(0.33)	-	>86
Gl 907.1	-	-	-	-	-	3.4	14.0+5.6-3.9
HIP 3121	-	-	-	-	-	17.0	2.21+0.5-0.4
HIP 6290	-	-	-	-	-	3.21	6.73+2.5-1.7
HIP 11437	-	-	-	-	-	5.0	8.98+3.0-2.3
HIP 14593A	0.1298 0.0028	-	+17.47	1.42-0.43+0.38	-	-	26.6+18-9.0
HIP 19410A	0.146 0.0030	-	+14.36	3.11-0.24+0.21	-	-	8.92+2.5-2.1
HIP 19410B	0.0936 0.0031	-	+9.32	<1	-	-	-
HIP 19410C	0.156 0.0031	-	+0.22	3.88-0.21+0.20	-	-	5.06+1.3-1.1
HIP 21865	0.1337 0.0028	-	+53.29	1.95-0.37+0.28	-	-	17.3+6.4-3.9
HIP 40170	-	-	-	-	-	0.53	53.9+71-23
HIP 42108A	0.135 0.0029	-	+27.10	2.09-0.34+0.27	-	-	13.5+4.9-3.2
HIP 42108B	0.134 0.0029	-	+38.56	1.99-0.37+0.27	-	-	14.1+5.7-3.4
HIP 42910	0.1361 0.0028	-	+0.23	2.19-0.30+0.27	-	-	19.0+6.3-4.6
HIP 50773	-	0.1628 0.0034	-16.67	-	(1.07)	-	(28.4)
HIP 51073	0.1325 0.0028	-	+57.04	1.79-0.38+0.33	-	-	18.5+9.3-5.7
HIP 51263A	0.1299 0.0028	-	+83.87	1.44-0.38+0.33	-	-	23.6+14-7.4
HIP 51263B	0.1165 0.0028	-	+46.32	<1	-	-	>70
HIP 53175	-	0.1702 0.0034	+14.72	-	2.48-0.45+0.45	-	15.0+6.4-4.4
HIP 56838	0.1319 0.0028	-	+39.26	1.71-0.40+0.35	-	-	21.4+9.6-5.6
HIP 58945	-	0.1682 0.0034	-7.02	-	2.21-0.54+0.45	-	14.3+7.8-4.4
HIP 59247	-	0.1702 0.0034	+4.45	-	2.48-0.45+0.45	-	13.8+6.1-4.2
HIP 60438	-	-	-	-	-	17.9	2.45+0.6-0.6
HIP 60501	-	0.1672 0.0034	+6.13	-	2.08-0.62+0.45	-	25.0+18-8.6
HIP 72044	-	0.1643 0.0034	-30.11	-	(1.58)	-	(19.1)
HIP 76550	0.1271 0.0028	-	-64.50	1.01-0.61+0.43	-	-	22.9+49-10
HIP 78395	0.1299 0.0028	-	+25.52	1.44-0.38+0.33	-	-	21.6+13-6.9
HIP 80083	0.1304 0.0028	-	-4.81	1.51-0.43+0.37	-	-	18.1+14-7.3
HIP 95223	-	-	-	-	-	1.90	18.0+11-5.8
HIP 103150	0.1230 0.0028	-	+15.77	<1	-	-	>30
HIP 110245	0.1475 0.0028	-	-8.87	3.23±0.21	-	-	12.3+3.0-2.6
HIP 110714	0.1294 0.0028	-	+6.62	1.36-0.45+0.39	-	-	24.6+17-8.3
HIP 113597	-	-	-	-	-	6.27	7.46+2.7-1.9
HIP 116011	-	0.1638 0.0034	+8.78	-	(1.46)	-	(19.4)
LHS 3060	-	-	-	-	-	4.9	6.20+1.4-1.1
STKM 1-607	-	-	-	-	-	40.0	-

[1]Rutten 1987